OUKA
The University of Osaka
Institutional Knowledge Archive

Title	Effects of Polymerization Temperature and Helical Pitch on the Electro-Optic Characteristics of Polymer/Cholesteric Liquid Crystal Nanocomposites
Author(s)	金, 會慶
Citation	大阪大学, 2016, 博士論文
Version Type	VoR
URL	https://doi.org/10.18910/59617
rights	
Note	

The University of Osaka Institutional Knowledge Archive : OUKA

https://ir.library.osaka-u.ac.jp/

The University of Osaka

Doctoral Dissertation

Effects of Polymerization Temperature and Helical Pitch on the Electro-Optic Characteristics of Polymer/Cholesteric Liquid Crystal Nanocomposites

「高分子/コレステリック液晶ナノ複合材料の電気光学特性に及ぼす重合温度および螺旋周期の効果に関する研究」

Hoekyung Kim
金會慶

July 2016

Graduate School of Engineering,
Osaka University

Contents

Chapter 1 Introduction 1

1.1 Liquid crystals 3
1.2 Light propagation in cholesteric liquid crystals 4
1.3 Textures of cholesteric liquid crystals 10
1.4 Polymer/liquid crystal composite 13

1.4.1 Electro-optic response of the polymer/cholesteric liquid crystal nanocomposites . 15
1.4.2 Response time of the polymer/liquid crystal nanocomposites 16

Chapter 2 Deformation-free switching of polymer-stabilized cholesteric liquid crystals by low-temperature polymerization 19

2.1 Introduction 19
2.2 Effects of monomer concentration and polymerization temperature on the driving voltage in deformation-free polymer/ChLC nanocomposites 20
2.3 Materials and experimental procedure 24

2.3.1 Materials 24
2.3.2 Fabrication of polymer/cholesteric liquid crystal cell 26
2.3.3 Fabrication of samples for measuring polymer morphologies 28
2.3.4 Measurement setup of the electro-optic characteristics 28

2.4 Electro-optic characteristics 29
2.5 Polymer network morphologies 31
2.6 Response time 34
2.7 Improvement of the electro-optic characteristics due to the low temperature polymerization 37
2.8 Summary 39

Chapter 3 Helical pitch dependence of the electro-optic characteristics in polymer/cholesteric liquid crystal nanocomposites having ultra-small liquid crystal domains 41

3.1 Introduction 41
3.2 Materials and experimental procedure 42

3.2.1 Materials and fabrication process 42
3.2.2 Measurement of the helical pitch 42

3.3 Electro-optic characteristics 43
3.4 Textures of polymer/ChLC nanocomposites 49
3.5 Polymer network morphologies 53

3.6 Fredericks-type reorientation of polymer/ChLC nanocomposite at a polymerization temperature of -20 °C 56
3.7 Summary 57
Chapter 4 Helical pitch dependence of the electro-optic characteristics in polymer/cholesteric liquid crystal composites having large-size liquid crystal domains 59
4.1 Introduction 59
4.2 Materials and sample preparation 60
4.3 Polymer network morphologies 61
4.4 Electro-optic characteristics 62
4.4.1 Electric field dependence of the selective reflection band 62
4.4.2 Response time 68
4.5 Textures of polymer/ChLC nanocomposites 69
4.6 Summary 70
Chapter 5 Conclusions 73
Acknowledgments 75
References 76
Achievements 82

Abstract

In this dissertation, a study on the electro-optic characteristics of polymer/cholesteric liquid crystal (ChLC) nanocomposites is reported to reduce the driving voltage and understand the physics of polymer/ChLC nanocomposites. A low-temperature polymerization process can manipulate the electro-optic switching mode; the result is that a low driving voltage is attained in low-monomer-concentration polymer/ChLC nanocomposite while maintaining a fast response time. The study on the helical pitch dependence of the electro-optic characteristics in polymer/ChLC nanocomposites should help understand the response mechanism of such polymer/ChLC nanocomposites. The details are described in the following chapters.

Chapter 1: Introduction

An introduction to the properties of LCs, ChLCs, and the polymer/ChLC nanocomposites is given. The research purpose and overview of the dissertation is also described.

Chapter 2: Deformation-free switching of polymer-stabilized cholesteric liquid crystals by low-temperature polymerization

The 'deformation-free' switching mode in polymer/ChLC nanocomposites usually occurs when the polymer concentration ranges from a few to several tens of wt% values. In this chapter, a qualitative change in the electro-optic response of polymer/ChLC nanocomposites with a monomer concentration of 6.6 wt% is demonstrated by reducing the polymerization temperature. The LC domains are formed by phase separation between the polymer and non-photopolymerizable LC molecules during the polymerization process. Because the domain size depends on the polymerization rate during polymerization-induced phase separation, smaller LC domains can be achieved by controlling the degree of phase separation via a change in the polymerization temperature. Suppressed phase separation leading to the formation of smaller LC domains is accomplished by reducing the polymerization temperature. The driving force leading to the formation of smaller domain sizes is believed to be the increased viscosity at lower temperatures. The low-monomer-concentration polymer/ChLC nanocomposites can achieve a lower driving voltage without any deterioration in the fast response. The electro-optic characteristics and polymer morphologies of low-monomer-concentration polymer/ChLC nanocomposites with different polymerization temperatures are investigated.

Chapter 3: Helical pitch dependence of the electro-optic characteristics in polymer/cholesteric liquid crystal nanocomposites having ultra-small liquid crystal domains

Studies on the helical pitch (p) dependence of the electro-optic characteristics in low-monomer-concentration polymer/ChLC composites are reported. Depending on the polymerization temperature, low-monomer-concentration polymer/ChLC composites show two response modes: a 'polymer-stabilized' response and a 'deformation-free' response. Despite the difference in the electro-optic response modes, the threshold electric field of the polymer/ChLC composites increases as the helical pitch decreases for both response modes. However, the threshold electric field shows differing dependencies on the helical pitch according to the electro-optic response modes. The 'polymer-stabilized' ChLC roughly shows a $p^{-0.57}$ dependence on the pitch, which is a consequence of the response being dominated by the Helfrich deformation. The 'deformation-free' polymer/ChLC, on the other hand, shows a smaller dependence on the pitch of approximately $p^{-0.33}$. The decrease in the pitch dependence is described as a consequence of the nano-confined LC molecules undergoing a Fredericks-type reorientation instead of a helix deformation.

Chapter 4: Helical pitch dependence of the electro-optic characteristics in polymer/cholesteric liquid crystal composites having large-size liquid crystal domains

The helical pitch dependence of the threshold electric field in high-monomer-concentration polymer/ChLC composites having pitch-length scale LC domains is investigated. In contrast to the previous chapter, the threshold electric field shows little dependence on the helical pitch. This difference in the behavior of the helical pitch dependence in the thresholds is thought to originate from the difference in the dynamics of the LC molecules in each of the domains. The dynamics of the LC molecules in each of the domains is determined by the ratio of domain size to pitch length, since the domain sizes are statistically distributed. The portion of LC domains showing the helix deformation in the polymer/ChLC composite increases with an increase in the ratio of domain size to pitch length. For short pitch samples, the decrease in thresholds due to the change in the dynamics of the LC molecules within the domains cancels out the increase in thresholds caused from the increased twist in the Fredericks-type reorientation.

Chapter 5: Conclusions

The results obtained from chapter 2 to chapter 4 are summarized and the main conclusions of the dissertation are drawn.

Chapter 1 Introduction

Liquid crystal (LC) is a state of matter that exists between the fluid and the solid states. Because of its unique characteristics, such as optical and dielectric anisotropy, LCs have been applied to various industrial fields, especially information display [1-3] and tunable electro-optic devices [4-6]. Optical anisotropy, called birefringence, is the difference between the extra-ordinary and ordinary refractive indices of a LC. The birefringence can provide an ability to change the optical characteristics of a LC, such as transmittance and phase, since the velocity of light with a polarization parallel to the director is different from that perpendicular to the director. Dielectric anisotropy is the difference between the relative permittivities when an electric field is applied parallel and perpendicular to the LC molecules. Therefore, the optical characteristics of a LC can be modulated by an external electric field because the orientation of molecules is changed in response to an external field. Self-organization is also a very important property of LCs, in which the molecules are spontaneously arranged with an ordered structure. It is a very interesting subject of research in the fields of both chemistry and physics, since it is possible to easily fabricate a variety of difficult complex structures, which are difficult to make artificially. The various functionalities of LC materials, which result from the collective molecular alignment, have attracted much attention for their potential use in optoelectronic applications.

The spontaneous formation of the periodic structure makes cholesteric LCs (ChLCs) potentially useful for optical applications such as optical switches [7], lasers [8-10], and displays [11-14], because the selective reflection (SR) band is tunable by external stimuli [15-19]. When light incidents on the ChLCs, they reflect circularly polarized light with the same handedness as the cholesteric helix in a certain wavelength band, called the SR band. The spectral position and the band-width of the SR band is determined by the helical pitch, defined as the distance required for the director to twist by 2π, the ordinary and the extra-ordinary refractive indices of the ChLCs. However, they show a slow decay time typically on the order of several seconds [20], hindering their use in electro-optic applications. The slow decay time originates from the field-induced deformation of the helical structure, which occurs on larger length and time-scales compared to the reorientation of the director in a nematic LC [21].

To overcome this intrinsic drawback, 'polymer-stabilized' ChLCs in which polymer networks are dispersed in ChLCs have been investigated intensively [22]. 'Polymer-stabilized' ChLCs are obtained by dissolving a small amount of a photopolymerizable monomer (5–10 wt %) in a low-molecular weight ChLC and polymerizing the sample *in situ* in the cholesteric phase. 'Polymer-stabilized' ChLCs show an improved response time; however, the movement of the polymer network with the LC molecules limits the response time to a few tens of milliseconds [23].

Recently, polymer/ChLC nanocomposites have been emerging as next-generation LC materials for various functional optical devices such as polarization rotators and polarization-independent phase modulators, due to their unique electro-optic response in which the decay time is fast (~ few 10 μs) without deforming the reflection band [24-28]. This electro-optic response is called 'deformation-free', since the reflection band is maintained. This 'deformation-free' tuning mode occurs when the size of the LC domains in a polymer/ChLC composite is reduced to several tens of nanometers, leading to the control of the effective refractive index only.

Under an electric field, the LC molecules are reoriented along the field, but the polymer matrix is strongly fixed by the cross-linked polymer chains and is immobile; the result is that the effective extra-ordinary refractive index is decreased, while the ordinary refractive index and helical pitch remain constant. The motion of the non-reactive LC molecules confined in the nano-sized domains exhibits a very short decay time of a few tens of microseconds, corresponding to a ~1000-fold improvement compared to that of conventional ChLCs. However, the driving voltage of polymer/ChLC nanocomposites showing a 'deformation-free' electro-optic response is too high to use in practical electro-optic devices. There is a limit to which the threshold voltage of 'deformation-free' polymer/ChLC nanocomposites can be decreased, because the nano-sized domains leading to the strong anchoring are required to implement the 'deformation-free' electro-optic response in polymer/ChLC nanocomposites. Also, the small amount of mobile LC molecules restricts the tuning range of the refractive index, since monomer concentrations of a few to several tens of wt% values are required to form the nano-sized LC domains in polymer/ChLC nanocomposites. Further studies on reducing the driving voltage in polymer/ChLC nanocomposites may lead to practical electro-optic devices.

From this perspective, in this dissertation, we focus on the method of implementing the 'deformation-free' switching behavior in 'polymer-stabilized' ChLCs by low-temperature polymerization and the understanding of the driving mechanisms of the 'deformation-free' polymer/ChLC nanocomposites.

The outline of this dissertation is as follows. The main subjects of this dissertation are the fabrication of low-monomer-concentration polymer/ChLC nanocomposites by a low-temperature polymerization process and investigation of their electro-optic characteristics. In the rest of this chapter, we will introduce the fundamentals of LCs, ChLCs and polymer/LC nanocomposites.

In chapter 2, we provide a detailed account of the low-temperature polymerization process in a low-monomer-concentration polymer/ChLC precursor that yields a qualitative change in the electro-optic response from 'polymer-stabilized' to 'deformation-free'. The suppressed polymerization-induced phase separation, due to the low polymerization temperature, results in

smaller LC domains which bring about a change in the electro-optic response. A low driving voltage with fast response in 'deformation-free' polymer/ChLC nanocomposite is demonstrated.

In chapters 3 and 4, we also show the helical pitch dependence of the electro-optic characteristics in polymer/ChLC nanocomposites having domains of different size to understand the response mechanism of polymer/ChLC nanocomposites.

In chapter 3, the helical pitch dependence of the threshold electric field in low-monomer-concentration polymer/ChLC composites showing different electro-optic response modes is investigated. Although the threshold electric field of the polymer/ChLC nanocomposites decreases as the helical pitch increases regardless of the electro-optic response mode, the dependences of the threshold electric field on the helical pitch are different depending on the electro-optic response modes. Fredericks-type reorientation of the LC molecules confined in nano-sized domains is introduced to understand the dynamics of the 'deformation-free' polymer/ChLC nanocomposites.

In chapter 4, we study the helical pitch dependence of the threshold electric field in polymer/ChLC composites having large domain sizes. In this case, the dependence of the threshold electric field on the helical pitch is completely different from the results discussed in Chapter 3. The reason is investigated that both Helfrich deformation and Fredericks-type reorientation affect the threshold electric field. The variation in the ratio of domain size to pitch length is proposed as the dominant parameter that determines the threshold electric field.

In chapter 5, we summarize the key results of each chapter and present conclusions drawn from this dissertation.

1.1 Liquid crystals

To date, LCs have mainly been studied from the viewpoint of display applications because of their large refractive index change with low driving voltage. However, LCs are potentially applicable to not only display applications, but also photonic devices, since a LC is a multi-functional material that can control various aspects associated with the propagation of light such as phase changes, scattering, diffraction, and reflection. As indicated by the name, a LC is an intermediate state of matter between an isotropic liquid and a solid crystal. A LC possesses properties of both liquid (fluidity) and crystal (anisotropy). A LC is classified by the shape and orientational order of its molecules. In the case of rod-like (calamitic) LCs, as shown in Fig. 1.1, the thermotropic LC phase occurs over a certain temperature range. The LC phase changes to the isotropic phase with an increase in the temperature; on the other hand, the LC phase changes to the crystal phase with a decrease in the temperature. The most common LC phase is the nematic phase, which is widely used in most LC display applications. In the nematic phase, the calamitic molecules have no positional order, but have an orientational order, i.e., the LC

molecules are aligned towards a preferred direction defined by the director vector. Unlike the nematic LC phase, the molecules in the smectic phase not only have orientational order, but also have partial positional order.

The ChLC, which is called a chiral nematic LC, is a liquid crystalline phase in which the constituent molecules self-organize into a helical structure. The ChLC exhibits the nematic phase locally; however, the LC molecules are twisted with a periodicity along the direction perpendicular to the director vector. The ChLC forming a helical periodic structure shows the unique optical characteristic of SR. In the following sections, we present an introduction to the basic electro-optic characteristics of the ChLC used in this dissertation.

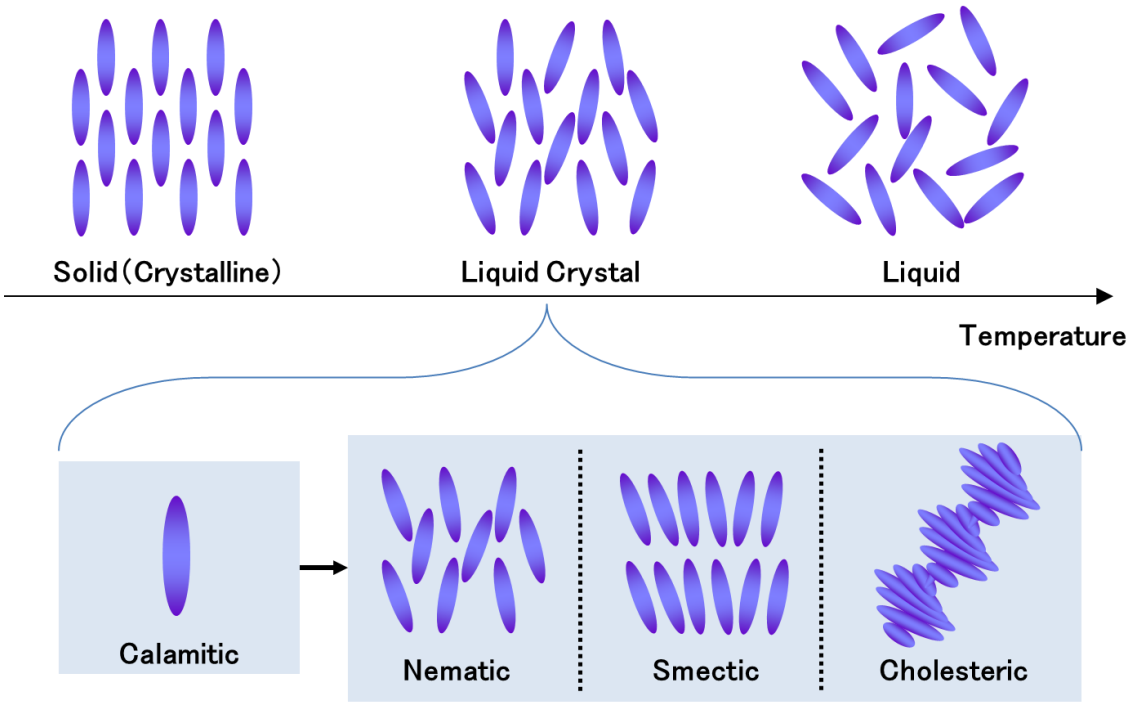

Figure 1.1 Categorization of liquid crystals.

1.2 Light propagation in cholesteric liquid crystals

In general, a ChLC is obtained from the nematic phase of a LC material by adding a chiral dopant. Figure 1.2 shows a schematic view of the self-assembled helical periodic structure formed by ChLC. This structure can be considered as a one-dimensional photonic crystal. It exhibits the so-called SR characteristics, in which light with the same circular polarization handedness as the helix is Bragg reflected. When the helical pitch, p, is defined as the distance required for the director to twist by 360°, the center wavelength, λ_c, and the band-width of the SR band, $\Delta\lambda$, is determined by the helical pitch, the average refractive index, $n_{avg} = \frac{n_e + n_o}{2}$,

and the birefringence $\Delta n = (n_e - n_o)$, i.e., $\lambda_c = n_{avg} \times p$ and $\Delta\lambda = \Delta n \times p$, where n_e and n_o are the extra-ordinary and ordinary refractive indices, respectively. The relations of the SR band are obtained by solving Maxwell's equations with respect to the light propagating in the direction of the helical axis [29,30].

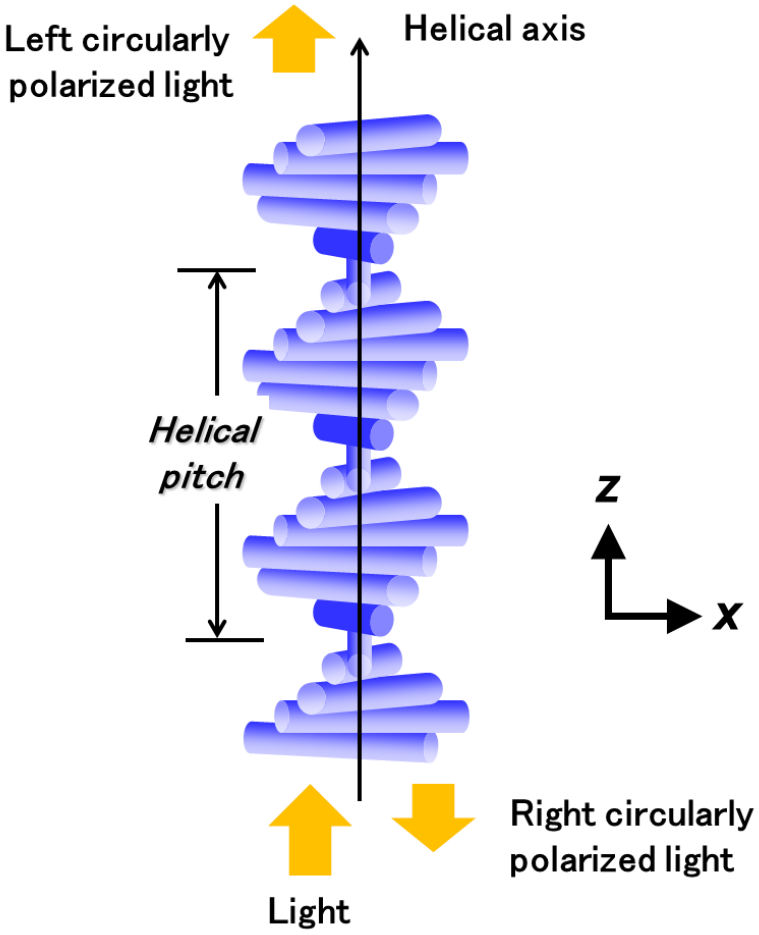

Figure 1.2 Selective reflection in the helical structure of the ChLC.

In a ChLC phase, the LC molecular director $\boldsymbol{n}$ turns around the helical axis, where $\boldsymbol{n}$ and helical axis are perpendicular to each other. When the helical axis is parallel to the $\boldsymbol{z}$ axis as shown in Fig. 1.2, the director $\boldsymbol{n}$ is expressed as

$$\boldsymbol{n}(z) = (\cos qz, \quad \sin qz, \quad 0), \tag{1.1}$$

where the chirality, q, is defined as $q = 2\pi / p$. The local directors of the LC molecules are twisted in the xy-plane, with a twist angle of qz. The dielectric constant in the local principal coordinate is expressed as

$$\varepsilon = \begin{pmatrix} \varepsilon_{\parallel} & 0 & 0 \\ 0 & \varepsilon_{\perp} & 0 \\ 0 & 0 & \varepsilon_{\perp} \end{pmatrix}, \tag{1.2}$$

where $\varepsilon_{\parallel}$ and $\varepsilon_{\perp}$ are the dielectric constants along the long and short molecular axes, respectively. In general, rod-like LC molecules satisfy the following relationship: $\Delta\varepsilon = \varepsilon_{\parallel} - \varepsilon_{\perp} > 0$.

When the light propagates to the direction of the helical axis of the ChLC ($\boldsymbol{z}$-axis), the electromagnetic wave and Maxwell's equation in a free-space are expressed as

$$\boldsymbol{E}(z,t) = \boldsymbol{E}(z)e^{-i\omega t}, \tag{1.3}$$

$$\boldsymbol{H}(z,t) = \boldsymbol{H}(z)e^{-i\omega t}, \tag{1.4}$$

$$\nabla \times \boldsymbol{E}(z,t) = -\mu_0 \frac{\partial \boldsymbol{H}(z,t)}{\partial t}, \tag{1.5}$$

$$\nabla \times \boldsymbol{H}(z,t) = \varepsilon_0 \hat{\varepsilon}(z) \frac{\partial \boldsymbol{E}(z,t)}{\partial t}, \tag{1.6}$$

where ω is the angular frequency ($\omega = 2\pi/\lambda$), and μ_0 and ε_0 are the magnetic permeability and dielectric tensor in vacuum, respectively. The dielectric tensor $\hat{\varepsilon}(z)$ of the ChLC can be expressed as

$$\begin{aligned} \hat{\varepsilon}(z) &= \begin{pmatrix} \cos(qz) & -\sin(qz) & 0 \\ \sin(qz) & \cos(qz) & 0 \\ 0 & 0 & 1 \end{pmatrix} \begin{pmatrix} \varepsilon_{\parallel} & 0 & 0 \\ 0 & \varepsilon_{\perp} & 0 \\ 0 & 0 & \varepsilon_{\perp} \end{pmatrix} \begin{pmatrix} \cos(qz) & \sin(qz) & 0 \\ -\sin(qz) & \cos(qz) & 0 \\ 0 & 0 & 1 \end{pmatrix} \\ &= \begin{pmatrix} \frac{\varepsilon_{\parallel}+\varepsilon_{\perp}}{2} + \frac{\varepsilon_{\parallel}-\varepsilon_{\perp}}{2}\cos(2qz) & \frac{\varepsilon_{\parallel}-\varepsilon_{\perp}}{2}\sin(2qz) & 0 \\ \frac{\varepsilon_{\parallel}-\varepsilon_{\perp}}{2}\sin(2qz) & \frac{\varepsilon_{\parallel}+\varepsilon_{\perp}}{2} - \frac{\varepsilon_{\parallel}-\varepsilon_{\perp}}{2}\cos(2qz) & 0 \\ 0 & 0 & \varepsilon_{\perp} \end{pmatrix} \\ &= \begin{pmatrix} \bar{\varepsilon} + \frac{\Delta\varepsilon}{2}\cos(2qz) & \frac{\Delta\varepsilon}{2}\sin(2qz) & 0 \\ \frac{\Delta\varepsilon}{2}\sin(2qz) & \bar{\varepsilon} - \frac{\Delta\varepsilon}{2}\cos(2qz) & 0 \\ 0 & 0 & \varepsilon_{\perp} \end{pmatrix}, \end{aligned} \tag{1.7}$$

with the average dielectric constant $\bar{\varepsilon} = \frac{\varepsilon_{\parallel} + \varepsilon_{\perp}}{2}$ and dielectric anisotropy $\Delta\varepsilon = \varepsilon_{\parallel} - \varepsilon_{\perp}$. Equation (1.5) and Eq. (1.6) are expanded to Eq. (1.8) using a curl operation.

$$\nabla \times \left(\nabla \times \boldsymbol{E}(z,t)\right) = -\mu_0 \varepsilon_0 \hat{\varepsilon}(z) \frac{\partial^2 \boldsymbol{E}(z,t)}{\partial t^2}. \tag{1.8}$$

Using the vector formula of $\nabla \times \left(\nabla \times \boldsymbol{E}(z,t)\right) = \nabla\left(\nabla \cdot \boldsymbol{E}(z,t)\right) - \nabla^2 \boldsymbol{E}(z,t)$ and the relation of $\nabla \cdot \boldsymbol{E}(z,t) = 0$, Eq. (1.8) can be expressed as

$$\nabla^2 \boldsymbol{E}(z,t) - \mu_0 \varepsilon_0 \hat{\varepsilon}(z) \frac{\partial^2 \boldsymbol{E}(z,t)}{\partial t^2} = 0. \tag{1.9}$$

By substituting Eq. (1.3) into Eq. (1.9), the following wave equation is yielded:

$$\frac{d^2}{dz^2}\boldsymbol{E}(z) + \mu_0 \varepsilon_0 \hat{\varepsilon}(z)\,\omega^2 \boldsymbol{E}(z) = \frac{d^2}{dz^2}\boldsymbol{E}(z) + \left(\frac{\omega}{c}\right)^2 \hat{\varepsilon}(z)\,\boldsymbol{E}(z) = 0. \tag{1.10}$$

Since the z component of the electric field is 0, it is sufficient to consider only the x and y components of electric field in Eq. (1.10). Therefore, the dielectric tensor can also be expressed in terms of a corresponding 2×2 matrix. To simplify this wave equation, new variables are introduced as

$$E_{\pm}(z) = E_x(z) \pm i E_y(z). \tag{1.11}$$

Using Eq. (1.10) and Eq. (1.11), the wave equation changes to

$$\frac{d^2}{dz^2}\begin{pmatrix} E_+(z) \\ E_-(z) \end{pmatrix} = -\left(\frac{\omega}{c}\right)^2 \begin{pmatrix} \bar{\varepsilon} & \frac{\Delta\varepsilon}{2} e^{i2qz} \\ \frac{\Delta\varepsilon}{2} e^{-i2qz} & \bar{\varepsilon} \end{pmatrix} \begin{pmatrix} E_+(z) \\ E_-(z) \end{pmatrix}. \tag{1.12}$$

The solutions of the above differential equations generally take the following forms:

$$E_+(z) = \mathrm{A} e^{i(l+q)z}, \tag{1.13}$$

$$E_-(z) = \mathrm{B} e^{i(l-q)z}. \tag{1.14}$$

By substituting Eq. (1.13) and Eq. (1.14) into Eq. (1.12), two coupled linear equations for amplitudes A and B are obtained.

$$\left[(l+q)^2 - \left(\frac{\omega}{c}\right)^2 \bar{\varepsilon}\right]\mathrm{A} - \left(\frac{\omega}{c}\right)^2 \frac{\Delta\varepsilon}{2}\mathrm{B} = 0, \tag{1.15}$$

$$\left[(l-q)^2-\left(\frac{\omega}{c}\right)^2\bar{\varepsilon}\right]\mathrm{B}-\left(\frac{\omega}{c}\right)^2\frac{\Delta\varepsilon}{2}\mathrm{A}=0. \tag{1.16}$$

The above equations can be written as

$$\begin{pmatrix}(l+q)^2-k_a^2 & -k_b^2\\ -k_b^2 & (l-q)^2-k_a^2\end{pmatrix}\begin{pmatrix}\mathrm{A}\\ \mathrm{B}\end{pmatrix}=0, \tag{1.17}$$

where

$$k_a^2=\left(\frac{\omega}{c}\right)^2\bar{\varepsilon}, \tag{1.18}$$

$$k_b^2=\left(\frac{\omega}{c}\right)^2\frac{\Delta\varepsilon}{2}. \tag{1.19}$$

To get non-trivial solutions of amplitudes A and B, the determinant of Eq. (1.17) must be zero.

$$\begin{vmatrix}(l+q)^2-k_a^2 & -k_b^2\\ -k_b^2 & (l-q)^2-k_a^2\end{vmatrix}=\left[(l+q)^2-k_a^2\right]\left[(l-q)^2-k_a^2\right]-k_b^4=0. \tag{1.20}$$

For a given ω, two independent modes are given by

$$l^2=l_1^2=\left(k_a^2+q^2\right)-\sqrt{4k_a^2q^2+k_b^4}, \tag{1.21}$$

$$l^2=l_2^2=\left(k_a^2+q^2\right)+\sqrt{4k_a^2q^2+k_b^4}. \tag{1.22}$$

From here on in, we discuss the dispersion relation between ω and l and the polarization states of modes l_1 and l_2. The detailed mathematics are presented in references 29 and 30.

The dispersion relation between ω and l is plotted in Fig. 1.3. As can be seen from Eq. (1.21) and Eq. (1.22), l_2 is always real; however, l_1 is always pure imaginary in some frequency range between $\omega_-(0)$ and $\omega_+(0)$, as shown in Fig. 1.3 ($\omega_+(0)>\omega_-(0)$). The real wave number means that the mode propagates in the medium, whereas the pure imaginary wave number signifies that the mode cannot propagate in the medium and undergoes the Bragg reflection, which is called the bandgap. In order to obtain a frequency boundary at which light propagation is forbidden, the special case of $l=0$ is considered. From Eq. (1.17), we can obtain the relation

$$k_a^2-q^2=\pm k_b^2. \tag{1.23}$$

Using Eq. (1.18) and Eq. (1.19), the angular frequencies of $\omega_\pm(0)$ are expressed as

$$\omega_{+}(0)=\frac{cq}{\sqrt{\varepsilon_{\perp}}}=\frac{cq}{n_{\mathrm{o}}}, \tag{1.24}$$

$$\omega_{-}(0)=\frac{cq}{\sqrt{\varepsilon_{\parallel}}}=\frac{cq}{n_{\mathrm{e}}}, \tag{1.25}$$

where $n_{\mathrm{o}}=\sqrt{\varepsilon_{\perp}}$ and $n_{\mathrm{e}}=\sqrt{\varepsilon_{\parallel}}$ are the ordinary and extra-ordinary refractive indices, respectively. These equations can be rewritten in terms of the wavelength for the sake of convenience,

$$\lambda_{\mathrm{long-edge}}=n_{\mathrm{e}}\times p, \tag{1.26}$$

$$\lambda_{\mathrm{short-edge}}=n_{\mathrm{o}}\times p, \tag{1.27}$$

where $\lambda_{\mathrm{long-edge}}$ and $\lambda_{\mathrm{short-edge}}$ are the long and short band-edge wavelengths of the reflection band, respectively. Therefore, the band-width, $\Delta\lambda$, and the center wavelength of the SR band, λ_{c}, are expressed as

$$\Delta\lambda=\lambda_{\mathrm{long-edge}}-\lambda_{\mathrm{short-edge}}=\Delta n\times p, \tag{1.28}$$

$$\lambda_{\mathrm{c}}=\frac{\lambda_{\mathrm{long-edge}}+\lambda_{\mathrm{short-edge}}}{2}=n_{\mathrm{avg}}\times p, \tag{1.29}$$

where $\Delta n=(n_{\mathrm{e}}-n_{\mathrm{o}})$ and $n_{\mathrm{avg}}=\frac{n_{\mathrm{e}}+n_{\mathrm{o}}}{2}$ are the birefringence and the average refractive index, respectively. Consequentially, circularly polarized light with the same handedness as the helical axis is reflected over the wavelength region between the long and the short band-edge wavelengths.

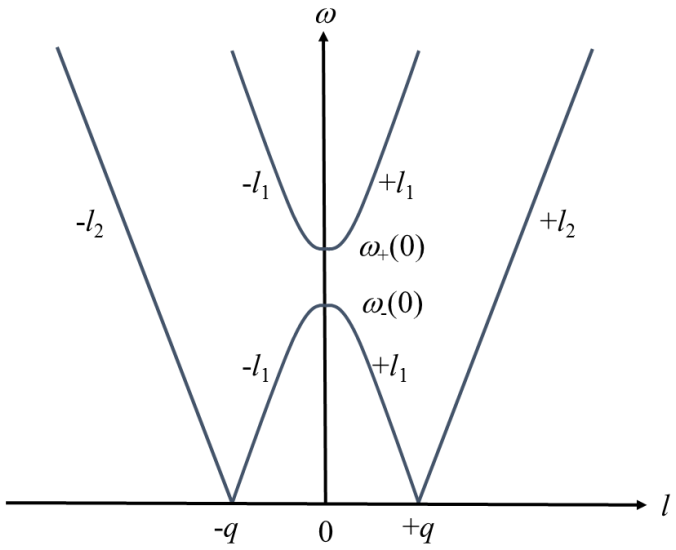

Figure 1.3 Dispersion relation ω versus l.

1.3 Textures of cholesteric liquid crystals

A ChLC sandwiched between two parallel substrates exhibits various textures depending on several parameters, such as an alignment layer and an external field. In this section, we briefly describe typical ChLC textures, which will be discussed later in this dissertation.

The most famous texture of a ChLC is the planar texture. In this case, the helical axis is parallel to the normal of the substrate. Figure 1.4 shows a schematic structure and a reflection polarizing optical micrograph of the planar texture. In some wavelength regions, a circularly polarized light with the same circular handedness as the helix is reflected from the planar texture because of Bragg reflection.

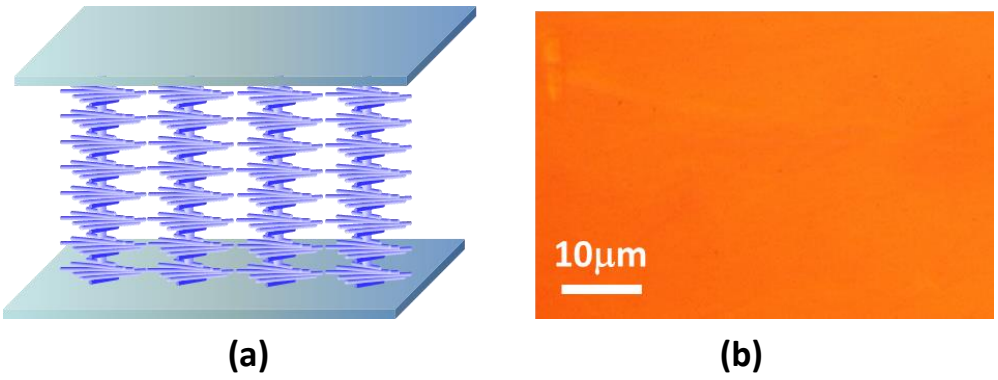

Figure 1.4 (a) Schematic of a planar texture. (b) Polarizing optical micrograph of a planar texture. White light was illuminated onto the cell.

The focal-conic texture is another texture of a ChLC. The focal-conic texture exhibits many different domains, where the helical axis of each domain is randomly oriented with the same pitch length. Due to the randomly oriented helical axis in each domain, this texture exhibits scattering of incident light. The focal-conic texture is typically obtained by applying a medium electric field in the planar texture of a ChLC. The schematic structure and a polarizing optical micrograph of the focal-conic texture are shown in Fig. 1.5.

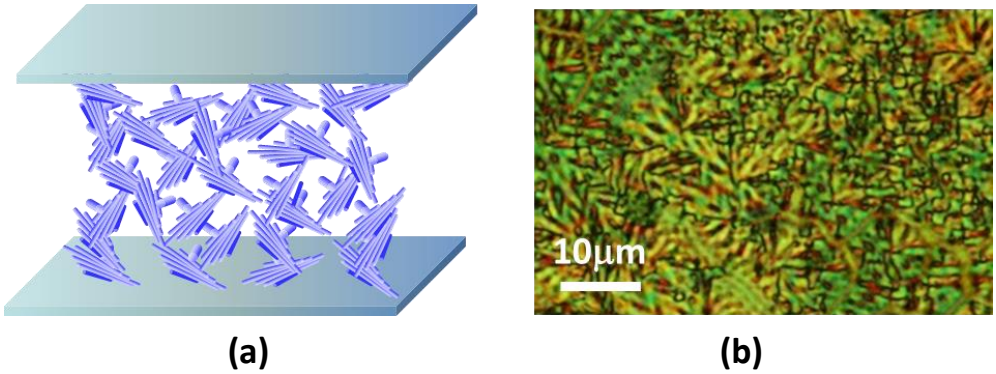

Figure 1.5 (a) Schematic of a focal-conic texture. (b) Polarizing optical micrograph of a focal-conic texture.

When a stronger electric field is applied in a direction perpendicular to the substrate, all the LC molecules are aligned along the electric field after the helix is completely unwound. This state is called as a homeotropic texture, shown in Fig. 1.6(a), and the polarized reflectance from the homeotropic texture becomes zero; this texture corresponds to the dark polarizing optical micrograph shown in Fig. 1.6(b).

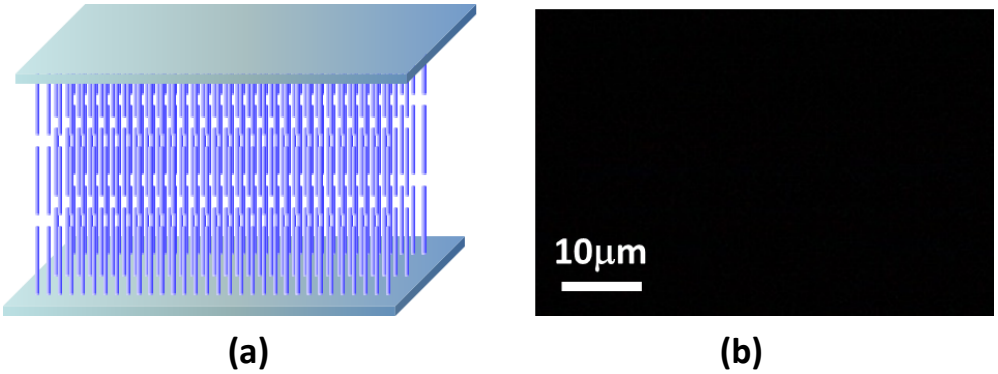

Figure 1.6 (a) Schematic of a homeotropic texture. (b) Polarizing optical micrograph of a homeotropic texture.

As mentioned above, the texture of a ChLC with positive dielectric anisotropy changes as an external electric field is applied normal to the substrate. Suppose that the initial texture of a ChLC is planar. When a medium electric field is applied, the planar texture breaks into a focal-

conic state while maintaining the pitch length. A sufficiently strong electric field is required to accomplish a transition from a focal-conic state to a homeotropic state, since a homeotropic state occurs after unwinding of the helix. The threshold electric field for unwinding of the helix is determined by minimizing the total free energy and is given by [31]

$$E_{\text{th}} = \frac{\pi^2}{p}\sqrt{\frac{K_{22}}{\varepsilon_0 \Delta\varepsilon}}, \tag{1.30}$$

where K_{22} is the twist elastic constant. This relation implies that the shorter the cholesteric helical pitch, the higher the electrical energy required to unwind the helical structure.

In general, the transition of bulk ChLC from a planar texture to a focal-conic texture occurs through two different processes. One is through the appearance of so-called oily streaks, which are bent cholesteric layers, and the other is through the so-called Helfrich deformation, which is an undulation of the helical axis [32]. In this dissertation, the Helfrich state, which will be investigated later, is one of the most important textures in ChLCs. Helfrich deformation is a two-dimensional undulation of the cholesteric layer without destroying the cholesteric layer structure, when an electric field above the Helfrich threshold, E_{H}, is applied to a planar texture in a direction parallel to the helical axis. Figures 1.7(a) and (b) show the schematic structure and a polarizing optical micrograph of the Helfrich deformation, respectively. Textures of two-dimensional square patterns are observed simultaneously everywhere. Theoretically, the Helfrich threshold is inversely proportional to the square root of the helical pitch length and is given by [33]

$$E_{\text{H}} \propto p^{-0.5}. \tag{1.31}$$

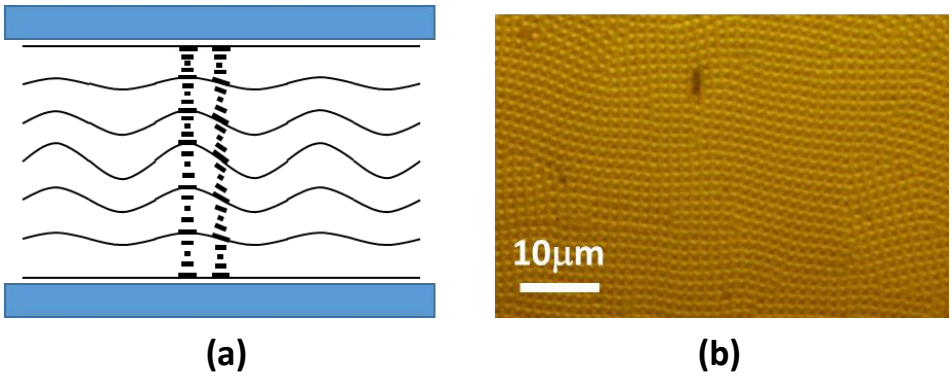

Figure 1.7 (a) Scheme of a Helfrich deformation. (b) Polarizing optical micrograph of a Helfrich deformation.

1.4 Polymer/liquid crystal composite

In general, a rod-like LC is composed of a rigid core consisting of benzene rings and flexible end parts consisting of alkyl groups. When an acrylate group is attached to this flexible end part of the LC molecule, the LC molecule undergoes radical polymerization by UV light irradiation. A cross-linked structure is obtained by successive addition of the mesogenic monomers while maintaining the liquid crystallinity of the materials. An example of the molecular structure of a popular mesogenic monomer with acrylate groups at the end parts is shown in Fig. 1.8.

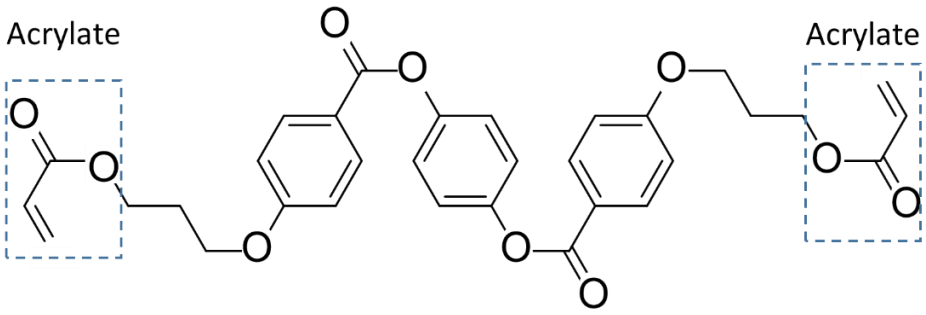

Figure 1.8 Molecular structure of the LC monomer having acrylate groups.

One of the advantages of utilizing materials having the self-organization property of LCs and the cross-linked property of polymers is that it is possible to easily make stable polymer ordered structures since a photo cross-linking reaction occurs at molecular level. For example, a photo cross-linking reaction of mesogenic ChLC with a helical periodic structure is capable of making a polymeric structure having a SR band originating from the helical order. It is very difficult to fabricate polymeric structures having a helical molecular arrangement by conventional chemical synthesis methods [34,35]. However, a polymerization process after aligning the molecules by using cross-linkable LCs [36-43] enables one to easily create a wide variety of ordered structures applicable to optical devices, compared with conventional processes [44-47].

One of the new types of materials for optoelectronic applications is a polymer-dispersed LC [48-55] consisting of micrometer-sized LC droplets that are randomly dispersed in a continuous polymer medium and separated from one another. The method of phase separation in precursor mixtures containing high-molecular-weight polymers and low-molecular-weight LCs is widely used for making polymer-dispersed LCs. When an electric field is applied to the polymer-dispersed LCs, the LC molecules, which are randomly oriented in the field-off state inside the droplets, are reoriented along the electric field. Therefore, owing to the difference in refractive index between LC droplets and the external polymer substance, it is possible to vary the transmittance of light passing through polymer-dispersed LCs. The monomer concentration of

the polymer-dispersed LCs is typically between 20 wt% and 70 wt%. The size of the LC droplets that can be controlled by the monomer concentration decreases with an increase in the monomer concentration.

There is another kind of polymer/LC composites in which a cross-linked polymer with a small amount of monomer concentration (less than 10 wt%) is dispersed in a fluid LC. This composite is called a polymer-stabilized LC [56-59]. Unlike the polymer-dispersed LC, a polymer-stabilized LC is made up of polymer networks that are dispersed in the LC. The voids in the polymer networks are typically on the order of several 100 nm ~ several μm. Interactions between the polymer networks and LCs stabilize the alignment of the LC molecules.

Recently, a new type of polymer/LC composite with nano-sized LC domains has been discovered [24]. This polymer/LC composite is completely different from the usual polymer-dispersed LC and polymer-stabilized LC. This polymer/LC composite consists of nano-sized LC domains (less than 40 nm) dispersed in an anisotropic polymer matrix. The nano-sized LC domains are fabricated by photopolymerizing a mesogenic monomer-LC mixture containing mesogenic monomer (~ 30 wt%). Because of the strong UV light intensity and high miscibility between the mesogenic monomers and the LCs, polymerization-induced phase separation is suppressed, and an anisotropic polymer matrix with nano-sized domains is obtained. The nano-sized domains result in a fast decay time of a few 10 μs; this will be explained in detail in section 1.4.2.

In general, a high monomer concentration of more than 70 wt% in a polymer-dispersed LC could give smaller LC droplets of approximately 100 nm [51]. The smaller LC droplets are thought to be due to the faster polymerization rate during the polymerization-induced phase separation of polymer-dispersed LC. This polymer-dispersed LC exhibits a faster response time of about 100 μs, which is improved by about two or three orders of magnitude compared to that of conventional polymer-dispersed LCs. However, a monomer concentration of more than 70 wt% means that the amount of the LC component decreases to less than 30 wt%, imposing a limit on the tuning range of the refractive index (on the order of 10^{-4}) [51]. In other words, there is a trade-off between the response time and the refractive index tuning range. Moreover, polymer-dispersed LC is optically isotropic since isotropic monomers are used. Consequently, the polymer-dispersed LC is not suitable for application to refractive index tuning devices. In the case of polymer-stabilized LCs, it is also impossible to have nano-sized LC domains, although mesogenic monomers have generally been used in the field of polymer-stabilized LCs. In contrast, a new kind of polymer/LC composite with nano-sized LC domains shows that the improvement in response time is compatible with the improvement in refractive tuning range, since the nano-sized LC domains of size less than 40 nm are attained when the LC component is more than 70 wt%. The fast response time and anisotropy of the polymer/LC nanocomposite

allows us to realize various photonic devices, such as optical amplitude modulators, electro-optic polarization rotators and polarization-independent phase modulators [24,26].

1.4.1 Electro-optic response of the polymer/cholesteric liquid crystal nanocomposites

As discussed in section 1.2, ChLCs are one-dimensional photonic band-gap materials in which the constituent LC molecules self-organize into a helical structure. They exhibit a so-called SR band, in which light with the same circular handedness as the helix is reflected: the SR band spans over the wavelength $n_o \times p - n_e \times p$, where n_e and n_o are the extra-ordinary and ordinary refractive indices and p is the helical pitch. Therefore, the reflection band can be modulated by changing the helical pitch. Control of the helical pitch by external stimuli such as electric field [15], temperature [16], pressure [17] and light irradiation [18,19] has been demonstrated. Among these methods, electric field tuning of the SR band is the best choice for practical use because of its switching speed and compatibility with other electro-optic devices. Some previous reports have demonstrated applications such as displays [11] and lasers [8-10] based on electro-optic switching of the SR band. Conventional ChLCs, however, are difficult to implement into electro-optic devices because the SR band tuning is irreversible and slow.

As shown in Fig. 1.9, the polymer/ChLC nanocomposites, which have nano-sized LC domains, do not follow the properties of the usual bulk ChLCs; under an electric field, only the unpolymerized LC molecules confined in the nano-sized domains are reoriented along the electric field, but the macroscopic helical structure is strongly fixed by the cross-linked polymer matrix. Therefore, the effective extra-ordinary refractive index of the nanocomposite is decreased, while the ordinary refractive index and helical pitch remain constant. Consequently, the polymer/ChLC nanocomposite can achieve the tuning of the SR band by shortening a long band-edge wavelength without affecting the short band-edge wavelength and the SR band shape as shown in Fig. 1.10.

Conventional control of the SR band in ChLCs by varying the helical pitch changes the wavelength of the SR band discretely [16]. When LC molecules are aligned in the sandwich cell, the LC molecules near the interface are fixed along the rubbing direction due to the anchoring of the substrate from the surface. Therefore, a change in the helical pitch in a usual ChLC is allowed only as an integer multiple of the half pitch ($\frac{p}{2}$), leading to a discrete SR band shift. On the other hand, the center wavelength of the SR band in the polymer/ChLC nanocomposites is continuously changing because the polymer/ChLC nanocomposites utilize a refractive index modulation, instead of a variation in the helical pitch. Furthermore, the motion of the LC molecules localized into the nano-sized domains demonstrates a very short decay

time of a few tens of microseconds, which is improved by a factor of 1000 compared to that of the bulk ChLC.

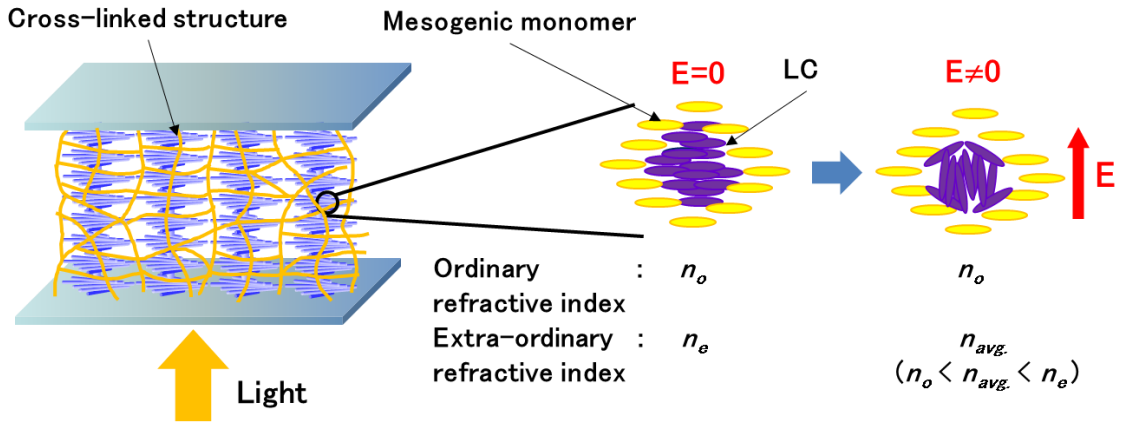

Figure 1.9 Schematic of an electric field response in the polymer/ChLC nanocomposite.

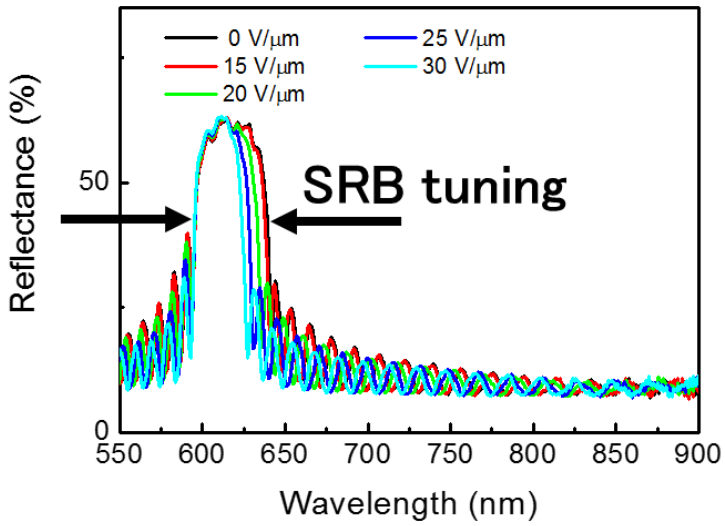

Figure 1.10 Electrical tuning of the SR band in the polymer/ChLC nanocomposite.

1.4.2 Response time of the polymer/liquid crystal nanocomposites

In this section, an interaction between the LC and the electric field is presented. When an electric field is applied to the LC molecules uniformly aligned in the sandwich cell, the LC molecules are reoriented along the electric field. The external field requires a critical value called threshold to change the director configuration gradually from a uniform status. Such a

phenomenon is called the Fredericks transition in which a sufficiently strong external electric field is required to change the director configuration.

For a bulk nematic LC sandwich cell, the rise time τ_r and decay time τ_d are expressed as [30]

$$\tau_r = \frac{\gamma}{\varepsilon_0 \Delta\varepsilon (E^2 - E_{th}^2)}, \tag{1.32}$$

$$\tau_d = \frac{\gamma}{K_{11}} \left(\frac{d}{\pi} \right)^2, \tag{1.33}$$

where γ is a rotational viscosity coefficient, K_{11} is the splay elastic constant, d is the cell gap of the sandwich cell, E and E_{th} are the external electric field and the threshold electric field, respectively. The driving force of the rise response is the electric field, whereas that of the decay response is the elastic restoring force. In other words, it is possible to improve the rise time up to a few tens of microseconds by increasing the strength of the applied electric field [60]. Therefore, the rise response is not too much of a problem in the study of response time. On the other hand, in the case of decay time, all parameters other than the cell gap are intrinsic to the material. It is necessary to increase the elastic constant [61] or decrease the rotational viscosity coefficient [62] in order to improve the decay time. However, since it is very difficult to change the material parameters, in general, the decay time is limited to approximately a few tens of milliseconds [60-63]. Therefore, the decay response is a big issue in the study of response time. From Eq. (1.33), we can reduce the decay time by decreasing the cell gap, which is the only device parameter. Actually, however, there is a limit to which the cell gap can be reduced, since an optimum thickness exists for optical device applications. Therefore, the decay time can be improved by changing the movement of the director locally.

The fast response in polymer/LC nanocomposites is explained by the localized motion of the nematic LC molecules confined in nano-sized domains [64]. The localized motion of the nematic LC molecules can be similarly understood in the case of the bulk nematic LC uniformly oriented in a sandwich cell. A very short decay time of a few tens of microseconds in polymer/LC nanocomposites is thought to originate from the small correlation length of a few tens of nanometers, which corresponds to the diameter of the domains, since the correlation length is much smaller than the usual cell gap of bulk nematic LC.

Chapter 2 Deformation-free switching of polymer-stabilized cholesteric liquid crystals by low-temperature polymerization

2.1 Introduction

The alignment of the conventional ChLC having a positive dielectric anisotropy ($\Delta\varepsilon > 0$) is changed when an electric field is applied along the helical axis, as shown in Fig. 2.1. When the ChLC is injected into a sandwich cell with planar alignment, the planar state, where the helix is normal to the substrate, is obtained. The focal-conic state, where the helix axis is randomly oriented, appears when a weak electric field is applied normal to the substrate. Because of the tilting of the cholesteric helix, the reflection band blue-shifts and the peak reflectance decreases with an increase in the electric field. When a sufficiently high electric field is applied, the homeotropic state, where the helix is completely unwound and the LC molecules are aligned along the electric field, is obtained and therefore the reflection band disappears.

In the focal-conic state, the incident light no longer experiences a periodic modulation in the dielectric constant, and the reflectance significantly decreases and the shape of the reflection spectrum is distorted at the same time. In addition, even if the electric field is removed, a long relaxation time of more than a few minutes is required to return to the original state. Thus, it is not possible to control the reflection band by applying an electric field in a direction along the helical axis of the ChLC having a positive dielectric anisotropy. Therefore, 'polymer-stabilized' ChLC has been investigated intensively to overcome this intrinsic drawback. 'Polymer-stabilized' ChLCs in which polymer networks are dispersed in ChLCs show an improved response time; however, the movement of the polymer network with the LC molecules limits the response time to a few tens of milliseconds [23]. Tuning of the SR band without deforming the macroscopic helical structure in the polymer/ChLC nanocomposites can lead to a tremendous improvement in the electro-optic response time [24,26]. This 'deformation-free' tuning mode is achieved by down-sizing the LC domains in a polymer/ChLC composite to several tens of nanometers such that the LC domains only contribute to the effective refractive index.

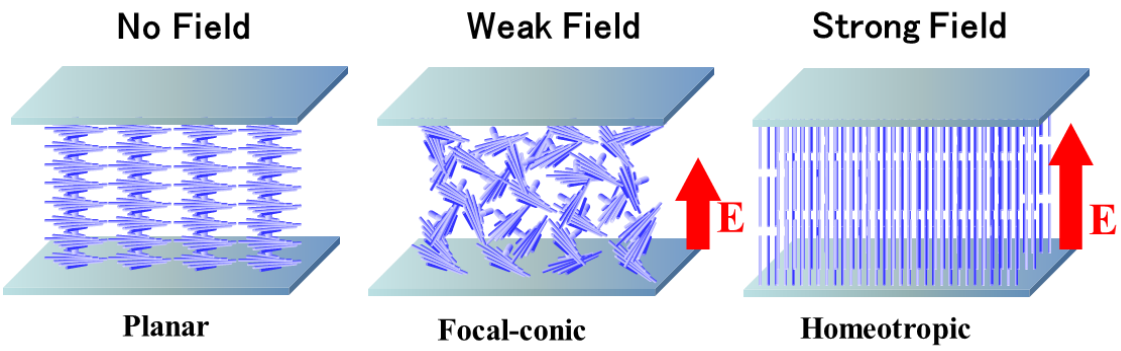

Figure 2.1 The ChLC state with respect to the applied electric field.

The formation of nano-sized LC domains typically requires polymer concentrations of few to several 10 wt% in the sample, which limits the tuning range because of the strong anchoring imposed, in conjunction with the small amount of mobile LCs. There is an urgent need to develop polymer/ChLC nanocomposites with reduced monomer concentrations, and hence larger tuning ranges (or lower driving voltages). In this chapter, the 'deformation-free' switching behavior can be achieved in 'polymer-stabilized' ChLCs with a monomer concentration of 6.6 wt%. On reducing the polymerization temperature, phase separation is suppressed in the composite, leading to the formation of smaller LC domains. As the size of the LC domain decreases from the 100 nm-range to the 10 nm-range, a qualitative change in the electro-optic response occurs, from 'polymer-stabilized' to 'deformation-free'. Not only is the response time improved by this change in electro-optic response, the polymer/ChLC nanocomposite fabricated with a low monomer concentration shows an improved tuning range compared to the nanocomposite fabricated with a high monomer concentration of 13.5 wt%. This is because of the increase in the number of LC molecules contributing to the refractive index tuning.

2.2 Effects of monomer concentration and polymerization temperature on the driving voltage in deformation-free polymer/ChLC nanocomposites

To date, it is thought that a low driving voltage in 'deformation-free' polymer/ChLC nanocomposites can be achieved by either decreasing the monomer concentration or increasing the polymerization temperature [24]. However, we do not know which parameter affects the driving voltage the most. In this section, we show the effects of monomer concentration and polymerization temperature on the driving voltage in 'deformation-free' polymer/ChLC nanocomposites before discussing a qualitative change in electro-optic switching response of 'polymer-stabilized' ChLC. It is expected that the optimization of the parameters can reduce the driving voltage of the polymer/ChLC nanocomposites showing a 'deformation-free' electro-optic response without degradation of other properties.

Firstly, the effect of monomer concentration on electro-optic characteristics in 'deformation-free' polymer/ChLC nanocomposites is briefly described. Details of the materials and experimental procedure used in this section will be presented in the next section of this chapter. The detailed composition of each polymer/ChLC precursor used in this experiment is listed in Table 2.1. All samples were photopolymerized at a temperature of +20 °C in the ChLC phase.

Table 2.1 Composition of the samples used in this section.

Mesogenic monomer (RM257) [wt%]	Nematic LC (MLC-6849-100) [wt%]	Chiral dopant (ZLI-4572) [wt%]	Photoinitiator (Irgacure 819) [wt%]
16.0	78.0	5.0	1.0
25.3	68.1	5.6	1.0
34.6	58.2	6.2	1.0

Figure 2.2 shows the voltage-dependent reflectance of the polymer/ChLC nanocomposites with different monomer concentrations. The horizontal axis shows the wavelength, and the vertical axis shows the applied electric field; the color corresponds to the reflectance in each graph. All samples showed a switching behavior typical of a 'deformation-free' polymer/ChLC nanocomposite; with increasing electric field, only the long band-edge wavelength was blue-shifted without a change in the short band-edge wavelength and peak reflectance. Figure 2.3 shows the dependence of the normalized SR band-width on the monomer concentration for the 'deformation-free' polymer/ChLC nanocomposites. The SR band-width is the full width at half maximum of the reflection spectrum, and the normalized SR band-width is defined as the relative band-width of the SR compared to the zero field. The threshold electric field increases with an increase in the monomer concentration. The higher threshold in high-monomer-concentration polymer/ChLC nanocomposite is thought to be attributed to the stronger anchoring force resulting from the polymer networks. In addition, the slope gradient above the threshold is larger for the lower-monomer-concentration sample. This implies that a more efficient tuning of the refractive index is possible in the lower-monomer-concentration polymer/ChLC nanocomposites, because of the increase in the number of non-photopolymerized LC molecules contributing to the refractive index tuning. The low-monomer-concentration polymer/ChLC nanocomposite exhibits improved electro-optic characteristics, such as lower threshold and higher effective refractive index tuning range.

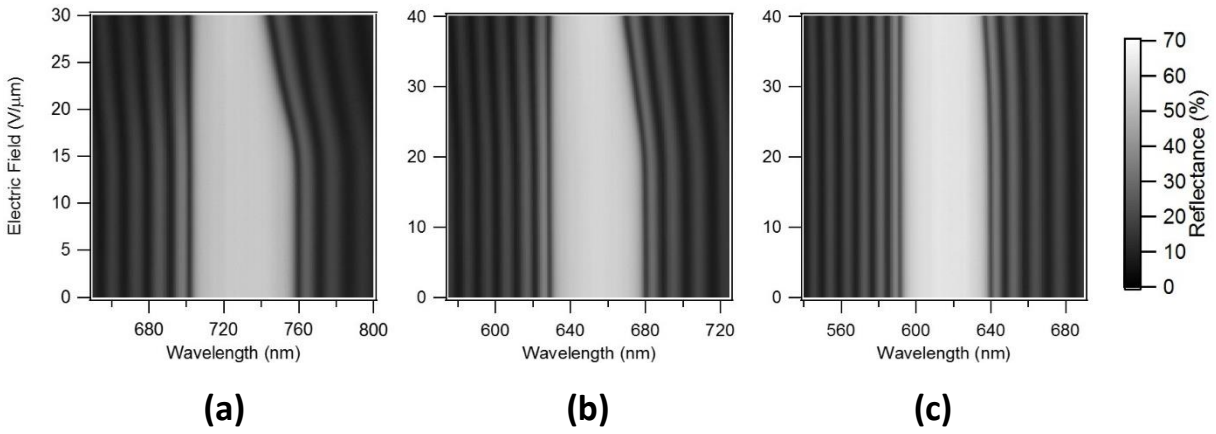

Figure 2.2 Electrical tuning of the SR band in the 'deformation-free' polymer/ChLC nanocomposite with different monomer concentrations (ϕ_{mono}) at a polymerization temperature of +20 °C: (a) ϕ_{mono} = 16.0 wt%, (b) ϕ_{mono} = 25.3 wt%, (c) ϕ_{mono} = 34.6 wt%.

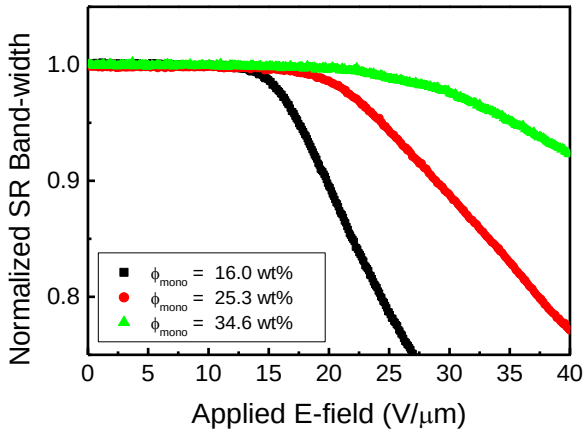

Figure 2.3 Normalized SR band-width with respect to the applied electric field in the 'deformation-free' polymer/ChLC nanocomposites polymerized at +20 °C with different monomer concentrations.

It is also possible to improve the driving voltage of 'deformation-free' polymer/ChLC nanocomposites by changing the polymerization temperature. The samples were fabricated from a polymer/ChLC precursor containing 15.8 wt% of mesogenic monomer, 77.2 wt% of host nematic LC, 6.0 wt% of chiral dopant and 1.0 wt% of photoinitiator. The polymerization temperature was varied from +20 °C to -20 °C at 20 °C intervals. Figure 2.4 shows the voltage-dependent reflectance of the polymer/ChLC nanocomposites with different polymerization temperatures. All the samples exhibited a switching behavior typical of a 'deformation-free'

polymer/ChLC nanocomposite. Figure 2.5 shows the normalized SR band-width with respect to the applied electric field in the 'deformation-free' polymer/ChLC nanocomposites at different polymerization temperatures. The threshold electric field decreases with an increase in the polymerization temperature. From the result of Fig. 2.6, we can attribute a decrease in the threshold electric field of 'deformation-free' polymer/ChLC nanocomposites to an increase in the LC domain size formed in the nanocomposite. The smaller the domain size, the stronger the anchoring force resulting from the polymer network. The effect of polymerization temperature on the domain size will be discussed in detail in section 2.5.

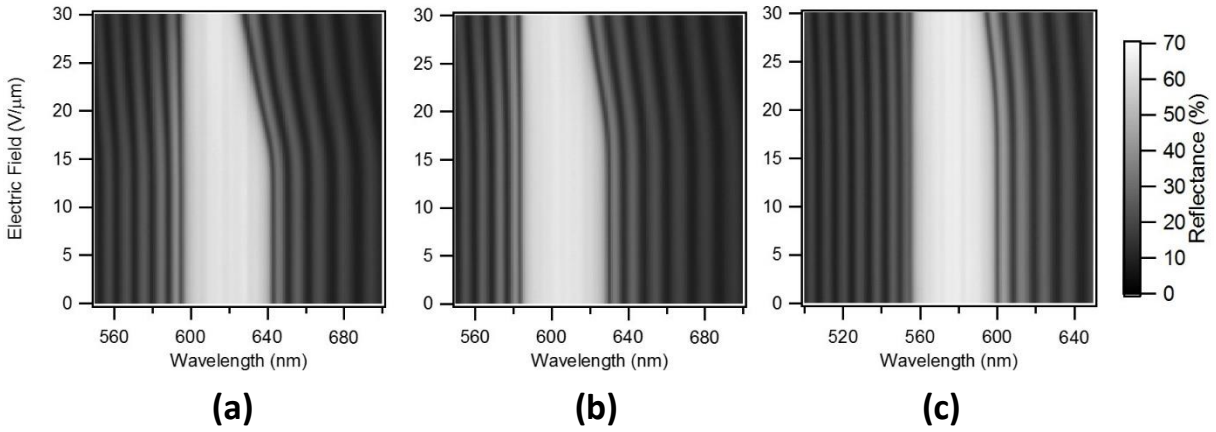

Figure 2.4 Electrical tuning of the SR band in the 'deformation-free' polymer/ChLC nanocomposites with monomer concentration of 15.8 wt% at different polymerization temperatures (T_p): (a) T_p = +20 °C, (b) T_p = 0 °C, (c) T_p = -20 °C.

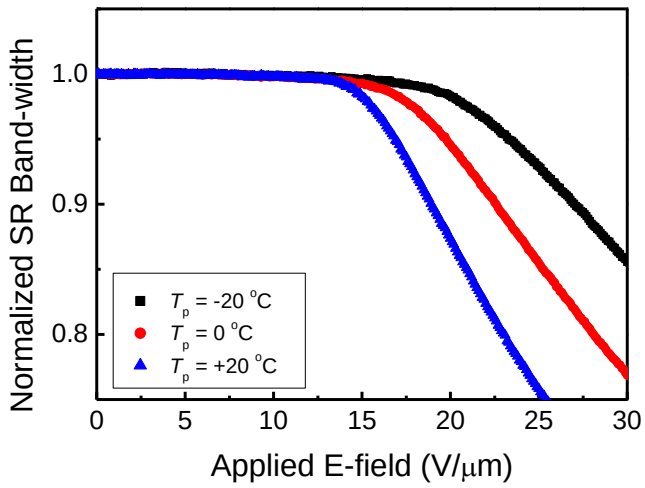

Figure 2.5 Normalized SR band-width with respect to the applied electric field in the 'deformation-free' polymer/ChLC nanocomposites with monomer concentration of 15.8 wt% at different polymerization temperatures.

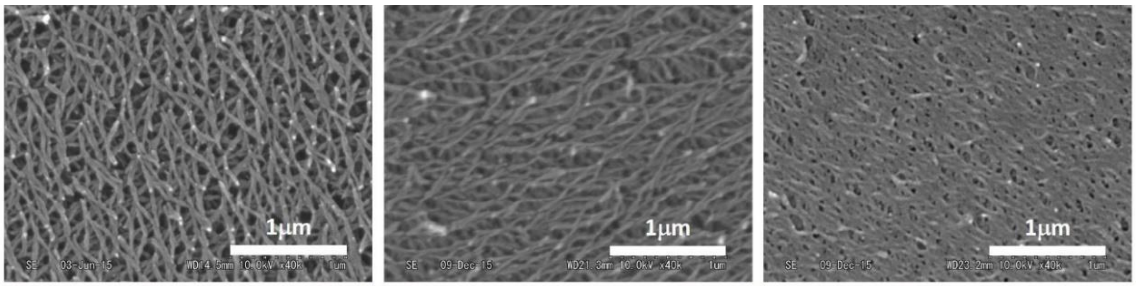

Figure 2.6 Polymerization temperature dependence of the SEM images in the polymer/ChLC nanocomposites with monomer concentration of 15.8 wt%: (a) T_p = +20 °C, (b) T_p = 0°C, (c) T_p = -20 °C.

The threshold electric field can be decreased by both a reduction in the monomer concentration and a rise in the polymerization temperature. However, the polymerization temperature has a smaller influence than the monomer concentration on the slope gradient above the threshold. This is because the number of unpolymerized LC molecules in all the samples used in the experiment of polymerization temperature change is almost the same. Therefore, a reduction in the monomer concentration is a more effective method for increasing the availability of the 'deformation-free' polymer/ChLC nanocomposites by lowering the driving voltage. However, there is a limit for reducing the monomer concentration, since the 'deformation-free' switching behavior requires polymer concentrations of a few to several tens of wt% values, as mentioned earlier. When the monomer concentration of polymer/ChLC composites is less than the minimum amount required for the 'deformation-free' switching mode, the 'polymer-stabilized' switching behavior is observed instead of the 'deformation-free' switching behavior; i.e., a qualitative change in the electro-optic response occurs. In the rest of this chapter, we focus on the effects of both monomer concentration and polymerization temperature on the qualitative change in the electro-optic response of the low-monomer-concentration polymer/ChLC composites from 'polymer-stabilized' to 'deformation-free'.

2.3 Materials and experimental procedure

2.3.1 Materials

In this chapter, the precursor mixtures of mesogenic monomer and ChLC were prepared by mixing four materials, namely, a photopolymerizable LC monomer (Merck, RM257), a nematic LC (Merck, MLC-6849-100), a chiral dopant (Merck, ZLI-4572) and a photoinitiator (Ciba, Irgacure 819). The detailed composition of each sample used in this chapter is listed in Table

2.2. The molecular structures of the mesogenic monomer RM257 and the chiral dopant ZLI-4572 are shown in Fig. 2.7 and Fig. 2.8, respectively. The physical properties of RM257 and MLC-6849-100 are listed in Table 2.3. The materials were dissolved in chloroform and left to evaporate for approximately 3 days.

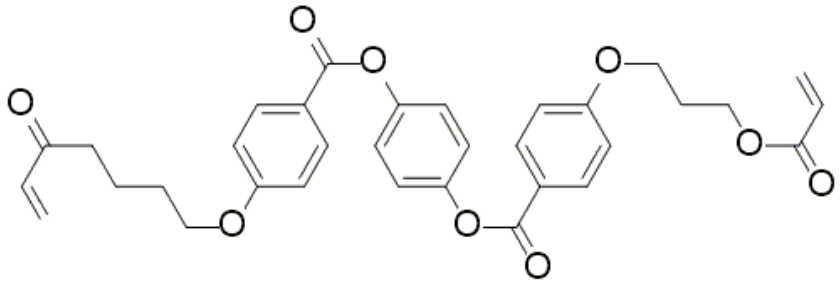

Figure 2.7 Molecular structure of the mesogenic monomer RM257.

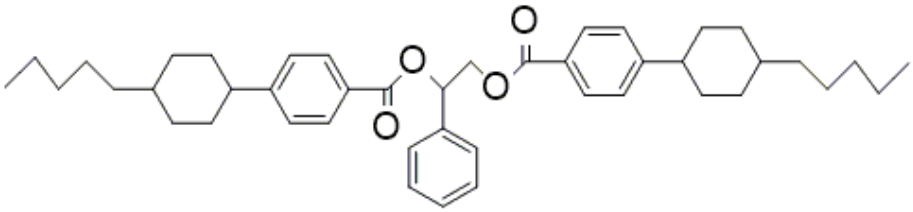

Figure 2.8 Molecular structure of the chiral dopant ZLI-4572.

Table 2.2 Composition of the samples used in this chapter.

Mesogenic monomer (RM257) [wt%]	Nematic LC (MLC-6849-100) [wt%]	Chiral dopant (ZLI-4572) [wt%]	Photoinitiator (Irgacure 819) [wt%]
6.6	87.0	5.4	1.0
8.9	84.5	5.6	1.0
11.2	82.1	5.7	1.0
13.5	79.6	5.9	1.0

Table 2.3 Physical properties of each material used in this study.

Material	Extra-ordinary refractive index (n_e)	Birefringence (Δn)	Dielectric anisotropy ($\Delta\varepsilon$)
RM257	1.687	0.179	-1.5
MLC-6849-100	1.6003	0.1138	11.3

2.3.2 Fabrication of polymer/cholesteric liquid crystal cell

The fabrication process of the polymer/ChLC cell is described in Fig. 2.9. The mixture was injected into an indium-tin-oxide (ITO)-coated planar sandwich cell with a cell-gap of 10 μm (purchased from E. H. C Co.) in the isotropic phase (100 °C). The helical axis of the ChLC was perpendicular to the glass substrate. The sample was cooled to the cholesteric phase, and polymerized by irradiating UV light with a wavelength of 365 nm and a power of 200 mW/cm^2 for 1 hour. The temperature of the sample was controlled by a temperature-controlled stage comprising a pure silver heating/cooling block, used for improved heat transfer, within the sample chamber (Linkam Scientific, LTS420E). Liquid nitrogen used as a coolant was injected into the block, and the recycled nitrogen gas was used for preventing moisture condensation. A platinum resistor was used as a temperature sensor, and the temperature stability of the temperature-controlled stage was less than 0.1 °C.

In general, irradiation of UV light from one side of the sample leads to a variation in polymer morphology along the depth direction of the cell, causing light reflectance to differ depending on the direction of light incidence [40,65,66]. Although the polymer/ChLC composites were fabricated under an asymmetrical irradiation condition, almost the same reflectance spectra were observed regardless of the observation direction, as shown in Fig. 2.10. The similarity between the two reflectance spectra is possibly due to the strong UV light intensity used. This implies that in our sample, the polymer network is more or less homogeneous throughout the sample.

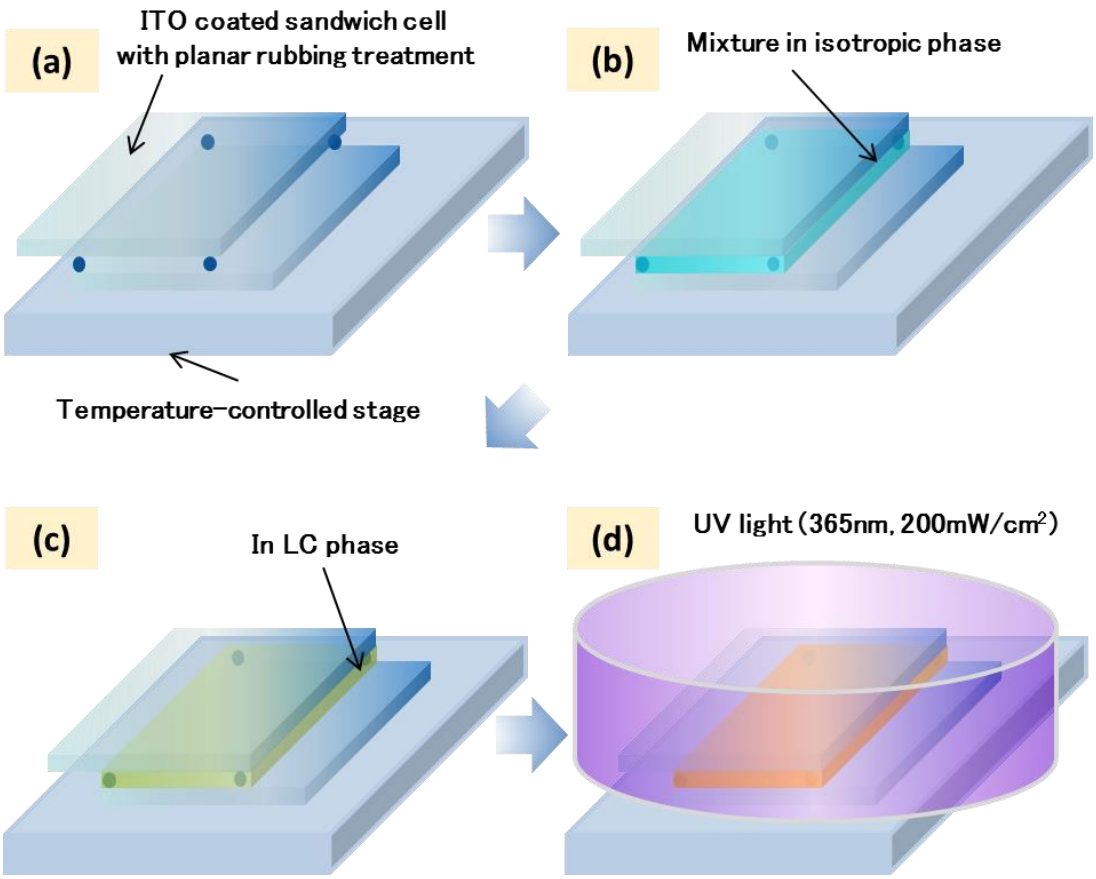

Figure 2.9 Fabrication process of the sample: (a) Preparation of the ITO-coated planar sandwich cell, (b) Injection of the LC materials in the isotropic phase, (c) Temperature cooling into the LC phase, and (d) Photo polymerization process.

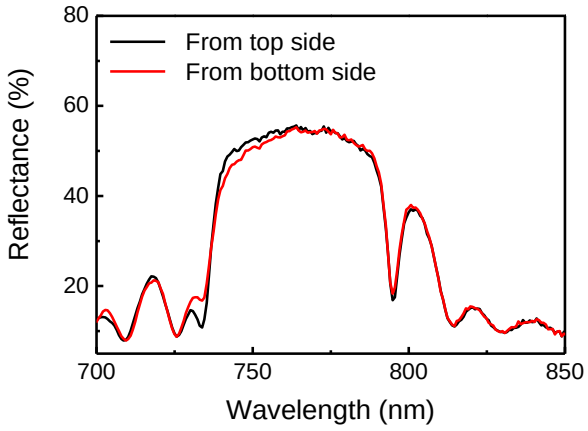

Figure 2.10 Reflectance spectra observed from top and bottom of the sample after curing under an asymmetrical irradiation condition.

2.3.3 Fabrication of samples for measuring polymer morphologies

The polymer morphologies of the polymer/ChLC nanocomposites were observed by field emission scanning electron microscopy (SEM) (Hitachi S-4300). For SEM observation, the cell was opened and rinsed with super-critical CO_2 (Rexxam Co. Ltd., SCRD401) after the polymerization process. Only the unpolymerized LC molecules inside the polymer network were removed without destroying the microstructure in the polymer. Ethanol was used as a washing solvent and super-critical CO_2 was used for drying. A gold thin film was coated on the polymer surface after removing the LC molecules to form a thin layer approximately 10 nm thick.

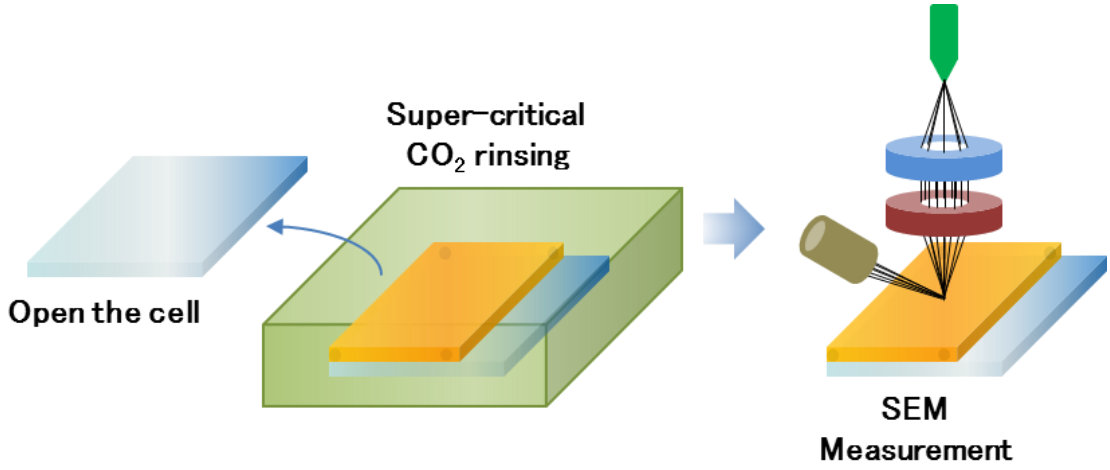

Figure 2.11 Schematic of the process followed for SEM measurements.

2.3.4 Measurement setup of the electro-optic characteristics

A schematic of the experimental setup for measurement of voltage-dependent reflectance and response time is shown in Fig. 2.12. The reflection spectra were measured on a polarizing optical microscope using a fiber-optic spectrometer (Hamamatsu Photonics, PMA-11, fiber diameter of ~ 1 mm) and a 10× objective lens (N.A. 0.3), as a square wave electric field with a frequency of 1 kHz was applied along the helical axis on the cell. The incident direction of the light coincided with the helical axis, and the SR band was observed in a direction normal to the substrate. The fiber-optic spectrometer has a simultaneous measurement wavelength range of 200 nm ~ 950 nm with a spectral resolution of 2 nm. A halogen lamp was used as a wideband light source with a spectral range of 400 nm ~ 900 nm and the incident light was focused onto a spot with diameter of ~ 0.3 mm. The response times were measured under the same conditions but by using a fiber patch cable with a diameter of 200 μm, a photomultiplier tube (Hamamatsu Photonics, H10722-20, spectral response wavelength of 230 nm ~ 920 nm) and a digital

oscilloscope (Tektronix, TDS 3012). The measured response time was the time required for the intensity to change from 10% to 90%.

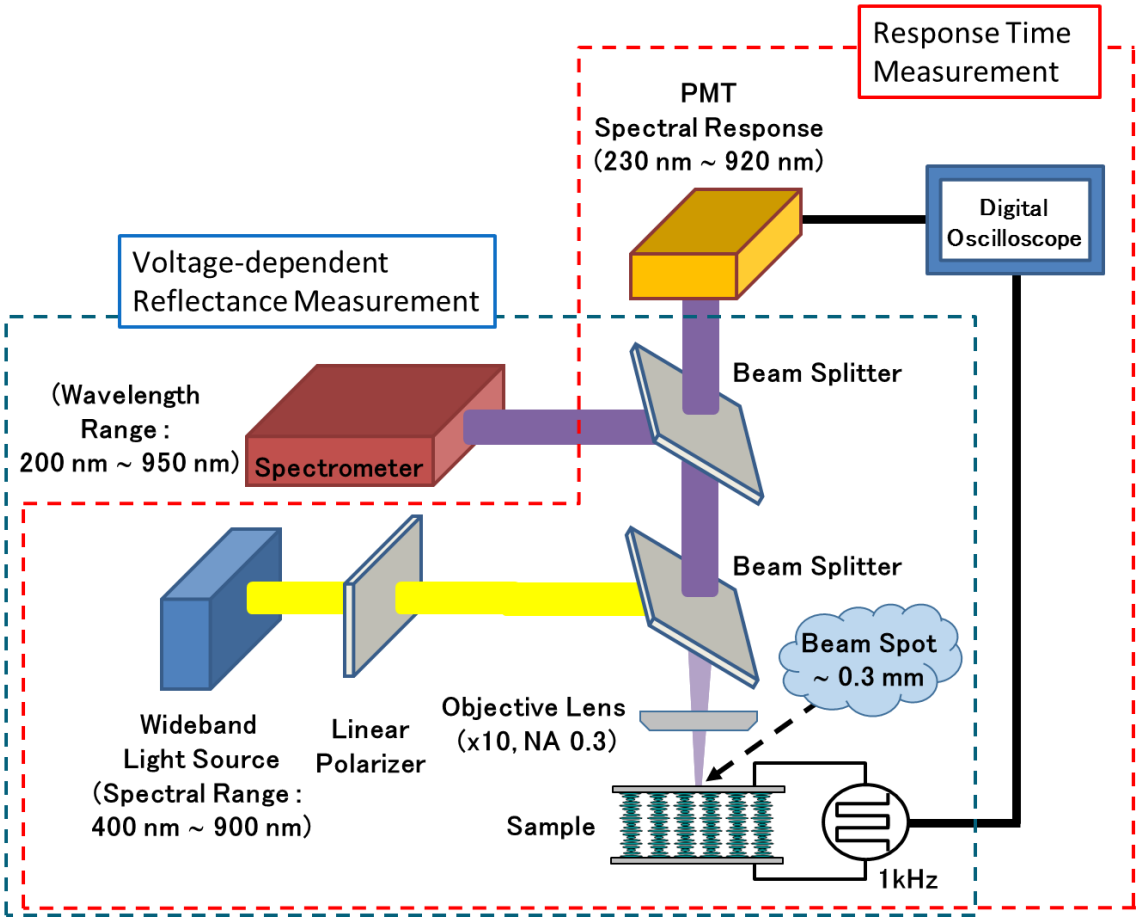

Figure 2.12 Experimental setup for measurement of voltage-dependent reflectance and response time.

2.4 Electro-optic characteristics

We first describe the change in electro-optic responses of polymer/ChLCs with various monomer concentrations. All samples were photopolymerized at a temperature of +20 °C in the ChLC phase. Figure 2.13 shows the voltage-dependent reflectance of the polymer/ChLC nanocomposites with monomer concentrations varying from 6.6 wt% to 13.5 wt%. In the SR band, only half of the unpolarized incident light, which is a circularly polarized light with the same handedness as the helical axis, is reflected from the sample. The nanocomposite with the monomer concentration of 6.6 wt% showed a switching behavior typical of a 'polymer-stabilized' ChLC; with increasing electric field, the reflection band blue-shifted and the peak reflectance decreased, eventually disappearing completely. This is explained by the tilting of

the cholesteric helix before becoming unwound [33]. The 8.9 wt% sample showed a different electro-optic response in that the SR band became narrower without a blue-shift and the peak reflectance also decreased. As the concentration was increased further, the red-shift of the short band-edge wavelength became smaller, and no further shift in the short band-edge wavelength was observed at monomer concentrations of 13.5 wt%. Considering the theoretical band-width of the SR band ($n_e \times p - n_o \times p$), the response of the 13.5 wt% sample indicates a decrease in n_e while p and n_o remain constant; i.e., a 'deformation-free' response is achieved, with the effective refractive index changing without distorting the helical structure.

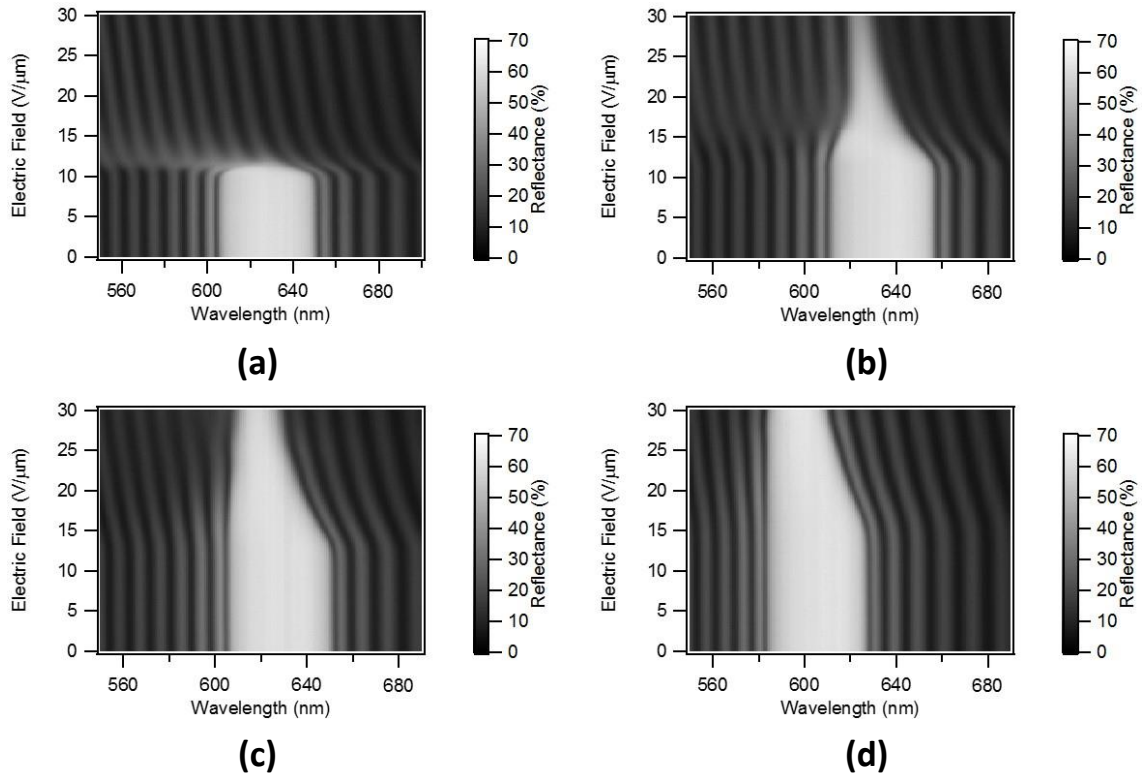

Figure 2.13 Electrical tuning of the SR band in the polymer/ChLC nanocomposites with different monomer concentrations at a polymerization temperature of +20 °C: (a) ϕ_{mono} = 6.6 wt%, (b) ϕ_{mono} = 8.9 wt%, (c) ϕ_{mono} = 11.2 wt%, (d) ϕ_{mono} = 13.5 wt%.

We will now show that a similar control over the electro-optic response can be achieved by modulating the degree of phase separation by changing the polymerization temperature. Figure 2.14 shows the voltage-dependent reflectance data of polymer/ChLC nanocomposites fabricated from a mixture containing 6.6 wt% of mesogenic monomer; the polymerization temperatures were varied between +20 °C and -20 °C in intervals of 10 °C in the ChLC phase. The switching behavior of the polymer/ChLC nanocomposites gradually changes in a similar

manner as for the monomer concentration. Similar to the sample with a high monomer concentration of 13.5 wt%, the nanocomposite at a polymerization temperature of -20 °C also exhibited the 'deformation-free' switching behavior.

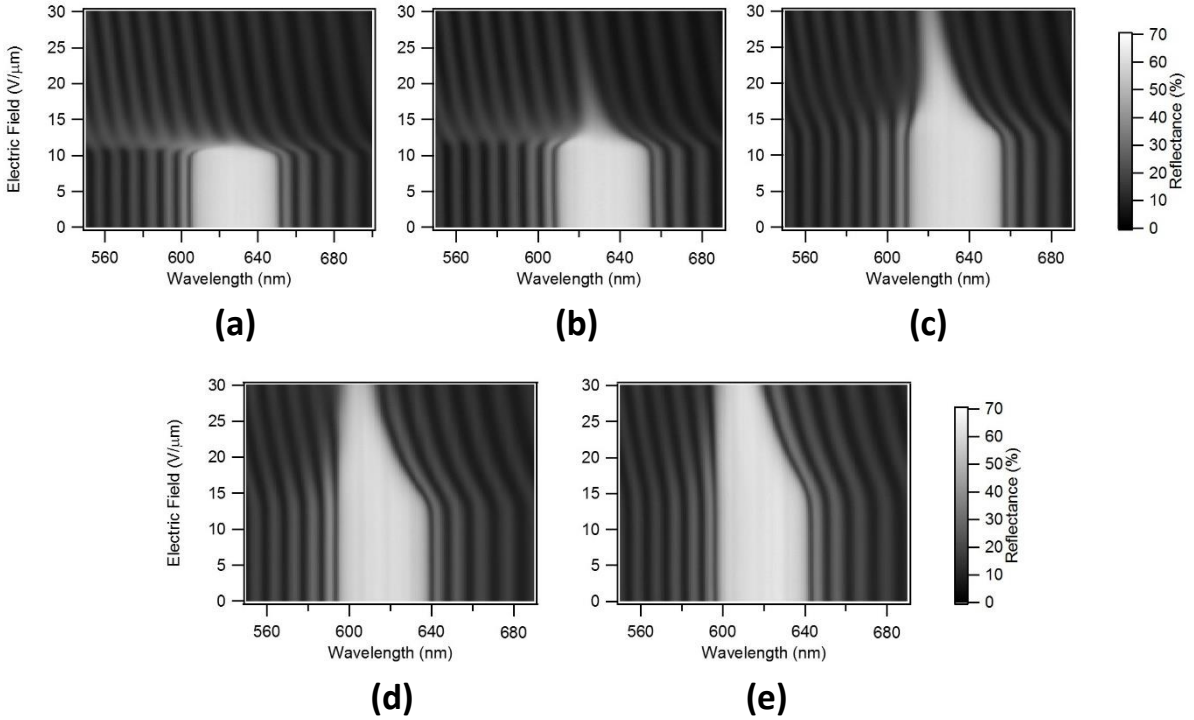

Figure 2.14 Electrical tuning of the SR band in the polymer/ChLC nanocomposites with low monomer concentration of 6.6 wt% at different polymerization temperatures: (a) T_p = +20 °C, (b) T_p = +10 °C, (c) T_p = 0 °C, (d) T_p = -10 °C, (e) T_p = -20 °C.

2.5 Polymer network morphologies

To investigate the mechanism driving the change in electro-optic response, the morphology of the polymer network in each sample was observed by SEM after rinsing out the unpolymerized LC with super-critical CO_2. As shown in Fig. 2.15, the size of the voids, which correspond to the LC domains, is smaller in the samples with lower polymerization temperatures. An analysis of the pores observed in the SEM images of Fig. 2.15 yields average sizes of ~ 297 nm (average over 20 voids), ~ 196 nm (average over 30 voids), ~ 129 nm (average over 30 voids), ~ 67 nm (average over 40 voids), and ~ 38 nm (average over 50 voids) at polymerization temperatures of +20 °C, +10 °C, 0 °C, -10 °C, and -20 °C, respectively. The average pore size is gradually reduced as the temperature decreases. We therefore attribute the change in electro-optic response to the change in LC domain size formed in the composite.

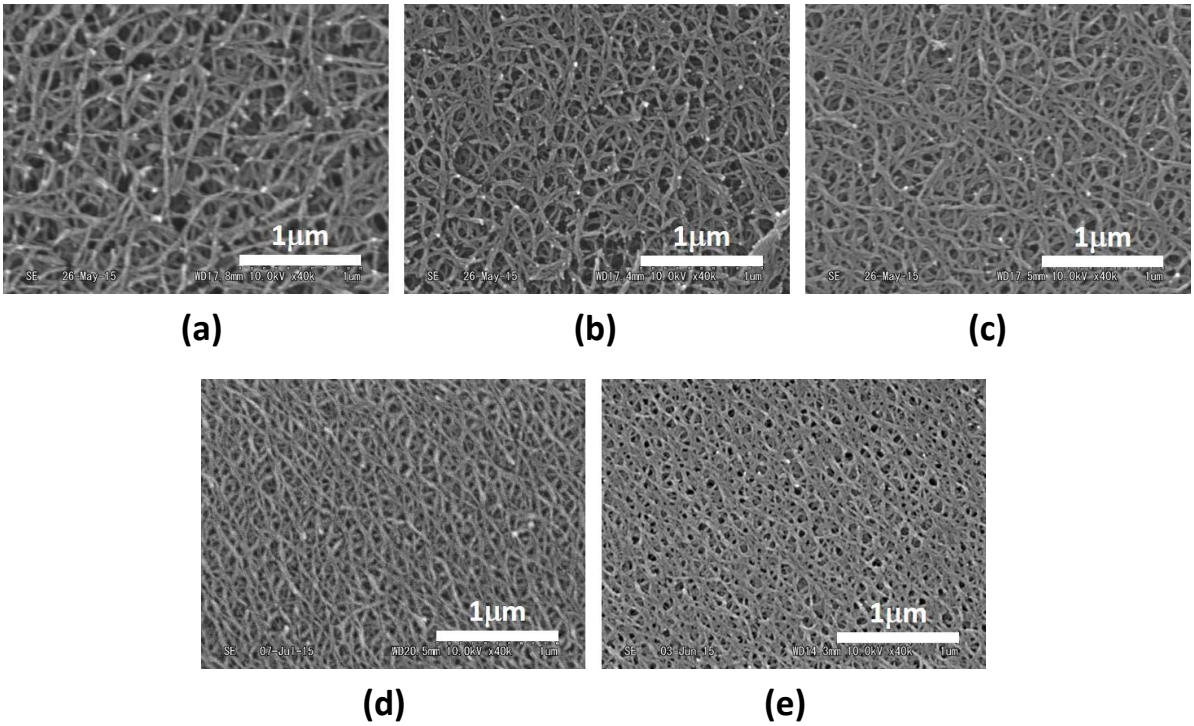

Figure 2.15 Polymerization temperature dependence of the SEM images in the polymer/ChLC nanocomposites with monomer concentration of 6.6 wt%: (a) T_p = +20 °C, (b) T_p = +10 °C, (c) T_p = 0 °C, (d) T_p = -10 °C, (e) T_p = -20 °C.

The driving force leading to the formation of smaller domain sizes is believed to be the increased viscosity at lower temperatures. LCs typically have viscosities that have an approximately Arrhenius-type dependence on the temperature [67,68].

The viscosity, η, following the Andrade's viscosity formula is expressed as

$$\eta = \mathrm{A}\exp\left(\frac{E_a}{k_B T}\right), \tag{2.1}$$

where A is a constant, E_a is the activation energy, k_B is the Boltzmann constant, and T is the absolute temperature. The activation energy is an intrinsic property of the material and does not vary with temperature. In the phase separation forming LC domains, the change in viscosity caused by temperature is considered to affect the size of the LC domains.

Here, we consider how the viscosity affects the formation of LC domains. According to Eq. (2.1), when the temperature reduces, the viscosity increases, thereby reducing the diffusion speed of the molecules. It is believed that when the diffusion speed of the molecules is slower, phase separation is suppressed since phase separation is a phenomenon in which LC molecules and polymers are aggregated to each other. Therefore, the LC domain size is believed to

decrease with an increase of viscosity. Assuming that the size of the LC domains is inversely proportional to viscosity to the power of g, Eq. (2.1) becomes:

$$D \sim \left(\frac{1}{\eta}\right)^{g} = \mathrm{B}\exp\left(-\frac{gE_a}{k_B T}\right), \tag{2.2}$$

where D is the diameter of the LC domain and B is a constant. Figure 2.16 shows the Arrhenius plot of the domain size. In this case, the natural log plot of domain size should yield a straight fitting line. The apparent activation energy gE_a is calculated as ~ 10 kJ/mol from the straight line fit.

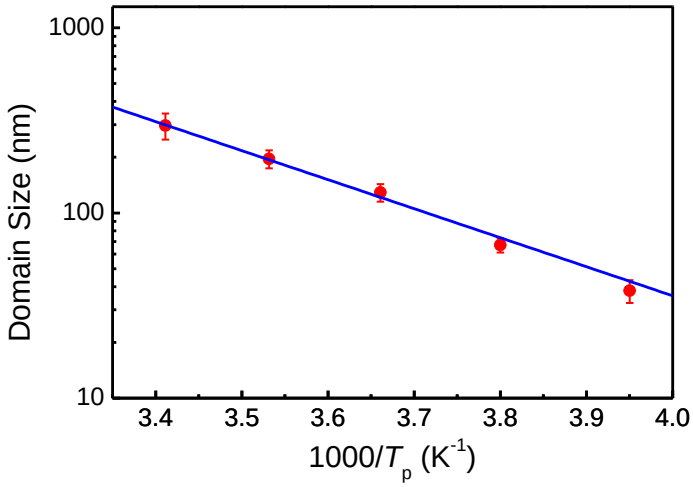

Figure 2.16 Arrhenius plot of the domain size distribution. The blue line is the fitting line.

From the results of this analysis, the reason for the smaller domain size with decreasing polymerization temperature seems to be a large viscosity due to the influence of the temperature dependence. Therefore, phase separation and diffusion of the polymerized monomers become suppressed at low temperatures, leading to smaller LC domains.

Low-temperature polymerization has proven useful in down-sizing the LC domains and improving the electro-optic response time in polymer/nematic LC composites [69]. Here, we have shown that low-temperature polymerization in a polymer/ChLC composite can lead to a qualitative change in the electro-optic response from 'polymer-stabilized' to 'deformation-free'.

Because the 'deformation-free' electro-optic response is caused by a change in the polymer morphology, the same effect can be expected in polymer/ChLC composites in general. However, the monomer concentration at which the 'deformation-free' response occurs would depend on the material parameters, such as viscosity, low temperature stability of the LC phase, reactivity of the polymer, and miscibility of the LC and polymer. In our material system, 6.6 wt% is close to the minimum concentration required to observe the effect, since the sample with 4.3 wt%

monomer concentration did not show the 'deformation-free' response even at a polymerization temperature of -40 °C as shown in Fig. 2.17.

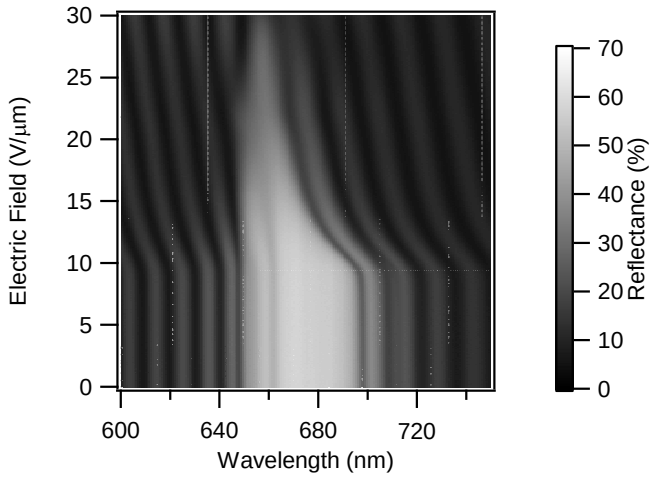

Figure 2.17 Electrical tuning of the SR band in the polymer/ChLC composite with monomer concentration of 4.3 wt% at a polymerization temperature of -40 °C.

2.6 Response time

In this section, we will discuss in detail the polymerization temperature dependence of the decay time in the low-monomer-concentration polymer/ChLC composite, since the rise time of the polymer/ChLC composite has an electric field dependence, rather than a polymerization temperature dependence, and is relatively fast (less than 100 μs) [67].

The reflected intensity of the light incident normally on to the polymer/ChLC composites decreases upon application of an electric field, and returns to its original value upon removal of the field (Fig. 2.13). The decay time was evaluated by measuring the variation in the entire reflected light intensity as an electric field was applied and then removed. Figure 2.18 shows typical transient responses obtained upon removal of a 1 kHz rectangular wave, for samples with different polymerization temperatures. The reflected light intensity of the sample polymerized at +20 °C varied gradually versus time, unlike the other samples. Therefore, the decay time was estimated from the time required for the reflected light intensity to change from 10% to 90% of its maximum value.

As shown in Fig. 2.19, the decay time showed little dependence on the electric field, but a large dependence on the polymerization temperature. The polymer/ChLC composite at a polymerization temperature of +20 °C showed a slow decay response of more than 20 ms. The decay time is faster with a decrease in the polymerization temperature. The polymer/ChLC nanocomposite at a polymerization temperature of -20 °C showed a fast decay time of

approximately 20 μs. The ~ 1000-fold improvement in the decay time was obtained by reducing the polymerization temperature from +20 °C to -20 °C.

This drastic improvement in the decay time is thought to originate from the localized motion of the LC molecules confined in small volumes. The results of the domain size analysis evaluated by SEM images of Fig. 2.15 are considered once again. The helical pitches of all samples used in this study are approximately 450 nm, which is estimated from the SR band-width and refractive index of LC materials. The average domain size in the sample at a polymerization temperature of -20 °C is approximately 38 nm, which is sufficiently smaller than (less than a tenth of) the helical pitch. In the case of smaller LC domains, these nano-sized domains are considered as a medium for controlling the effective refractive index in the polymer/ChLC nanocomposites without affecting the macroscopic helical structure. The fast relaxation response is thought to be attributed to the Fredericks-type reorientation of the unpolymerized LC molecules within small LC domains [64]. As described in section 1.4, the decay time in the polymer/ChLC nanocomposites decreases as the correlation length, which corresponds to the distance between the anchoring walls of the polymer networks, decreases. Therefore, a fast decay time of 20 μs was achieved, when the correlation length was limited to the LC domain size of a few tens of nanometers.

On the other hand, the average domain size in the sample at a polymerization temperature of +20 °C is approximately 297 nm. Moreover, domains having a size over 500 nm (more than the helical pitch) were observed. In such a large LC domain, the relaxation dynamics is thought to be mainly affected by the tilting of the cholesteric helix before becoming unwound. Therefore, a decay response of more than 20 ms was achieved. Under an electric field, the tilting of the helix of the unpolymerized ChLC causes the blue-shift and the reduction in the peak reflectance in the SR band as shown in Fig. 2.14. The reduction in peak reflectance is attributed to light scattering due to the deviation of the helical axis from the planar state. The detailed relaxation dynamics of the sample at polymerization temperatures of both -20 °C and +20 °C will be discussed in chapter 3.

For other samples at polymerization temperatures of +10 °C, 0 °C, and -10 °C, a few small domains follow the fast relaxation dynamics related to the Fredericks-type reorientation of the unpolymerized LC molecules, while the others follow the dynamics of the tilting of the helix of the unpolymerized ChLC, since the size of the each LC domain in a single sample is distributed statistically. Therefore, the decay response in the polymer/ChLC nanocomposites at polymerization temperatures of +10 °C, 0 °C, and -10 °C is thought to be a combination of two different relaxation dynamics. If the number of small domains is large, the motion of the non-reactive LC molecules is mainly governed by the fast relaxation dynamics. The fast decay time was obtained by reducing the polymerization temperature, since the average domain size decreased with a decrease in the polymerization temperature.

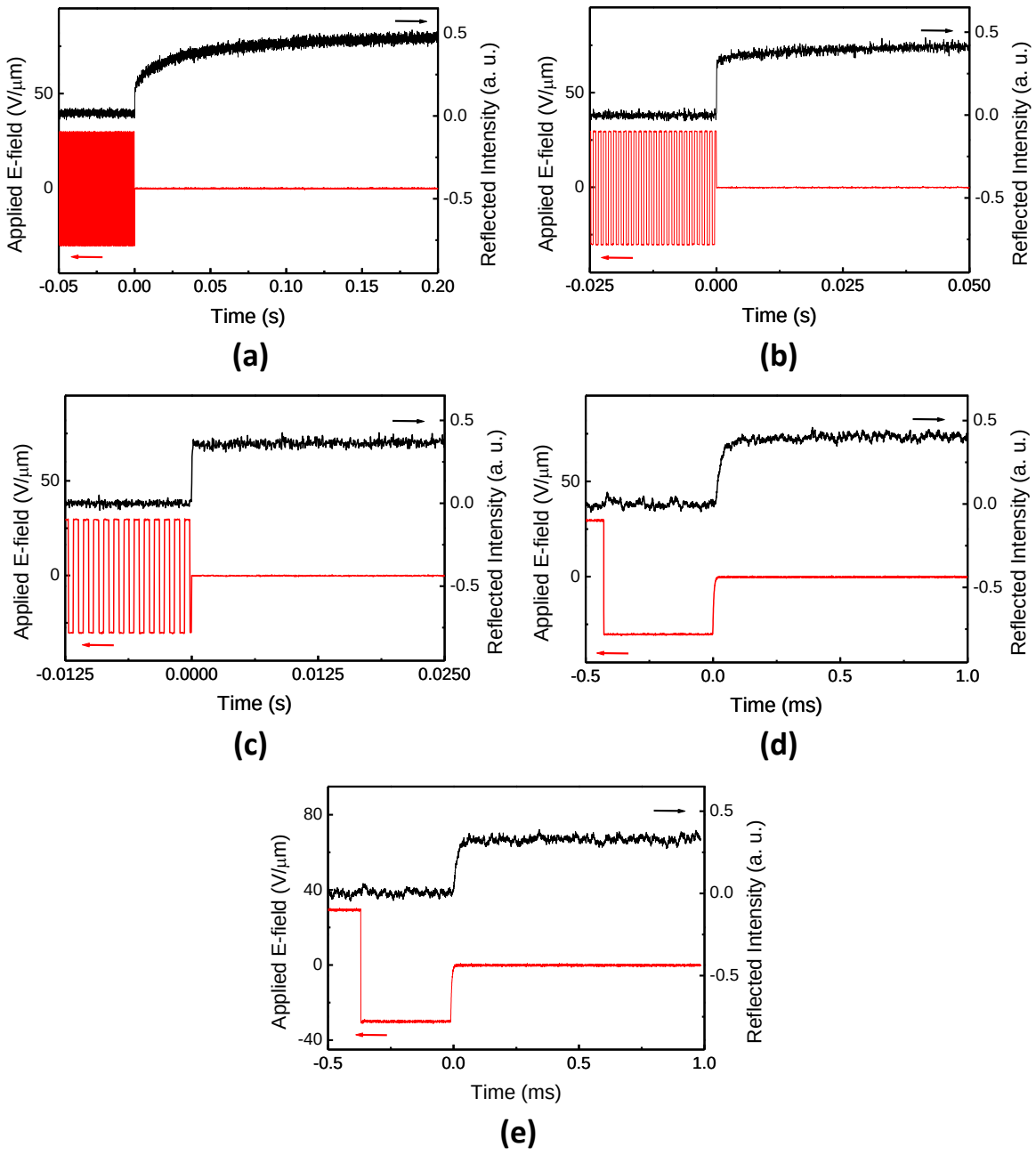

Figure 2.18 Typical transient responses obtained upon removal of a 1 kHz rectangular wave in the polymer/ChLC nanocomposites with low monomer concentration of 6.6 wt% at different polymerization temperatures: (a) T_p = +20 °C, (b) T_p = +10 °C, (c) T_p = 0 °C, (d) T_p = -10 °C, (e) T_p = -20 °C.

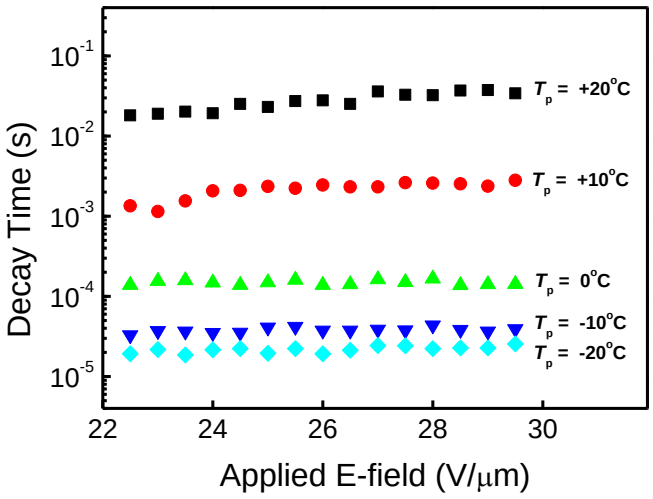

Figure 2.19 Electric field dependence of decay time in the polymer/ChLC nanocomposites with low monomer concentration of 6.6 wt% at different polymerization temperatures.

2.7 Improvement of the electro-optic characteristics due to the low temperature polymerization

Until now, we have discussed the change in electro-optic response mode of the low-monomer-concentration polymer/ChLC nanocomposites. In this section, we verify the improvement in electro-optic characteristics of the low-monomer-concentration polymer/ChLC nanocomposite at a polymerization temperature of -20 °C by comparing to the composite containing a higher monomer concentration of 13.5 wt%. All samples showed a switching behavior typical of a 'deformation-free' ChLC, as shown in Fig. 2.13 and Fig. 2.14. Figure 2.20(a) compares the electro-optic response of the polymer/ChLC nanocomposites fabricated from a high monomer concentration of 13.5 wt% at a polymerization temperature of +20 °C and that fabricated from a low monomer concentration of 6.6 wt% at a polymerization temperature of -20 °C. From Eq. (1.28), the SR band-width, $\Delta\lambda$, is determined by the product of the helical pitch, p, and the anisotropy, Δn, i.e., $\Delta\lambda = \Delta n \times p$. The normalized SR band-width ($\Delta\lambda / \Delta\lambda_0$) is the width of the SR band ($\Delta\lambda$) relative to the width at zero field ($\Delta\lambda_0$) and, because the short band-edge wavelength is immobile in both samples, the normalized SR band-width corresponds to the efficiency in tuning the refractive index ($\Delta n / \Delta n_0$). Figure 2.20(b) depicts the decay time (for the intensity to change from 10% to 90%) for various applied field strengths and shows that comparable response times of about 20 μs are obtained for the two nanocomposites. The decay time for the 'polymer-stabilized' ChLC (ϕ_{mono} = 6.6 wt%, T_{p} = +20

°C) is also presented as a reference, and shows that the change in electro-optic response mode improves the response time by ~ ×1000.

We can draw the following conclusions regarding the electro-optic response. First, the two samples showed similar thresholds around 15 V/μm regardless of the difference in the polymer concentration. This implies that the threshold voltage of the nanocomposite is determined not only by the concentration of the polymer but also by the size of the LC domains in the composite. The fact that comparable decay times were obtained also supports the presence of similar-sized pores in the two nanocomposites. Second, the slope gradient above the threshold improved from 0.0296 to 0.0397 on lowering the monomer concentration, implying a more efficient tuning of the refractive index. The normalized SR band-width ($\Delta\lambda / \Delta\lambda_0$) changes from 0.583 to 0.494 when an electric field of 30 V/μm is applied. This can likely be attributed to the increased number of LC molecules that can contribute to the refractive index in the low-monomer-concentration sample. In order to obtain the normalized SR band-width of 0.6, the high- and low-monomer-concentration samples require an electric field intensity of 29.2 V/μm and 25.5 V/μm, respectively. In other words, the required electric field is decreased by 12.7%. Since the field required to drive the tuning of the refractive index by a given amount is determined both by the threshold and slope gradient, low-temperature polymerization leads to polymer/ChLC nanocomposites with improved properties, i.e., comparable response times but with reduced driving voltage, making them more practical for real-life applications.

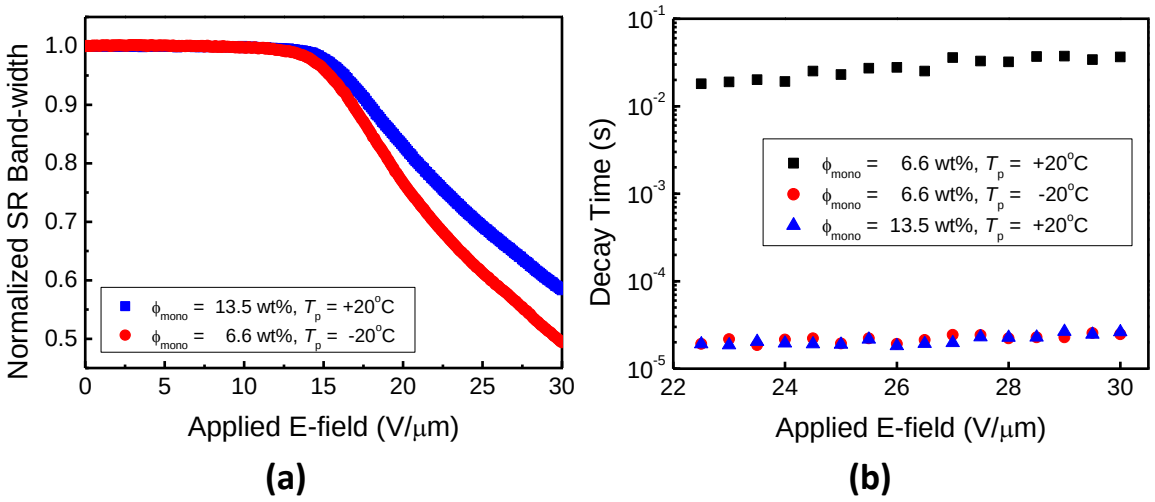

Figure 2.20 Electro-optic characteristics of the polymer/ChLC nanocomposites showing 'deformation-free' electro-optic switching mode with high monomer concentration of 13.5 wt% and low monomer concentration of 6.6 wt% at each polymerization temperatures. (a) Electric field dependence of the normalized SR band-width. (b) Electric field dependence of decay time.

2.8 Summary

To conclude, we showed that polymer/ChLC nanocomposites showing the 'deformation-free' electro-optic response can be prepared in a sample containing only 6.6 wt% of monomer, by controlling the degree of polymerization-induced phase separation through polymerization temperature control. The appearance of the 'deformation-free' switching mode is determined by the size of the LC domains dispersed in an anisotropic polymer matrix. The low monomer concentration samples can reduce the driving voltage by increasing the number of the LC molecules in response to an external electric field. The low-temperature polymerization procedure is a step towards realizing polymer/ChLC composites with practical driving voltages.

Chapter 3 Helical pitch dependence of the electro-optic characteristics in polymer/cholesteric liquid crystal nanocomposites having ultra-small liquid crystal domains

3.1 Introduction

The fabrication of polymer/ChLC composites by *in-situ* polymerization of a mesogenic monomer and ChLC has been proven to be effective in improving the response time of ChLCs. Depending on the size of pores in the composite, polymer/ChLC composites show two response modes: 'polymer-stabilized' response, in which the reflection band blue-shifts and the peak reflectance decreases with an increase in the electric field [23], and 'deformation-free' response, in which only the long band-edge wavelength blue-shifts [24]. The 'deformation-free' mode appears in composites with nano-sized LC domains. Consequently, the 'deformation-free' polymer/ChLC nanocomposites show a faster response time on the order of 10 μs. The 'deformation-free' mode enables new functionalities to be achieved for the nanocomposites, such as tunable optical rotation and phase modulation [24,26]. An important parameter for ChLC-based devices is their pitch, as it determines the spectral position of the SR band, and hence in most cases, the operating wavelength. However, the dependence of the electro-optic performance on the helical pitch in the polymer/ChLC composites has not yet been clarified. Gaining insight into the characteristics of polymer/ChLC composites is important for the future development of devices based on these materials.

In this chapter, different types of helical pitch dependence of the threshold electric field for polymer/ChLC nanocomposites showing 'polymer-stabilized' and 'deformation-free' responses are investigated. As described in chapter 2, two different electro-optic response modes appear in the same polymer/ChLC precursor due to change in the polymerization temperature [27]. Four polymer/ChLC precursors with different helical pitches were prepared, and polymerized in the ChLC phase at either +20 °C or -20 °C to fabricate composites showing the 'polymer-stabilized' and 'deformation-free' responses, respectively. Both samples showed a decrease in the threshold electric field with increasing pitch; however, with regard to the electro-optic response modes, the dependences were different, with the 'deformation-free' samples displaying lesser dependence. The helical pitch dependence of the 'polymer-stabilized' nanocomposites is explained by the tilting of the helix, or Helfrich deformation. On the other hand, the helical pitch dependence of the low-temperature-polymerized nanocomposites is attributed to the Fredericks-transition-like response of the LC molecules confined in nano-sized LC domains.

3.2 Materials and experimental procedure

3.2.1 Materials and fabrication process

Four kinds of mesogenic monomer/ChLC mixtures with different chiral dopant concentrations were used in this chapter. The materials for preparing the mesogenic monomer/ChLC mixtures are the same as those used in chapter 2. Detailed composition of each sample used in this chapter is listed in Table 3.1. The relative weight ratio of RM257 and MLC-6849-100 was fixed, while the concentration of ZLI-4572 was varied between 4.4 wt% and 7.4 wt% in 1 wt% steps to clarify the helical pitch dependence of the threshold electric field in the polymer/ChLC nanocomposites. The materials were dissolved in chloroform and left to evaporate for approximately 3 days.

The fabrication process of the samples for investigating the electro-optic characteristics and polymer morphologies is the same as that used in chapter 2. The polymerization temperature of the samples was either +20 °C or -20 °C.

Table 3.1 Composition of the samples used in this chapter.

Mesogenic monomer (RM257) [wt%]	Nematic LC (MLC-6849-100) [wt%]	Chiral dopant (ZLI-4572) [wt%]	Photoinitiator (Irgacure 819) [wt%]
6.67	87.93	4.40	1.00
6.60	87.00	5.40	1.00
6.53	86.07	6.40	1.00
6.46	85.14	7.40	1.00

3.2.2 Measurement of the helical pitch

In a conventional ChLC system, the helical pitch, p, follows Eq. (3.1) [70]

$$p = \frac{1}{c \times HTP}, \tag{3.1}$$

where c is the concentration of the chiral dopant and HTP is the helical twisting power of it. From Eq. (3.1), the helical pitch is inversely proportional to the chiral dopant concentration. In other words, it is possible to control the helical pitch by changing the chiral dopant concentration.

There are many methods to determine the helical pitch. In this dissertation, the Grandjean-Cano wedge method was used for determining the helical pitches of the samples [71]. Figure 3.1(a) shows a schematic illustration of the Grandjean-Cano wedge method. The wedge angle is expressed by $\tan^{-1}\left(\frac{d_2 - d_1}{L_2}\right)$. When two polished substrates are used, the number of turns enabled for the helical structure must be quantized so that the thickness of the cell is an integral multiple of the half-pitch, $p/2$, due to the anchoring between the LC molecules and the substrates of the wedge cell. The ChLC inside the wedge cell is separated by domains as shown in Fig. 3.1(b), since the number of half-turns is different in each domain. The disclination lines appear when the local cell gap of the wedge cell is different. Therefore, the helical pitch is related to the distance between the disclination lines, L_1, and the wedge angle by

$$p = 2L_1 \times \frac{d_2 - d_1}{L_2}. \tag{3.2}$$

For making a wedge cell, two glass substrates with planar alignment, prepared by rubbing a polyimide-coated glass substrate, were assembled with an angle. A polyimide film (AL1254, JSR) was coated onto the surface of the glass substrates by spin coating method. A wedge angle of ~ 0.04° was obtained by using two other spacers having thickness of 3 μm and 6 μm.

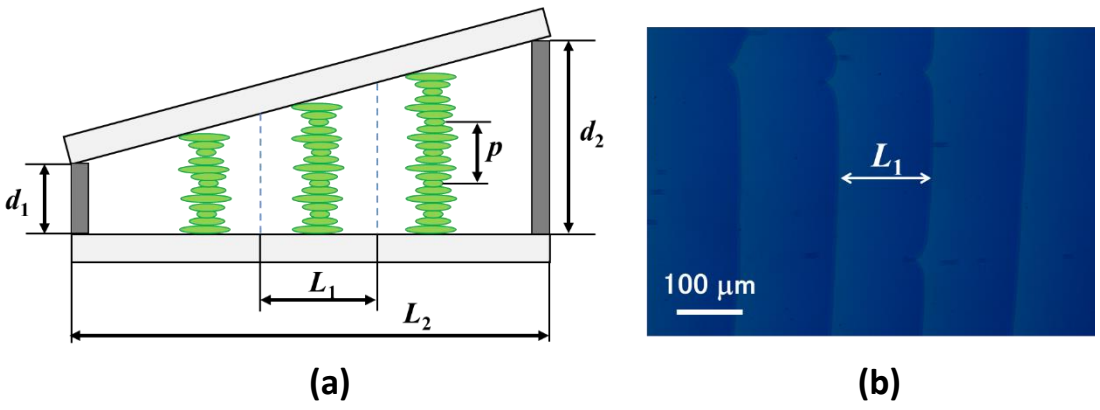

Figure 3.1 (a) Schematic illustration of the Grandjean-Cano wedge method. (b) Typical micrograph of a Grandjean-Cano wedge cell filled with polymer/ChLC.

3.3 Electro-optic characteristics

To discuss the helical pitch dependence of the threshold electric field, we first show the chiral dopant concentration dependence of the helical pitch. Figure 3.2 shows the dependence of the helical pitch on the chiral dopant concentration in samples polymerized at the

temperatures of +20 °C and -20 °C. The helical pitch lengths of the samples polymerized at the temperatures of +20 °C and -20 °C varied between 340 nm and 550 nm. As shown in Fig. 3.2, the helical pitch of the samples polymerized at both the temperatures of +20 °C and -20 °C decreases as the chiral dopant concentration increases.

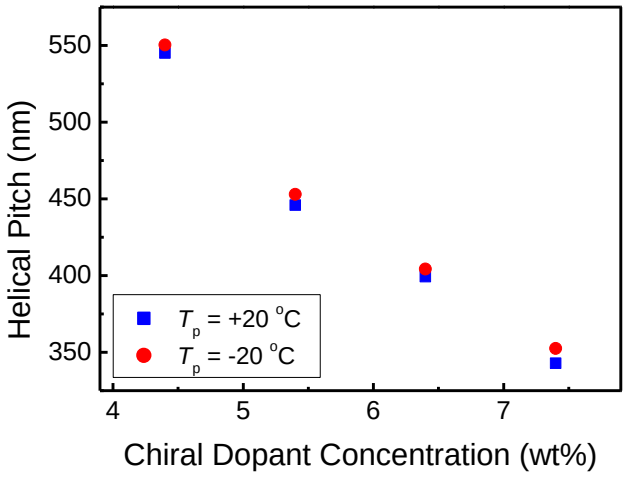

Figure 3.2 Dependence of the helical pitch on the chiral dopant concentration in samples with polymerization temperature of +20 °C and -20 °C.

The electric-field-dependent reflectance spectra of the polymer/ChLC composites polymerized at +20°C are shown in Fig. 3.3. All nanocomposites showed a switching behavior typical of a 'polymer-stabilized' ChLC; with increasing electric field, the reflection band broadened and the peak reflectance decreased. This is explained by the tilting of the cholesteric helix. In general, the transition of pure ChLC from the planar to the focal-conic state occurs through two different processes. One is through the appearance of the oily streaks, which are bent cholesteric layers and the other is through the Helfrich deformation, which is an undulation of the helical axis [32]. In the case of 'polymer-stabilized' ChLC, the nucleation of the oily streaks is suppressed by the polymer network [72]. Therefore, the electro-optic response of the polymer/ChLC composites polymerized at +20 °C is thought to be mainly affected by the Helfrich deformation.

Theoretically, the Helfrich threshold, E_H, for the transition from the planar to the Helfrich state in a bulk ChLC, is inversely proportional to the square root of the helical pitch length, p ($E_H \propto p^{-0.5}$) [33]. To determine the threshold electric field to tilt the helix in the polymer/ChLC nanocomposites polymerized at +20 °C, we plot the electric field dependence of the normalized peak reflectance of the SR band (Fig. 3.4(a)) and determine the electric field at which the normalized peak reflectance begins to decline; this corresponds to the cholesteric layers becoming undulated. The threshold electric field, E_{th}, is determined by fitting the data below

and above threshold with a line function and taking the point of intersection. As shown in Fig. 3.4(b), the threshold electric field increases with decreasing pitch in the 'polymer-stabilized' ChLCs. An analysis of the data using a power law equation $E_{th} = Ap^{-\beta}$ yields a best fit for β = 0.57, which is close to the predicted value from Helfrich threshold. The results therefore suggest that the response of the 'polymer-stabilized' ChLCs is dominated by the Helfrich deformation of the helix.

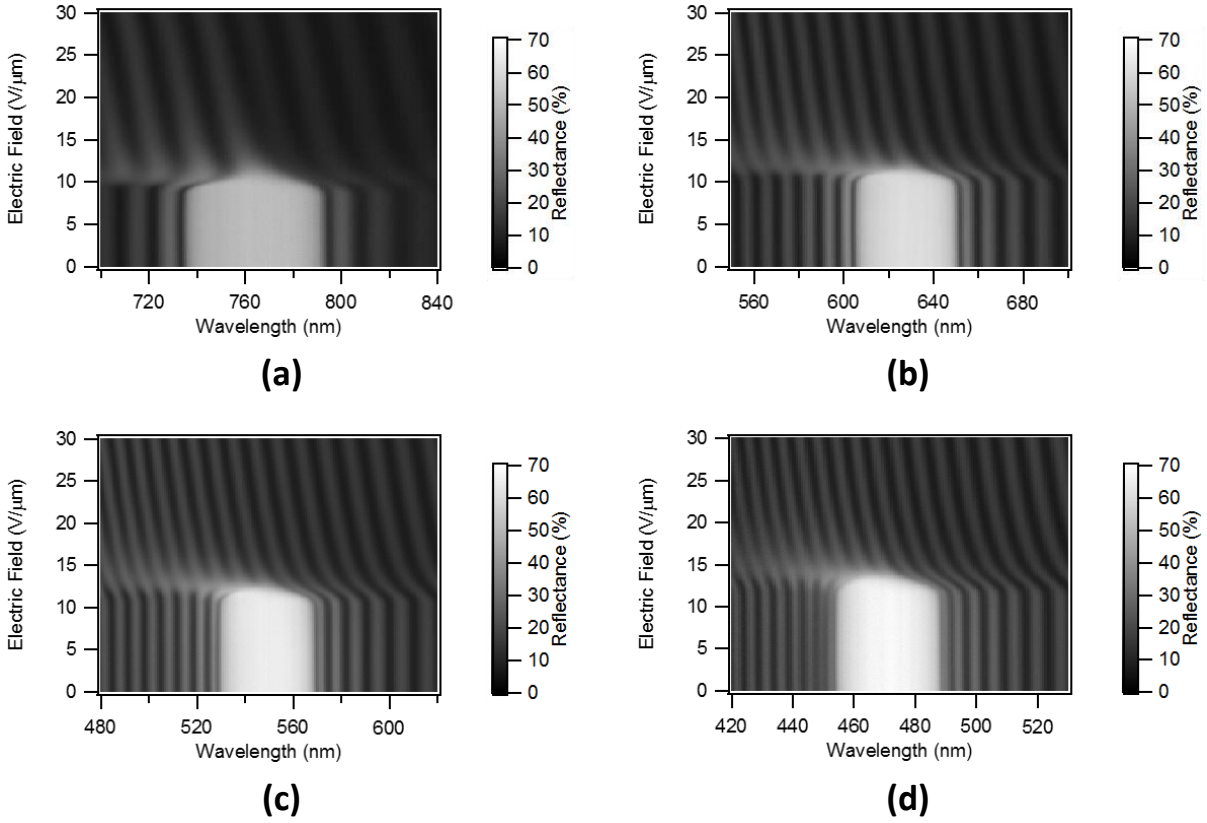

Figure 3.3 Electrical tuning of the SR band in the polymer/ChLC nanocomposites with different chiral dopant concentrations (ϕ_{chiral}) at a polymerization temperature of +20 °C: (a) ϕ_{chiral} = 4.4 wt%, (b) ϕ_{chiral} = 5.4 wt%, (c) ϕ_{chiral} = 6.4 wt%, (d) ϕ_{chiral} = 7.4 wt%.

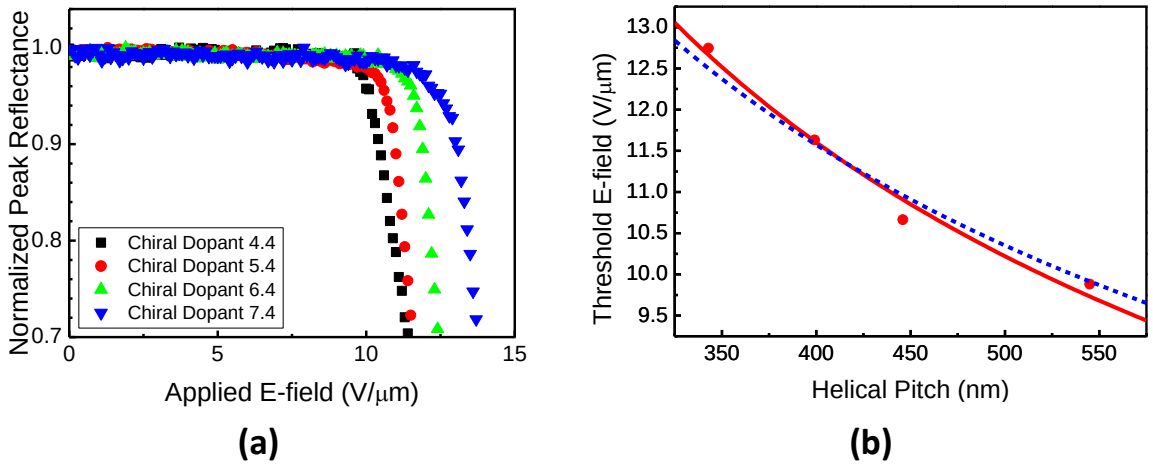

Figure 3.4 Dependence of the electro-optic switching on the helical pitch in the polymer/ChLC nanocomposites polymerized at +20 °C. (a) Normalized peak reflectance with respect to the applied electric field at different chiral dopant concentrations. (b) Helical pitch dependence of the threshold electric field. The red solid circles represent the measured data points and the red curve is the fitting curve. The blue dotted curve is the fitting curve for β = 0.5.

Figure 3.5 shows the electro-optic response of the nanocomposites polymerized at -20 °C, and Fig. 3.6 shows the electric field dependence of the SR band position. The 'deformation-free' response is observed, where only the long band-edge wavelength blue-shifts without showing a reduction in reflectance. Figure 3.7(a) shows the electric-field dependence of the normalized SR band-width on the helical pitch for the 'deformation-free' polymer/ChLC nanocomposites. The normalized SR band-width is defined as the relative band-width of the SR band compared to the band-width at zero field, and the threshold electric field is evaluated from the intersection point of the two line functions describing the response below and above the threshold. Similar to the 'polymer-stabilized' samples, the threshold decreases with an increase in the helical pitch; however, a fit with the power function yields a smaller value for the exponent β of approximately 0.33 (Fig. 3.7(b)). The smaller value compared to that predicted from the Helfrich model implies that unlike the 'polymer-stabilized' samples, the electro-optic response in the 'deformation-free' polymer/ChLC nanocomposites is not dominated by the tilting of the helix. In the following sections, we will study the textures and the polymer network morphologies of the polymer/ChLC composites with different chiral dopant concentrations in order to unveil the driving mechanism governing the 'deformation-free' electro-optic response.

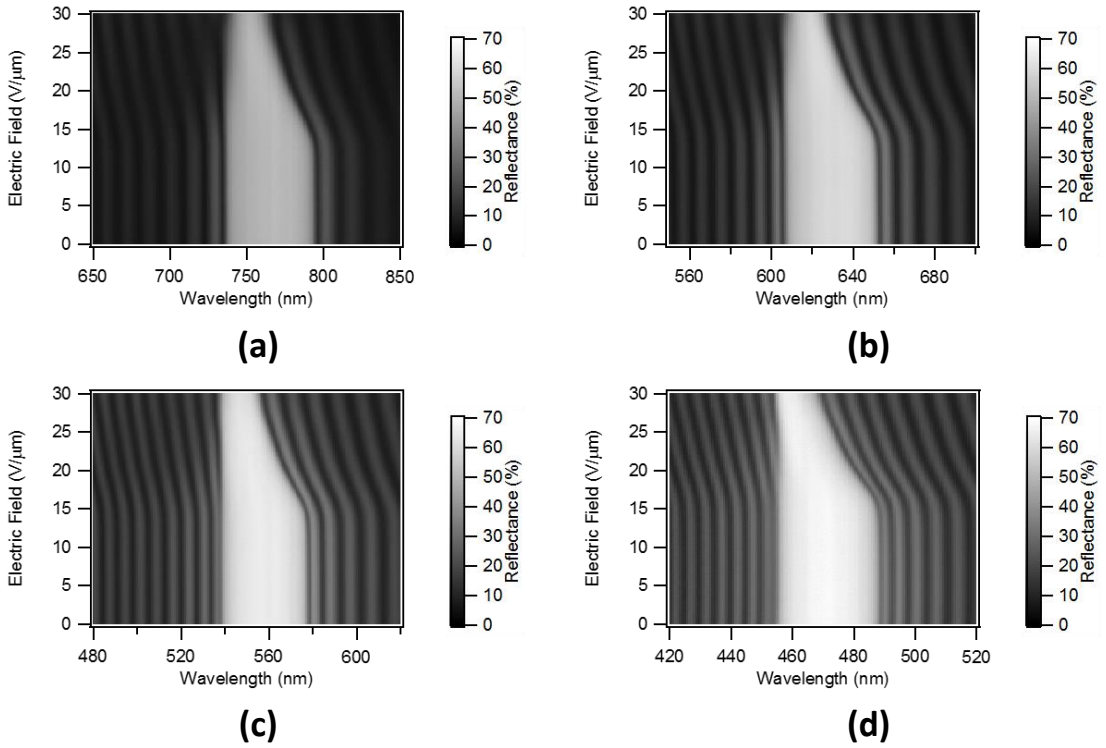

Figure 3.5 Electrical tuning of the SR band in the polymer/ChLC nanocomposites with different chiral dopant concentrations at a polymerization temperature of -20 °C: (a) ϕ_{chiral} = 4.4 wt%, (b) ϕ_{chiral} = 5.4 wt%, (c) ϕ_{chiral} = 6.4 wt%, (d) ϕ_{chiral} = 7.4 wt%.

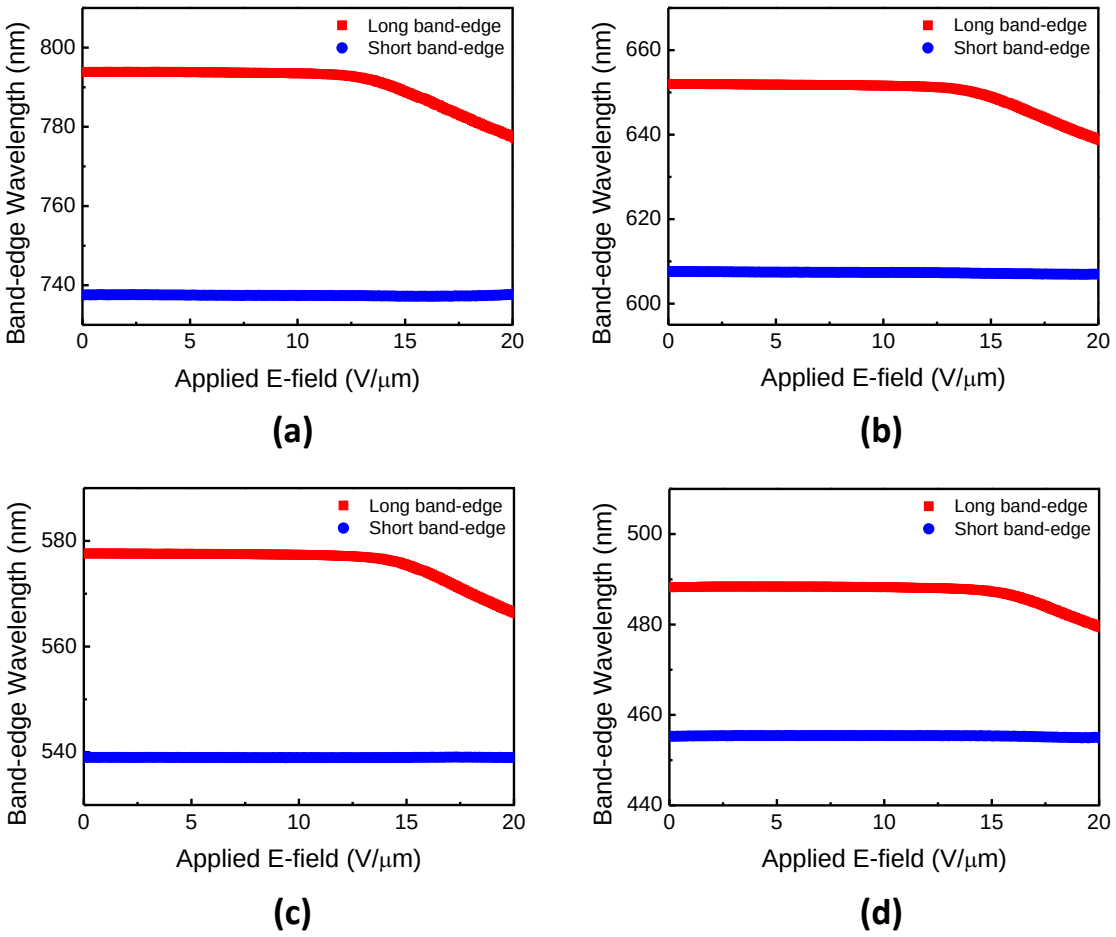

Figure 3.6 Electric field dependence of the SR band position in the polymer/ChLC nanocomposites with different chiral dopant concentrations at a polymerization temperature of -20 °C: (a) ϕ_{chiral} = 4.4 wt%, (b) ϕ_{chiral} = 5.4 wt%, (c) ϕ_{chiral} = 6.4 wt%, (d) ϕ_{chiral} = 7.4 wt%.

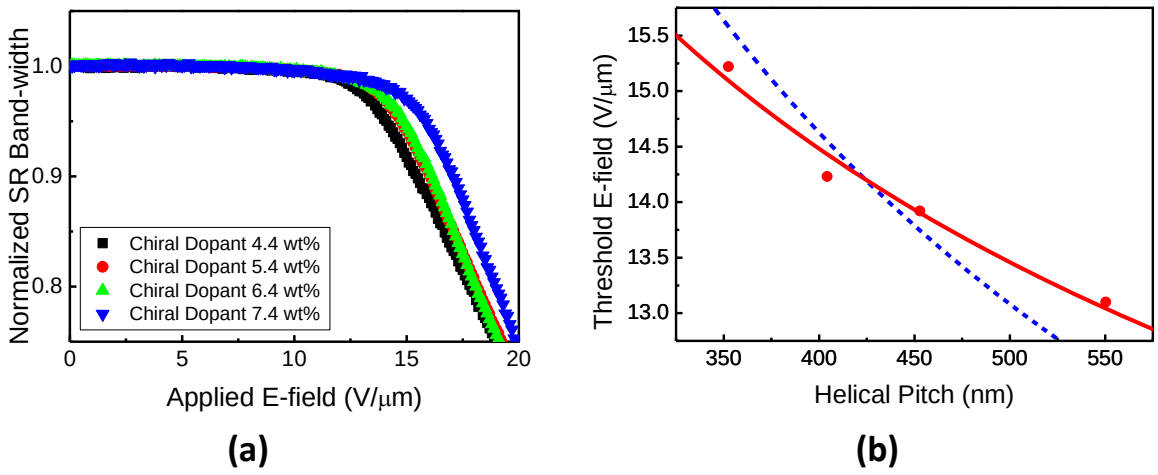

Figure 3.7 Dependence of the electro-optic switching on the helical pitch in the polymer/ChLC nanocomposites polymerized at -20 °C. (a) Normalized SR band-width with respect to the applied electric field at different chiral dopant concentrations. (b) Helical pitch dependence of the threshold electric field. The red solid circles represent the measured data points and the red curve is the fitting curve. The blue dotted curve is the fitting curve for β = 0.5.

3.4 Textures of polymer/ChLC nanocomposites

The difference in the response mechanisms is also supported by the polarizing optical micrographs of the samples. First, textures of the unpolymerized polymer/ChLC precursors were investigated, in order to compare with the textures in the polymer/ChLC nanocomposites polymerized at +20 °C and -20 °C. Figure 3.8 shows the reflective polarizing optical micrographs of the unpolymerized polymer/ChLC precursors with and without electric field. A long band pass filter with cut-off wavelength of 575 nm was used to avoid unintended photopolymerization. As shown in Fig. 3.8, the unpolymerized samples showed planar textures at zero electric field. Upon applying an electric field, both a Helfrich texture with two-dimensional square patterns [32], and the growth of oily streaks were observed. The two textures appeared almost at the same time, but the oily streaks gradually expanded to cover the whole field of view. When the electric field was removed, the Helfrich texture appeared to revert to the planar texture instantaneously, while the oily streaks reverted slowly.

The change in texture of the 'polymer-stabilized' ChLC caused by the polymer network was reported by another group [72]. The polymer network was thought to hinder the transition from a planar state to a focal-conic state. As a result, the modified Helfrich texture appeared, although the two-dimensional square patterns were modified. As the monomer concentration increased,

the shape of the square pattern was considerably changed. The polymer/ChLC composites polymerized at +20 °C showed distorted planar textures upon the application of an electric field, as shown in Fig. 3.9. These distorted planar textures of the samples polymerized at +20 °C are similar to the modified Helfrich texture reported by the other group. Similar to the Helfrich texture, the textures of the samples polymerized at +20 °C also showed instantaneous appearance and disappearance when the electric field was applied and removed, respectively. Unlike the unpolymerized samples, the growth of the oily streaks was suppressed and the focal conic textures did not appear even under a strong electric field. Therefore, the distorted planar textures are also thought to be due to the Helfrich deformation. On the other hand, the samples polymerized at -20 °C maintained the uniform planar cholesteric textures and only changed the color of the reflected light even under a high electric field of 20 V/μm (Fig. 3.10), i.e., the effective refractive index of the material was changed while maintaining the macroscopic helical structure. Therefore, the electro-optic response of the samples polymerized at -20 °C is not a consequence of the Helfrich deformation.

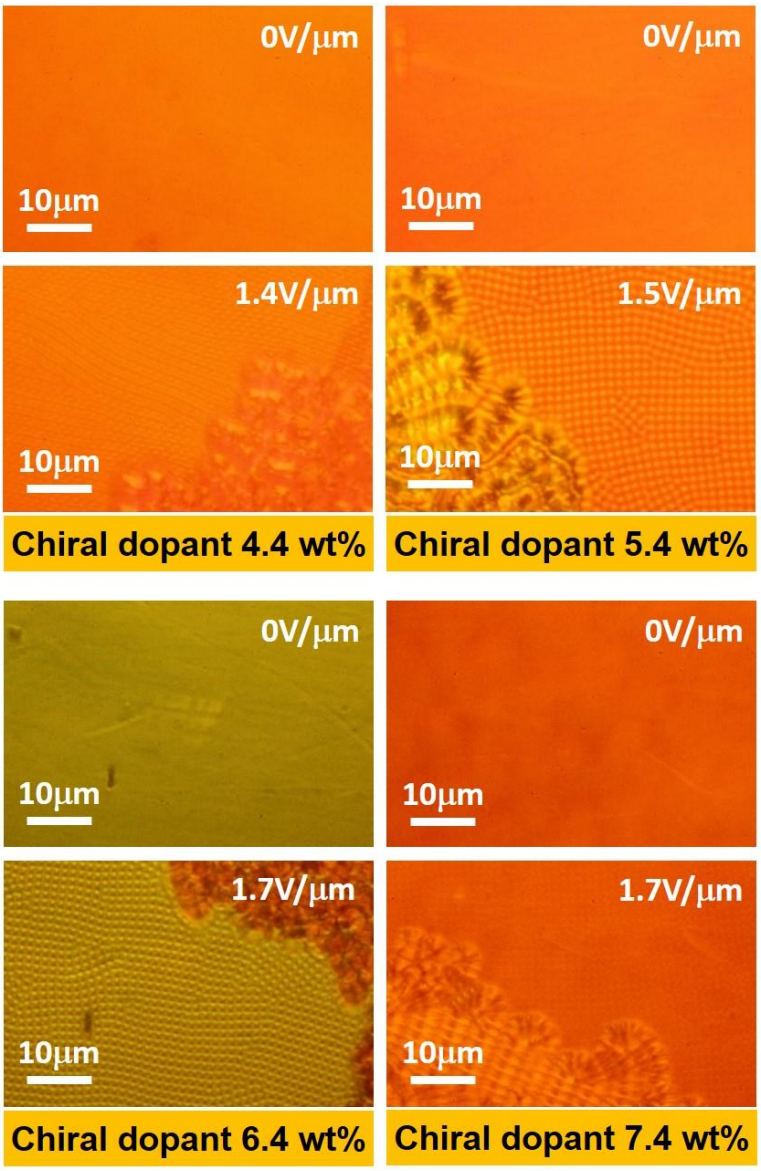

Figure 3.8 Polarizing optical micrographs of the unpolymerized polymer/ChLC precursors with different chiral dopant concentrations.

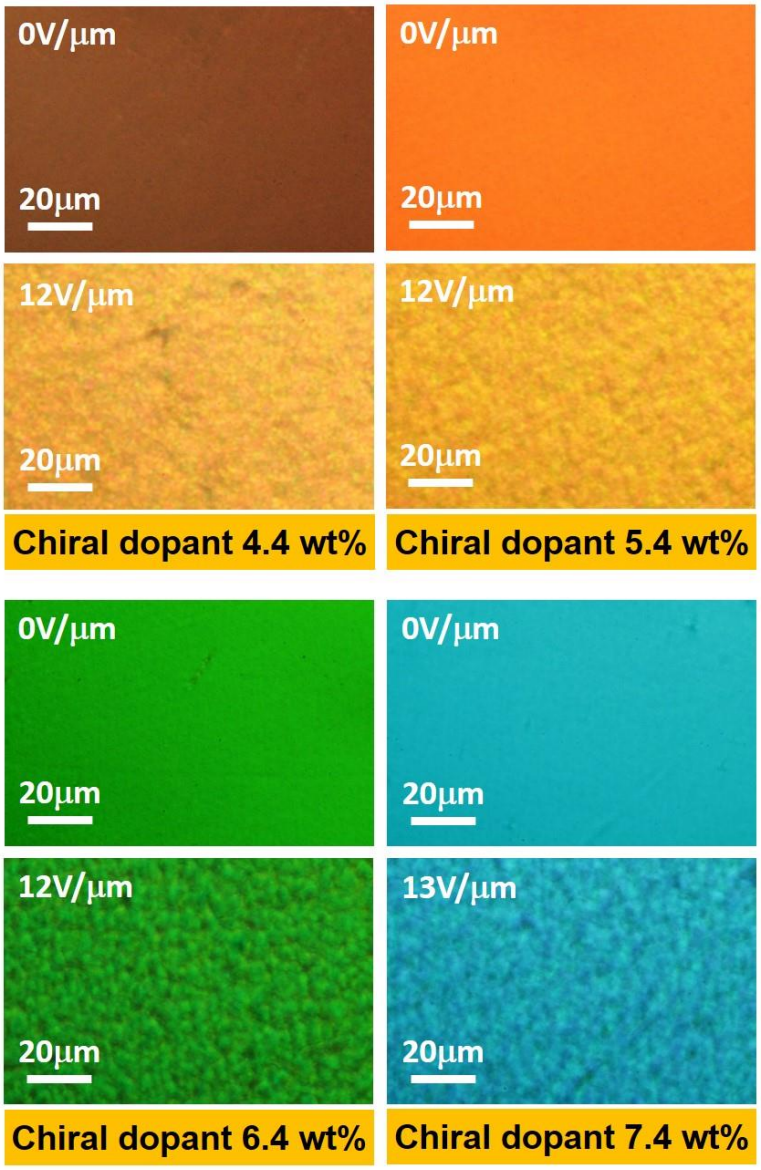

Figure 3.9 Polarizing optical micrographs of the polymer/ChLC composites polymerized at +20 °C with different chiral dopant concentrations.

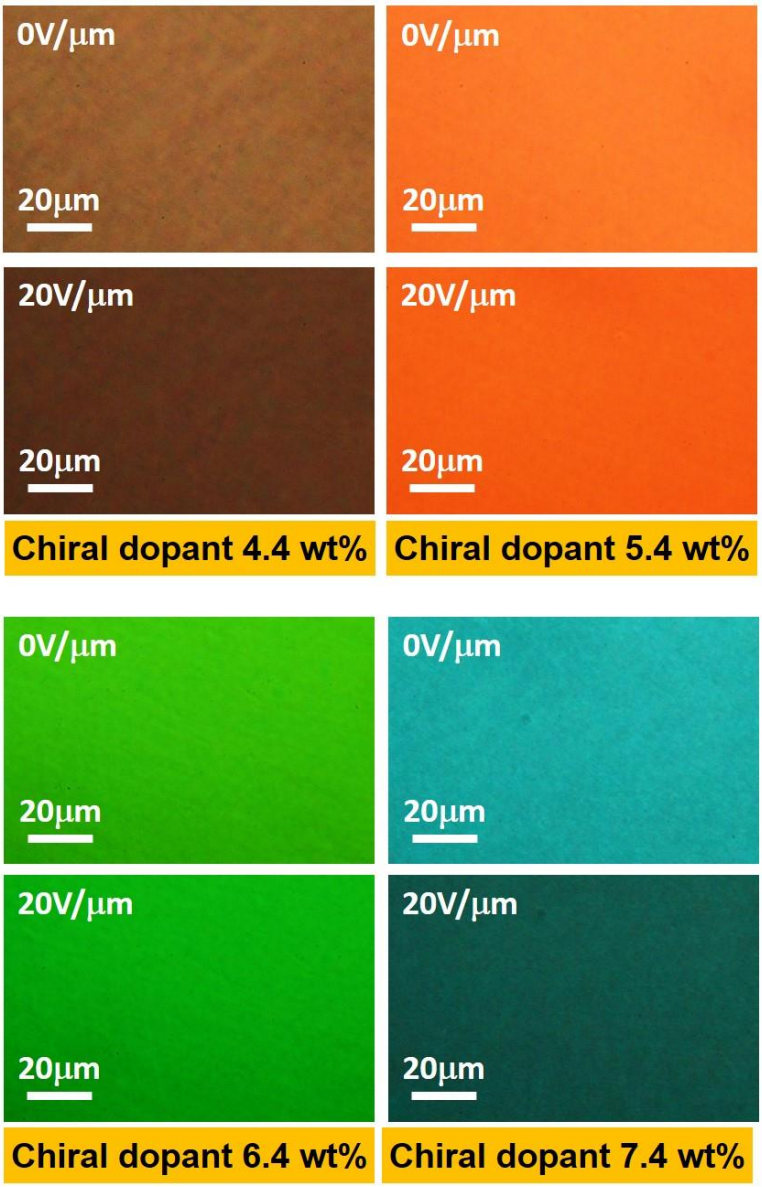

Figure 3.10 Polarizing optical micrographs of the polymer/ChLC composites polymerized at -20 °C with different chiral dopant concentrations.

3.5 Polymer network morphologies

In chapter 2, we mentioned that the threshold electric field increased with a decrease in the domain size, despite having approximately the same pitch lengths. The change in LC domain size caused by a change in pitch, if it exists, could be one of the causes for the change in threshold. Figure 3.11 and Fig. 3.12 show the morphologies of the polymer networks in the polymer/ChLC composites, after removing the unpolymerized LC molecules by super-critical CO_2. Figure 3.13 shows the dependence of the void size on the chiral dopant concentration,

obtained by analyzing the images in Fig. 3.11 and Fig. 3.12. The void sizes were defined as the diameter of the polymer-free regions enclosed by the polymer strands and evaluated from the SEM images. The void sizes in Fig. 3.11 and Fig. 3.12 were averaged over 20 voids and 50 voids, respectively. The sizes of voids, which correspond to the LC domains, depend strongly on the polymerization temperature [73]: the samples polymerized at +20 °C have pore sizes of approximately 295 nm, while the samples polymerized at -20 °C have pore sizes of approximately 40 nm. On the other hand, the effect of the helical pitch on the domain size is hardly detectable. The decrease in the domain size depending on the polymerization temperature can be attributed to the increased viscosity at a lower temperature, suppressing polymerization-induced phase separation of the polymer and LC [27]. The difference in LC domain sizes resulted in different reorientation mechanisms for the composites polymerized at +20 °C and -20 °C. However, the negligible dependence of the domain size on the helical pitch implies that the LC domain size is not a major cause of the difference in the threshold electric fields.

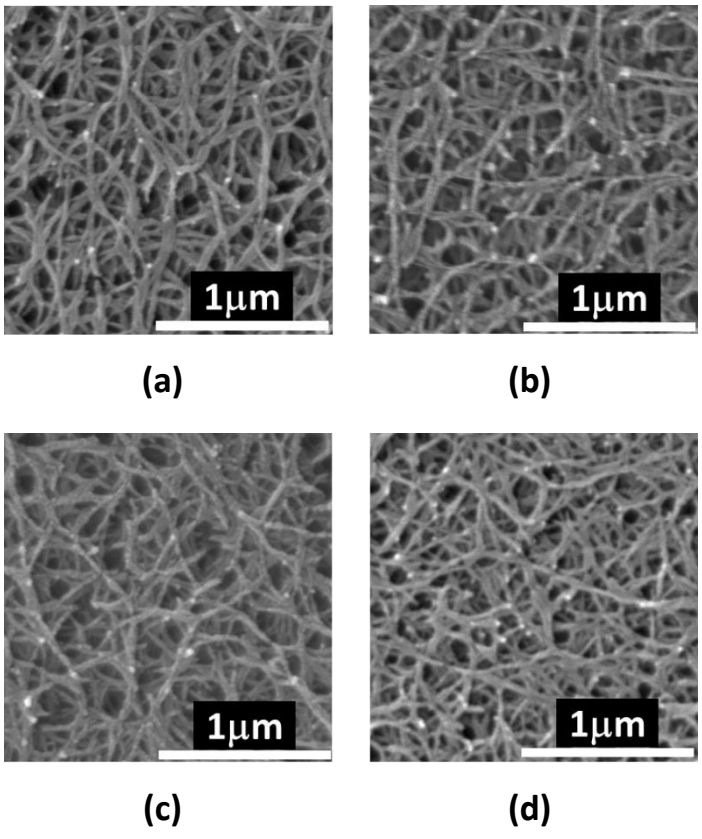

Figure 3.11 Chiral dopant concentration dependence of the polymer network morphologies in the polymer/ChLC nanocomposites polymerized at +20 °C: (a) ϕ_{chiral} = 4.4 wt%, (b) ϕ_{chiral} = 5.4 wt%, (c) ϕ_{chiral} = 6.4 wt%, (d) ϕ_{chiral} = 7.4 wt%.

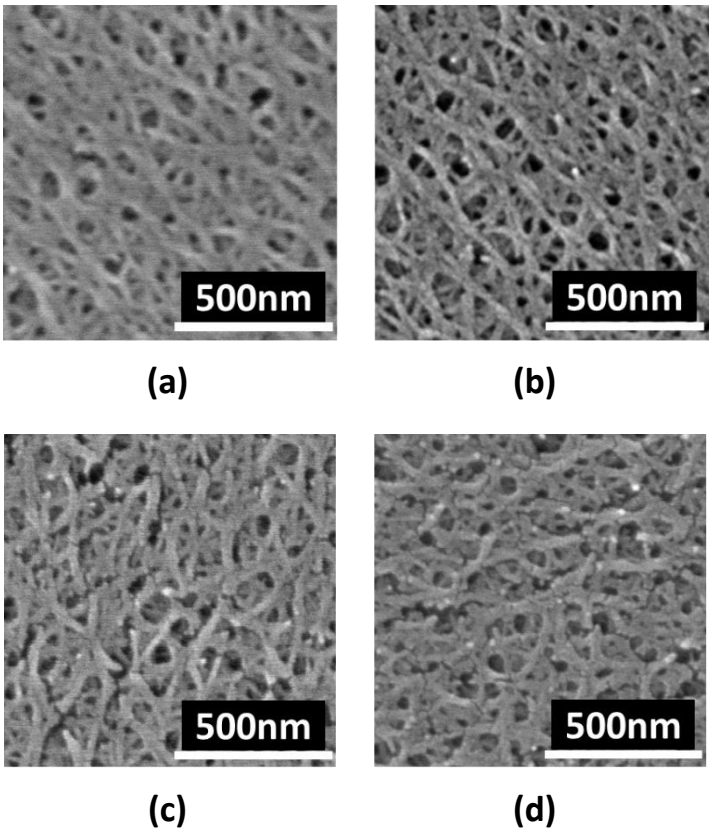

Figure 3.12 Chiral dopant concentration dependence of the polymer network morphologies in the polymer/ChLC nanocomposites polymerized at -20 °C: (a) ϕ_{chiral} = 4.4 wt%, (b) ϕ_{chiral} = 5.4 wt%, (c) ϕ_{chiral} = 6.4 wt%, (d) ϕ_{chiral} = 7.4 wt%.

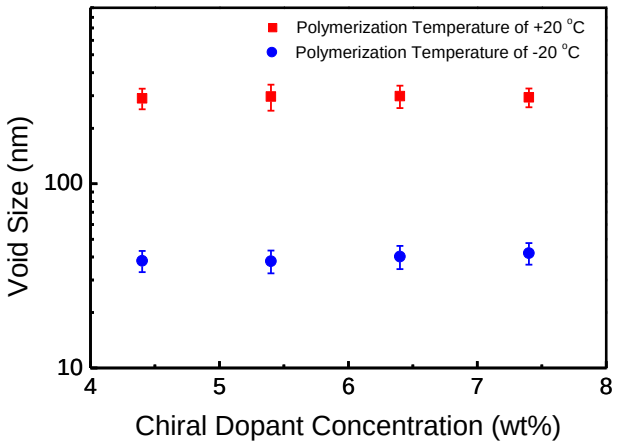

Figure 3.13 Chiral dopant concentration dependence of void-size distribution in the polymer/ChLC nanocomposites polymerized at +20 °C and -20 °C.

3.6 Fredericks-type reorientation of polymer/ChLC nanocomposite at a polymerization temperature of -20 °C

The improved response time of the polymer/nematic LC nanocomposites having ultra-small LC domains is caused by the effective decrease in the confined volume [64]. The Fredericks transition of the nematic LC molecules confined in nano-sized domains of few tens of nanometers was considered as an origin of the fast decay. This argument was limited to the nematic phase and did not consider the effect of twist that is present in the ChLC. To extend our discussion to the case of ChLC, we consider the Fredericks transition of twisted nematic LC molecules confined between two anchoring walls with a correlation length of ξ, as shown in Fig. 3.14. From the results shown in section 3.4, the macroscopic helical structure is retained even under a strong electric field. The non-polymerized LC molecules confined in nano-sized polymer walls are regarded as twisted nematic LC molecules. For a ChLC with pitch, p, the total twist angle, Φ, in the domain is given by

$$\Phi = \frac{2\pi\xi}{p}. \tag{3.3}$$

When an electric field is applied along the twist-axis, the threshold electric field, E_{th}, is expressed as [30]

$$E_{\text{th}} = \frac{\pi}{\xi}\frac{\sqrt{K_{11}}}{\sqrt{\Delta\varepsilon}}\left[1+\left(\frac{K_{33}-2K_{22}}{K_{11}}\right)\left(\frac{\Phi}{\pi}\right)^2\right]^{\frac{1}{2}}, \tag{3.4}$$

where K_{11}, K_{22}, K_{33} are the splay, twist and bend elastic constants, respectively. By substituting Eq. (3.3) into Eq. (3.4), we get

$$E_{\text{th}} = \pi\frac{\sqrt{K_{11}}}{\sqrt{\Delta\varepsilon}}\left[\frac{1}{\xi^2}+4\left(\frac{K_{33}-2K_{22}}{K_{11}}\right)\frac{1}{p^2}\right]^{\frac{1}{2}}. \tag{3.5}$$

From Eq. (3.5), the threshold electric field increases when the helical pitch becomes smaller. The proposed model has some limitations such as the anchoring imposed from the side-walls is not incorporated. However, the model qualitatively provides a physical explanation for the dependence of threshold electric field on the helical pitch.

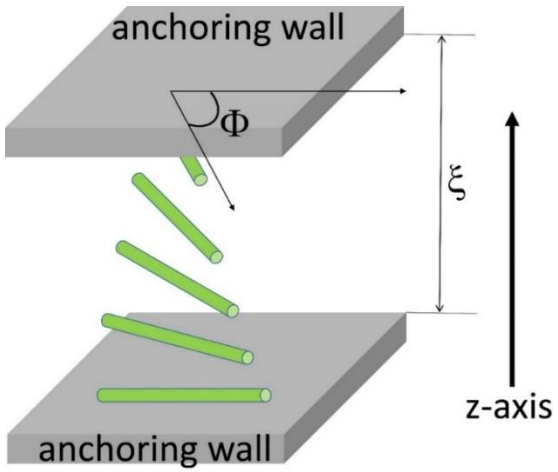

Figure 3.14 Schematic of the possible driving mechanism of the polymer/ChLC nanocomposite having small domains.

3.7 Summary

In this chapter, the helical pitch dependence of the threshold electric field in low-monomer-concentration polymer/ChLC nanocomposites was investigated. The polymerization temperature changes the electro-optic switching response of the polymer/ChLC nanocomposites from a 'polymer-stabilized' response (room temperature polymerization) to a 'deformation-free' response (low-temperature polymerization). The threshold electric fields of the nanocomposites increased as the helical pitch became smaller for both response modes, but the dependence was lesser in the 'deformation-free' sample, reflecting the difference in the driving mechanisms. The properties of polymer/ChLCs revealed here should aid the application of these materials in tunable electro-optic devices, such as phase modulators and tunable filters.

For the polarization-independent phase modulation, a polymer/short-pitch ChLC nanocomposite can be utilized by tuning the effective refractive index instead of tuning the SR band [26]. In this case, the operating wavelength of the polymer/short-pitch ChLC device is longer than the spectral position of the SR band. Since the spectral position of the SR band is not employed for the phase modulation, it does not matter if the helical pitch of the polymer/ChLC nanocomposite is sufficiently short to implement the phase modulation. Therefore, the threshold electric field can be lowered as the helical pitch of the polymer/ChLC nanocomposite increases within the limit that phase modulation can be achieved.

Chapter 4 Helical pitch dependence of the electro-optic characteristics in polymer/cholesteric liquid crystal composites having large-size liquid crystal domains

4.1 Introduction

In the previous chapter, small LC domains with an average diameter of 40 nm were observed in the polymer/ChLC nanocomposites showing the 'deformation-free' electro-optic switching mode. The threshold electric field of the 'deformation-free' polymer/ChLC nanocomposites having small LC domains increased as the helical pitch decreased. The driving mechanism of the 'deformation-free' response mode is thought to originate from the Fredericks-type reorientation of the LC molecules confined in small LC domains.

In this chapter, we investigate the helical pitch dependence of the threshold electric field in a special case of polymer/ChLC nanocomposites having pitch-length scale LC domains. Five samples with different helical pitches are prepared, and their electro-optic characteristics are compared before and after polymerization. Unlike the case in chapter 3, the threshold electric field of the nanocomposites showed little dependence on the helical pitch, while the unpolymerized samples showed a clear inversely proportional relationship with the helical pitch. The results are explained to be a consequence of the difference in the dynamics of the LC molecules in each of the domains, since the domain sizes in the same sample are statistically distributed. The polymer/ChLC composites that will be discussed in this chapter have pitch-length scale LC domains. The dynamics of the LC molecules in each of the domains are determined by the ratio of domain size to pitch length. When the helical pitch is sufficiently larger than the domain size, Fredericks-type reorientation occurs within most of the LC domains. In contrast, when the domain size is larger than the helical pitch, the dynamics of the LC molecules in the domains are attributed to the helix deformation. The ratio of domain size to pitch length is inversely proportional to the helical pitch, since the average domain size has no dependence on the helical pitch. For short pitch samples, the driving mechanism tends to change from the Fredericks-type reorientation to the helix deformation in some of the large LC domains. The proportion of LC domains that show the helix deformation in the polymer/ChLC composite increases as the helical pitch decreases. Therefore, the decrease in the threshold due to the change in the driving mechanism in some of the large LC domains should countervail the increase in the threshold caused by the reduced helical pitch observed in typical 'deformation-free' polymer/ChLC nanocomposites having small LC domains.

4.2 Materials and sample preparation

Five types of mesogenic monomer/ChLC mixtures with different chiral dopant concentrations are discussed in this chapter. The composition of each sample is listed in Table 4.1. The mesogenic monomer/ChLC mixtures comprised three materials from Merck: a photopolymerizable LC monomer (RM257); a nematic LC (MLC-6657-000); and a chiral dopant (ZLI-4572). No photoinitiator was used in this study. The physical properties of MLC-6657-000 and RM257 are listed in Table 4.2. The relative weight ratios of RM257 and MLC-6657-000 were set to 19.9 and 80.1, respectively, and the chiral dopant ZLI-4572 was added to this mixture to change the helical pitch of the polymer/ChLC nanocomposite. The chiral dopant concentration was varied from 6 wt% to 10 wt %. The materials were dissolved in chloroform and left to evaporate for approximately 1 day.

Table 4.1 Composition of the samples used in this chapter.

Mesogenic monomer (RM257) [wt%]	Nematic LC (MLC-6657-000) [wt%]	Chiral dopant (ZLI-4572) [wt%]
18.7	75.3	6.0
18.5	74.5	7.0
18.3	73.7	8.0
18.1	72.9	9.0
17.9	72.1	10.0

Table 4.2 Physical properties of each materials used in this chapter.

Material	Extra-ordinary refractive index (n_e)	Birefringence (Δn)	Dielectric anisotropy ($\Delta\varepsilon$)
RM257	1.687	0.179	-1.5
MLC-6657-000	1.6767	0.1702	37.34

The helical pitches of the samples were measured using the Grandjean-Cano wedge method using home-made, planar alignment wedge cells with a wedge angle of ~0.04°. The principles and fabrication method for the Grandjean-Cano wedge cell are described in detail in section 3.2.2. The helical pitches obtained for the samples before and after polymerization with

different chiral dopant concentrations are plotted in Fig. 4.1. The pitch lengths of the samples before and after polymerization varied between 273 nm and 458 nm.

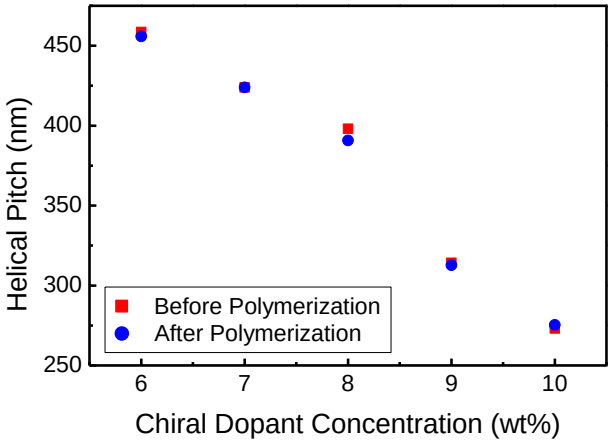

Figure 4.1 Dependence of helical pitch on chiral dopant concentration both before and after polymerization. The red solid squares and blue solid circles denote the measured results before and after polymerization, respectively.

The fabrication processes of the samples for measuring the electro-optic characteristics and polymer morphologies are almost the same as the processes in chapter 2. However, ITO-coated planar sandwich cells with a cell-gap of 6 μm (purchased from E. H. C Co.) were used. The polymerization temperature and polymerization time for the samples were +25 °C and 40 min, respectively.

4.3 Polymer network morphologies

From chapter 3, it was confirmed that the helical pitch cannot affect the domain size, whereas the fabrication conditions such as polymerization temperature can. Figure 4.2 shows the SEM images of the polymer/ChLC nanocomposites with different chiral dopant concentrations after rinsing out the unpolymerized LC with super-critical CO_2. All samples have approximately the same void size of 200 nm ~ 400 nm and polymer network morphology, likely attributed to the fact that the relative concentration of the LC monomer to the nematic LC and the fabrication procedure are the same for all samples.

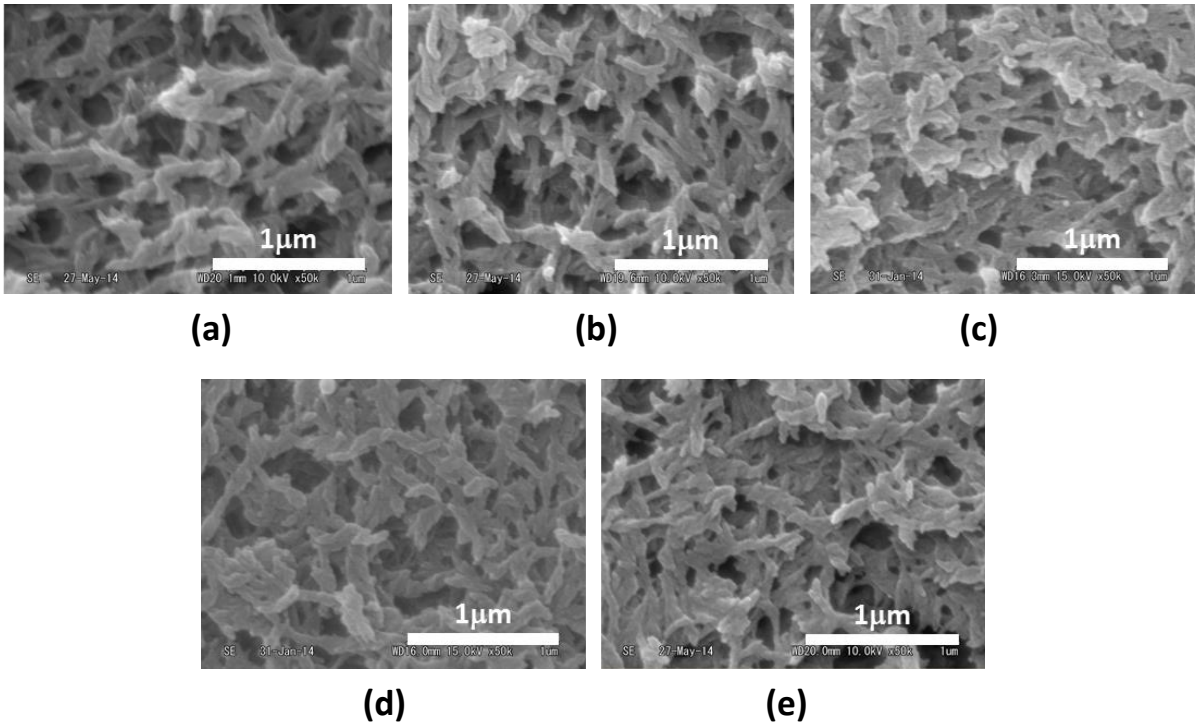

Figure 4.2 SEM images of the polymer/ChLC nanocomposites with different chiral dopant concentrations: (a) ϕ_{chiral} = 6 wt%, (b) ϕ_{chiral} = 7 wt%, (c) ϕ_{chiral} = 8 wt%, (d) ϕ_{chiral} = 9 wt%, (e) ϕ_{chiral} = 10 wt%.

In general, it is necessary to reduce the size of the LC domains to several tens of nanometers for the implementation of the 'deformation-free' response mode in polymer/ChLC nanocomposites. However, it is possible to control the long band-edge wavelength without changing the short band-edge wavelength, by using high monomer concentration polymer/ChLC composites, even though the domain size is larger. In the following sections, we will present in detail the electro-optic characteristics and textures of polymer/ChLC composites having large-size LC domains.

4.4 Electro-optic characteristics

4.4.1 Electric field dependence of the selective reflection band

Figure 4.3 shows the electro-optic characteristics of the polymer/ChLC nanocomposites before polymerization with different chiral dopant concentrations. All samples showed similar electro-optic switching behavior. Before polymerization, the electro-optic response varies depending on the applied field intensity. When a weak electric field is applied, the reflection band becomes narrower, and the peak reflectance decreases with an increase in the electric field.

At higher electric fields, the reflection band shifts to shorter wavelengths and eventually disappears. This is explained by the gradual unwinding of the helical structure, showing a transition to the focal-conic state where the helix axis is randomly oriented, before becoming completely unwound [74]. Because the helical structure is deformed from a perfect sinusoid, the reflectance decreases compared to the voltage off state.

On the other hand, once the material is polymerized, a completely different behavior is observed, as shown in Fig. 4.4: above the threshold electric field, only the long band-edge wavelength shortens, while the short band-edge wavelength remains constant. Because the long and short band-edge wavelengths are given by $\lambda_{\text{long-edge}} = n_e \times p$ and $\lambda_{\text{short-edge}} = n_o \times p$, the result implies that only the extra-ordinary refractive index decreases, while the ordinary refractive index and helical pitch remain constant. In contrast to the sample before polymerization, the helical structure, stabilized by the cross-linked polymer network, is not destroyed by the electric field. However, unlike the switching behavior typical of 'deformation-free' polymer/ChLC nanocomposites described in chapters 2 and 3, the peak reflectance gradually decreases as the electric field increases. The reduction in peak reflectance is probably caused by scattering due to the large domain size, which is comparable to the wavelength of light. The LC domains are considered to act as scattering domains, since the effective refractive indices of the LC domains are changed by the variation in the orientation direction of the LC molecules within each domain by an electric field.

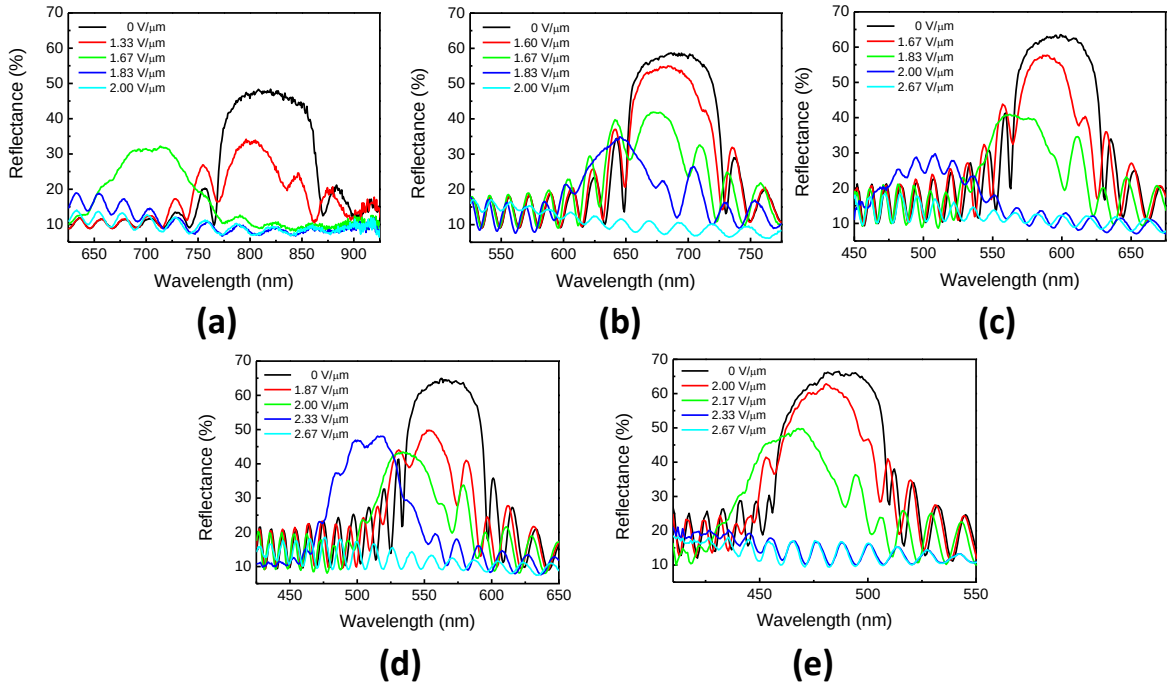

Figure 4.3 Electrical tuning of the SR band in the polymer/ChLC nanocomposites before polymerization with different chiral dopant concentrations: (a) ϕ_{chiral} = 6 wt%, (b) ϕ_{chiral} = 7 wt%, (c) ϕ_{chiral} = 8 wt%, (d) ϕ_{chiral} = 9 wt%, (e) ϕ_{chiral} = 10 wt%.

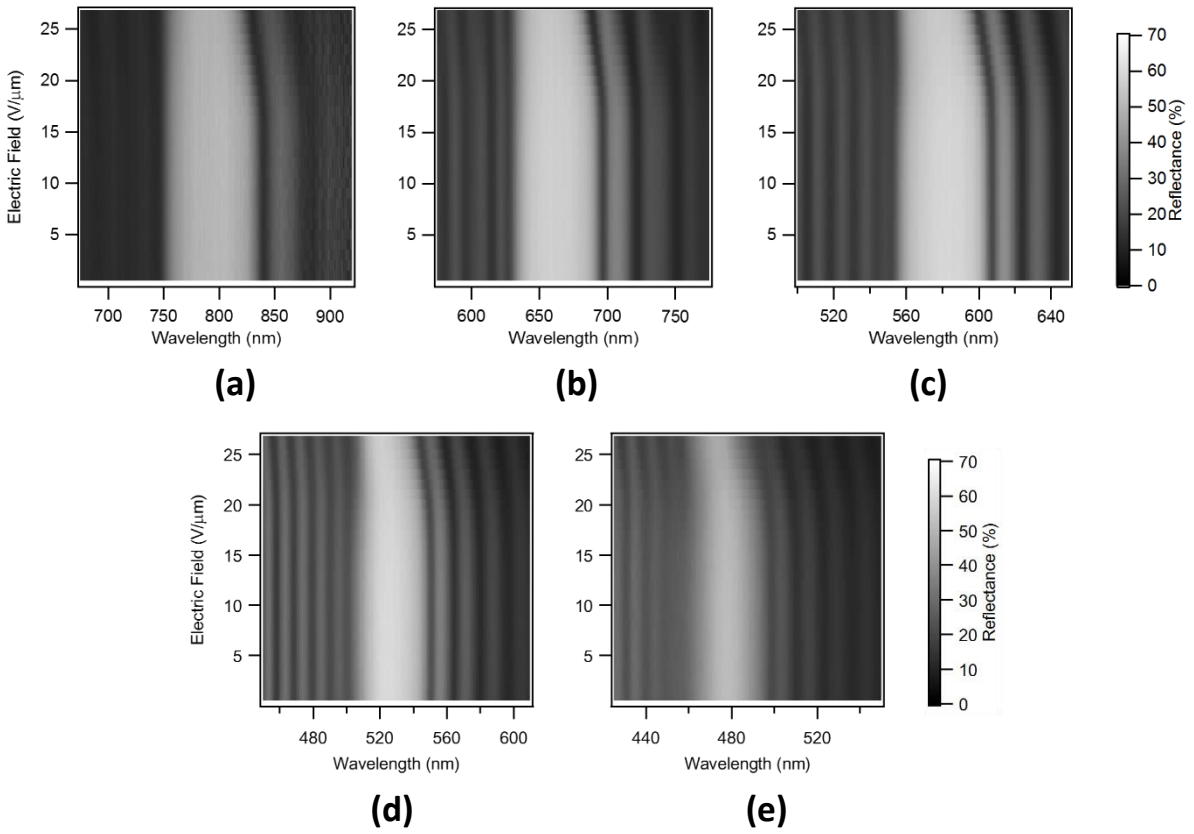

Figure 4.4 Electrical tuning of the SR band in the polymer/ChLC nanocomposites after polymerization with different chiral dopant concentrations: (a) ϕ_{chiral} = 6 wt%, (b) ϕ_{chiral} = 7 wt%, (c) ϕ_{chiral} = 8 wt%, (d) ϕ_{chiral} = 9 wt%, (e) ϕ_{chiral} = 10 wt%.

The threshold electric field, E_{th}, of a conventional ChLC is inversely proportional to the helical pitch, p, as shown in Eq. (1.30). This relation implies that the shorter the cholesteric helical pitch, the higher is the electrical energy required to unwind the helical structure [30]. To find the threshold electric field for unwinding the helix in the samples before polymerization, we measure the polarized reflectance from the samples and determine the electric field at which the reflectance becomes zero; this corresponds to the situation when all molecules are aligned along the electric field, thereby resulting in zero birefringence. Figure 4.5(a) shows the polarized reflection intensity integrated over the wavelength range 480 nm ~ 730 nm. The reflectance was integrated over the wavelength range 480 nm ~ 730 nm since the limited spectral range of the polarizers made it difficult to carry out measurements at the central reflection wavelength of each sample. As the chiral dopant concentration increases, or the helical pitch shortens, the threshold electric field increases. Figure 4.5(b) shows the threshold electric field with respect to the helical pitch. Analysis of the data using the power law equation

$E_{th} = Ap^{-\beta}$ yields a best fit for $\beta = 0.97$, which is close to the predicted value from Eq. (1.30). The threshold is almost inversely proportional to the pitch, as shown in Fig. 4.5(b).

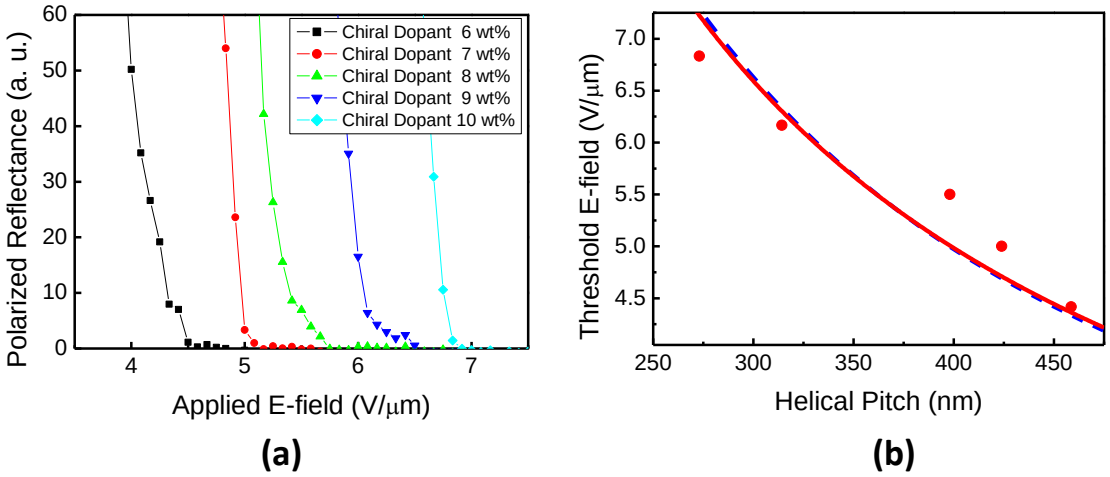

Figure 4.5 Dependence of the electro-optic response on the chiral dopant concentration of the samples before polymerization. (a) Polarized reflection intensity integrated over the wavelength range 480 nm ~ 730 nm with respect to the applied electric field at different chiral dopant concentrations. (b) Threshold electric field with respect to the helical pitch. The red solid circles represent the measured data points and the red curve is the fitting curve. The blue dotted curve is the fitting curve for $\beta = 1$.

Figure 4.6(a) shows the applied electric field dependence of the normalized SR band-width after polymerization. The threshold electric field is defined as the electric field required for the reflection band to start shifting. In contrast to the case of the unpolymerized samples, the threshold electric field shows little dependence on the helical pitch. As shown in Fig. 4.6(b), the thresholds for samples with different helical pitches vary slightly, between 5.5 V/μm and 5.9 V/μm. Consequently, the threshold electric field of the polymer/ChLC nanocomposites has no dependence on the helical pitch.

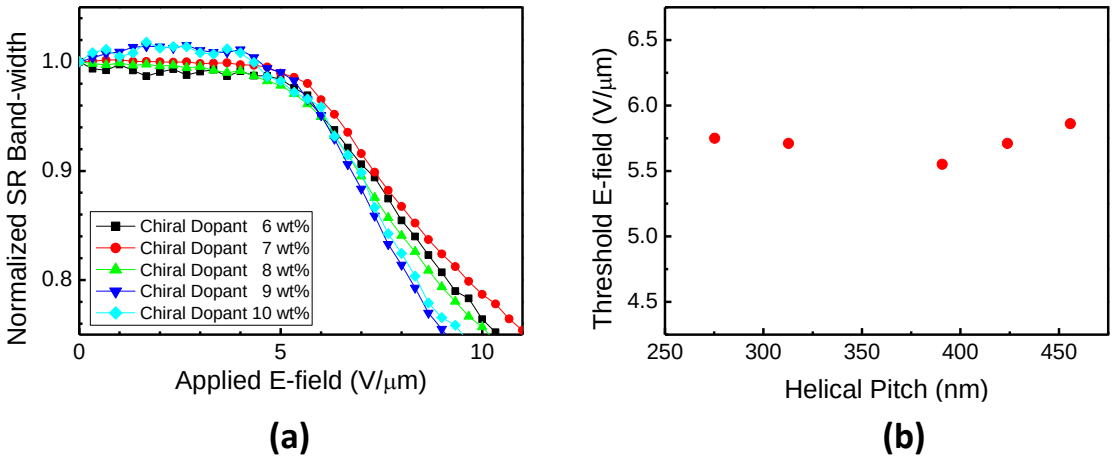

Figure 4.6 Dependence of the electro-optic response on the chiral dopant concentration of the polymer/ChLC nanocomposites after polymerization. (a) Normalized SR band-width with respect to the applied electric field at different chiral dopant concentrations. (b) Threshold electric field with respect to the helical pitch.

Let us consider why the helical pitch dependence of the threshold electric field for the samples investigated in this chapter is different from that of the usual 'deformation-free' polymer/ChLC nanocomposites. The difference in the helical pitch dependence of the electro-optic response is most likely attributed to the difference in the driving mechanism. From the results presented in chapter 3, the helical pitch dependence in polymer/ChLC nanocomposites having ultra-small LC domains is thought to be a consequence of the nano-confined LC molecules undergoing a Fredericks-type reorientation instead of a helix deformation. However, the LC domains in the composites studied in this chapter are relatively larger than those of the usual 'deformation-free' polymer/ChLC nanocomposites. It is impossible for the polymer/ChLC composites to show an undulation of the helical axis under an electric field when the domain size is less than half of the helical pitch. On the other hand, the probability of appearance of the helix deformation in each of the LC domains increases as the domain size increases. The ratio of domain size to pitch length, D/p, is inversely proportional to the helical pitch, since the average domain size being determined by the fabrication conditions of all the samples is approximately the same. Therefore, D/p is an important parameter for determining the driving mechanism.

Although we have discussed the results using the average domain size of the LC domains, in reality, the domain sizes are statistically distributed. For the short pitch samples with helical pitches shorter than 320 nm (or those with chiral dopant concentration of more than 9 wt%), there exist some of the domains whose size is larger than the helical pitch. The unpolymerized LC molecules in the larger domains follow the dynamics of the helix deformation, whereas

those in the other smaller domains follow the dynamics of the Fredericks-type reorientation. Therefore, the electro-optic response would be affected by both the helix deformation and the Fredericks-type reorientation. The number of LC domains showing the helix deformation increases as the helical pitch decreases. On the other hand, when the helical pitch is longer than 400 nm, or the chiral dopant concentration is less than 8 wt%, most of the LC domains are smaller than the helical pitch. The Fredericks-type reorientation tends to occur within most LC domains. Therefore, the electro-optic response would be affected by only the Fredericks-type reorientation. It can be thought that the samples with two different dynamics do not follow the conventional helical pitch dependence of the threshold electric field, since the level of the threshold electric field required by the Fredericks-type reorientation is different from the Helfrich threshold. In the case of a short helical pitch, the increase in threshold affected by the Fredericks-type reorientation is compensated by the decrease in the threshold due to the change in the driving mechanism of the unpolymerized LC molecules.

Figure 4.7 shows the reflection spectra before and after the application of an electric field in the polymerized polymer/ChLC composites with different chiral dopant concentrations. When the electric field was removed, the spectrum of the SR band in the low chiral dopant concentration samples returned to the original state. However, a different phenomenon, in which the spectrum of the SR band is different before and after an electric field is applied, was observed in the high chiral dopant concentration samples. As the chiral dopant concentration increases, or the helical pitch shortens, a larger difference is observed in the SR band before and after applying an electric field. The results are also thought to be a consequence of the variation in the ratio of domain size to pitch length. It is thought that reversibility of the SR band in the long pitch samples, similar to the phenomenon observed in the usual 'deformation-free' response mode, is due to the Fredericks-type reorientation of the LC molecules confined in the LC domains. On the other hand, the irreversibility of the SR band in the short pitch samples before and after applying an electric field, which is observed in bulk ChLC, is thought to be somewhat influenced by the Helfrich deformation. The difference in the electro-optic response mechanism between the long pitch and short pitch samples is also supported by the reflection spectra before and after applying an electric field.

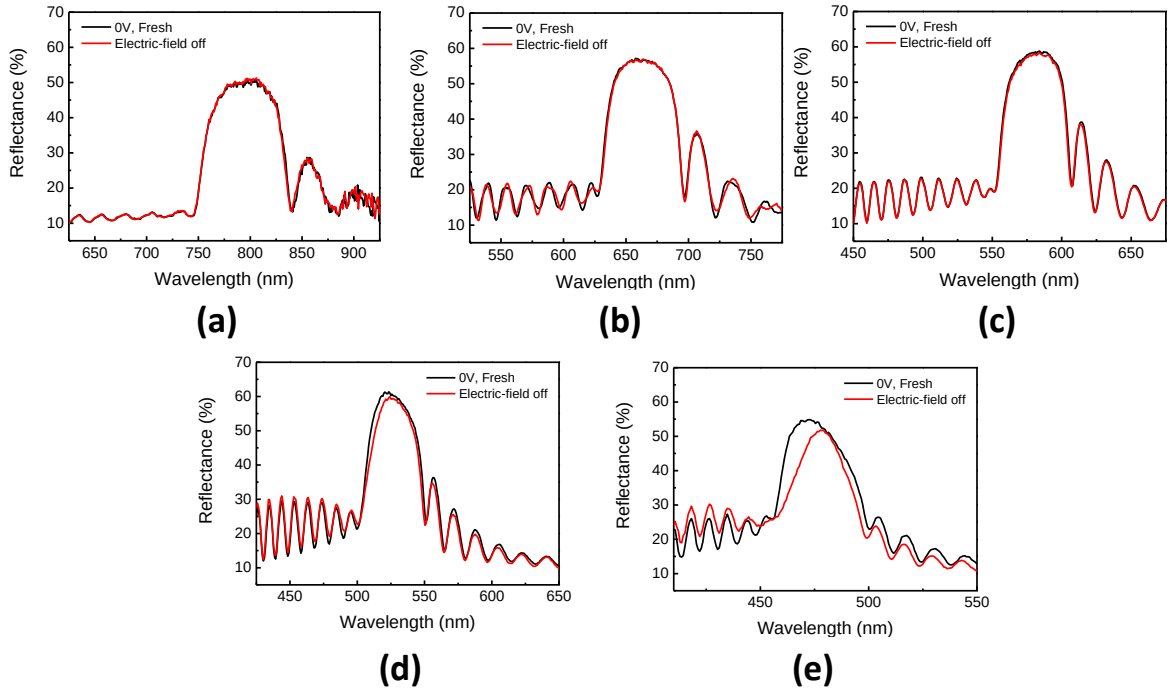

Figure 4.7 Reflection spectra before and after applying an electric field in the polymerized polymer/ChLC nanocomposites with different chiral dopant concentrations: (a) ϕ_{chiral} = 6 wt%, (b) ϕ_{chiral} = 7 wt%, (c) ϕ_{chiral} = 8 wt%, (d) ϕ_{chiral} = 9 wt%, (e) ϕ_{chiral} = 10 wt%.

4.4.2 Response time

In this section, we will discuss how fast the response time of the polymer/ChLC nanocomposites having large size LC domains is as compared with that of the 'polymer-stabilized' ChLCs. Figure 4.8 shows the electric field dependence of the rise and decay times of the polymer/ChLC nanocomposite with the 8 wt% chiral dopant concentration sample after polymerization. The response characteristics were measured by monitoring the reflected light intensity from the samples, while applying a pulse electric field with a width of 0.5 ms to the cell. The change in the reflected light intensity is caused by the SR band shift. The response times were estimated from the time difference when the reflected light intensity changes between 10% and 90% of its maximum value. The rise time was on the order of several tens of microseconds and decreased with an increase in the electric field. This is thought to be due to the increased electric field-induced torque on the LC molecule with increasing electric field. On the other hand, the decay times showed little dependence on the applied electric field. All samples with different chiral dopant concentrations had the same order of decay time (less than 500 μs).

The decay time of a few hundred microseconds is fast enough compared to that of the few tens of milliseconds in the usual 'polymer-stabilized' polymer/ChLC composites [23]. Therefore, these samples are competitive for photonic applications, although the decay time of a few hundred microseconds is not as fast as that of the polymer/ChLC nanocomposites having ultra-small LC domains.

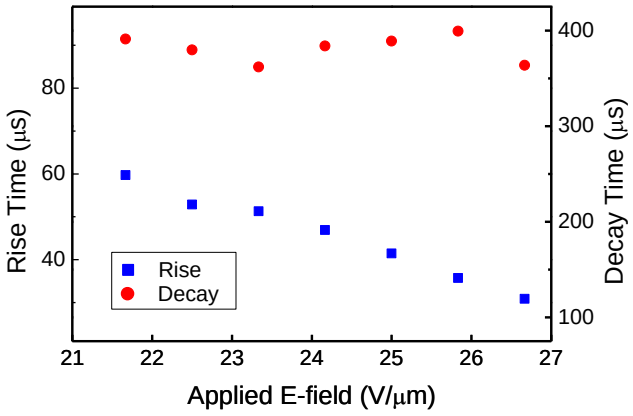

Figure 4.8 Electric field dependence of the rise and decay times of the polymer/ChLC nanocomposite with 8 wt% chiral dopant concentration after polymerization.

4.5 Textures of polymer/ChLC nanocomposites

The reflection images also suggest that the electro-optic response mechanism of the high chiral dopant concentration samples is different from that of the low chiral dopant concentration samples. Figure 4.9 shows the reflective textures of the photopolymerized polymer/ChLC nanocomposite samples under an electric field of 26.67 V/μm. The polymer/ChLC nanocomposite samples with a chiral dopant concentration of 6 wt% showed a planar cholesteric texture upon the application of a high electric field of 26.67 V/μm, i.e., the macroscopic helical structure was maintained. On the other hand, the polymer/ChLC nanocomposite samples with a chiral dopant concentration of 10 wt% showed a distorted planar texture, similar to the low monomer concentration polymer/ChLC composites polymerized at +20 °C presented in chapter 3. The two-dimensional pattern of the high chiral dopant concentration sample also showed simultaneous appearance and disappearance when the electric field was applied and removed. This is explained by the tilting of the cholesteric helix. The extent of change in the texture from planar was larger as the chiral dopant concentration was increased. Therefore, the relaxation dynamics in the high chiral dopant concentration samples is thought to be affected by the Helfrich deformation to a certain degree. The influence

of the Helfrich deformation on the electro-optic response mechanism increases as the chiral dopant concentration increases, or the helical pitch shortens.

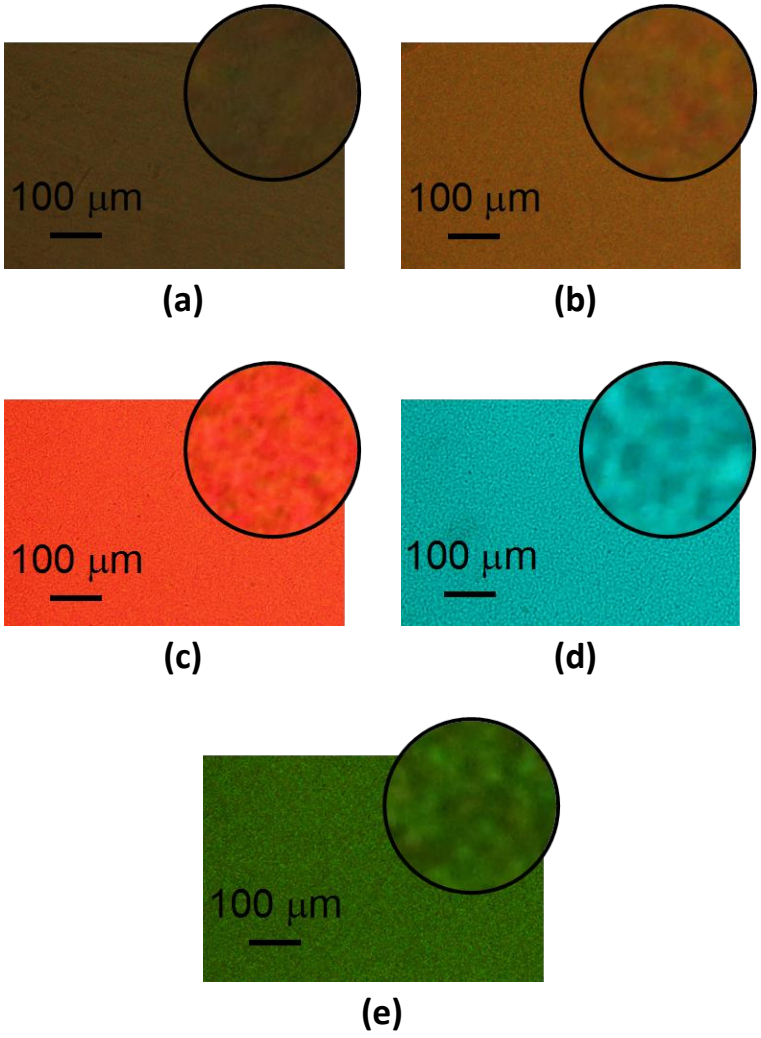

Figure 4.9 Reflection micrographs of the polymer/ChLC nanocomposites at 26.67 V/μm with different chiral dopant concentrations. The inset pictures show images magnified by a factor of 10: (a) ϕ_{chiral} = 6 wt%, (b) ϕ_{chiral} = 7 wt%, (c) ϕ_{chiral} = 8 wt%, (d) ϕ_{chiral} = 9 wt%, (e) ϕ_{chiral} = 10 wt%.

4.6 Summary

In this chapter, the electro-optic properties of polymer/ChLC nanocomposites with pitch lengths varying between 273 nm and 458 nm were investigated by spectroscopy and SEM observations. Although the domain size is large, tuning of the long band-edge wavelength only is achieved by using high-monomer-concentration polymer/ChLC precursors with a decay time of less than 500 μs. The threshold electric field of the polymer/ChLC nanocomposites had no

dependence on the helical pitch, in contrast to conventional ChLCs that have a threshold inversely proportional to the helical pitch. The reason why thresholds have no dependence on the helical pitch is probably because the dynamics of the LC molecules in each of the domains are not the same. The dynamics of the LC molecules are determined by the ratio of domain size to pitch length. The percentage of LC domains that show helix deformation in the polymer/ChLC composite increases as the ratio of domain size to pitch length increases. Therefore, for the short pitch samples, the increase in thresholds caused by the Fredericks-type reorientation and the decrease in thresholds due to the change in the driving mechanism in some of the LC domains would appear to cancel out each other. From these results, it is possible to control the effective refractive index with a relatively low threshold electric field of less than 6 V/μm as compared to the usual 'deformation-free' polymer/ChLC nanocomposites and a fast decay time of less than 500 μs.

Chapter 5 Conclusions

In this dissertation, various experiments were conducted with the aim of achieving a decrease in the driving voltage and an understanding of the driving mechanism of polymer/ChLC nanocomposites. We summarize the important contents from each chapter as follows.

In chapter 2, a low-temperature polymerization method was investigated to reduce the driving voltage of polymer/ChLC nanocomposites. We showed that by lowering the polymerization temperature, the electro-optic switching mode of the low-monomer-concentration polymer/ChLC nanocomposite could be changed from 'polymer-stabilized' to 'deformation-free', maintaining a fast response time of ~20 μs. Ultra-fast response time was achieved by the formation of nano-sized LC domains in the low-monomer-concentration polymer/ChLC nanocomposite. Smaller LC domains can be achieved by controlling the degree of phase separation through control of the polymerization temperature, since phase separation between the polymer and the non-photopolymerizable LC molecules during the polymerization process is the origin of formation of the LC domains. The formation of smaller domain sizes is caused by the increased viscosity at lower temperatures. 'Deformation-free' electro-optic response is achieved by decreasing the domain size to the order of a few tens of nanometers. The reduction in driving voltage, with a fast response of the low-monomer-concentration polymer/ChLC nanocomposites, is achieved by the low-temperature polymerization process. The increased number of unpolymerized mobile LC molecules contributes to the reduced driving voltage.

In chapters 3 and 4, the helical pitch dependences of the electro-optic characteristics in polymer/ChLC composites were investigated to understand the driving mechanisms of the polymer/ChLC composites. Various conditions for the polymer/ChLC composites, such as low monomer concentration with low temperature polymerization, low monomer concentration with room temperature polymerization, and high monomer concentration without a photoinitiator were investigated. In the case of low-monomer-concentration polymer/ChLC composites, the threshold electric field increases as the helical pitch decreases, regardless of the polymerization temperature. However, different dependencies of the threshold electric field on the helical pitch are observed depending on the electro-optic response modes. The 'polymer-stabilized' response mode is attributed to the Helfrich deformation, whereas the 'deformation-free' response mode is attributed to the Fredericks-type reorientation. However, the samples with high monomer concentration, without a photoinitiator, having pitch-length scale LC domains showed a completely different behavior. The larger size of the LC domains is attributed to the reduced polymerization rate caused by the absence of the photoinitiator in the

high-monomer-concentration polymer/ChLC composite. In contrast to the other cases, the threshold electric field showed little dependence on the helical pitch, probably due to the variation in the ratio of domain size to pitch length. Since the size of each LC domain in the same sample is statistically distributed, the size of some of the LC domains in the short pitch polymer/ChLC nanocomposites is larger than the helical pitch. The unpolymerized LC molecules in the larger domains undergo helix deformation rather than Fredericks-type reorientation. The resultant electro-optic responses in each sample would be affected by both Fredericks-type reorientation and helix deformation. The amount of domains showing the helix deformation increases as the ratio of domain size to pitch length increases. Therefore, the increase in the threshold due to the increased twist in the Fredericks-type reorientation is offset by the decrease in the threshold caused by the change in the driving mechanism, from the Fredericks-type reorientation to the helix deformation, in some large LC domains.

Acknowledgments

I sincerely appreciate to my supervisor Professor Masanori Ozaki, who has guided me in finishing this Ph.D dissertation. I have learned a lot under his tutelage. This dissertation would not have been possible without his encouragement. I would also like to thank Associate Professor Akihiko Fujii for his guidance and advice. I would also like to extend my gratitude to Assistant Professor Hiroyuki Yoshida. I can have a wide knowledge of liquid crystals and photonics through many discussions with him.

I would like to extend my gratitude to all the Professors at the Division of Electrical, Electronic and Information Engineering at Osaka University. I especially appreciate Professor Toshimichi Ito and Associate Professor Akihiko Fujii for reviewing this dissertation. I also deeply appreciate Professor Yusuke Mori, Professor Mitsuhiro Katayama, Professor Ryuji Katayama, Professor Masahiko Kondow, Professor Nobuya Mori, Professor Tetsuya Yagi, for serving on my dissertation committee.

I thank also both present and former members of Ozaki laboratory: Dr. Giichi Shibuya, Dr. Quang-Duy Dao, Mr. Junji Kobashi, Mr. Masashi Ohmori, Mr. Koki Imamura, Mr. Toshiki Usui, Mr. Dai Nakagawa, Ms. Chika Nakano, Mr. Kento Fujita, Mr. Yasutaka Maeda, Mr. Yoshinori Mouri, Mr. Yusaku Anzai, Mr. Takuma Ohkawa, Mr. Kanta Sunami, Mr. Yuya Nakata, Mr. Mitsuhiro Nakatani, Mr. Shohei Yamano, Mr. Ken Watanabe, Mr. Tomohiro Ouchi, Mr. Masaru Ono, Mr. Takahiro Kitagawa, Ms. Misaki Takahashi, Mr. Yuuki Nishikawa, it has been a pleasure working with you and I really enjoyed the times we had together. I deeply thank Dr. Jaeki Kim, who helped me a lot.

I thank KETI for allowing me an opportunity to study abroad.

Most of all, I deeply thank my wife Dr. Boyoung Kang, my son Taeyoung, my parents and parents-in-law for their love and encouragement.

References

[1] P. P. Crooker and D. K. Yang, “Polymer-dispersed chiral liquid crystal color display,” Appl. Phys. Lett. **57**(24), 2529-2531 (1990).

[2] M. Oh-e and K. Kondo, “Electro-optical characteristics and switching behavior of the in-plane switching mode,” Appl. Phys. Lett. **67**(26), 3895-3897 (1995).

[3] C. Y. Xiang, X. W. Sun, and X. J. Yin, “The electro-optic properties of a vertically aligned fast response liquid crystal display with three-electrode driving,” J. Phys. D: Appl. Phys. **37**, 994-997 (2004).

[4] V. I. Kopp, B. Fan, H. K. M. Vithana, and A. Z. Genack, "Low-threshold lasing at the edge of a photonic stop band in cholesteric liquid crystals," Opt. Lett. **23**(21), 1707-1709 (1998).

[5] J. Hwang, M. H. Song, B. Park, S. Nishimura, T. Toyooka, J. W. Wu, Y. Takanishi, K. Ishikawa, and H. Takezoe, “Electro-tunable optical diode based on photonic bandgap liquid-crystal heterojunctions," Nature Mater. **4**, 383-387 (2005).

[6] Y. Matsuhisa, Y. Huang, Y. Zhou, S. –T. Wu, R. Ozaki, Y. Takao, A. Fujii and M. Ozaki, “Low-threshold and high efficiency lasing upon band-edge excitation in a cholesteric liquid crystal,” Appl. Phys. Lett. **90**(9), 091114 (2007).

[7] D. –K. Yang, L. C. Chien, and J. W. Doane, “Cholesteric liquid crystal/polymer dispersion for haze-free light shutters,” Appl. Phys. Lett. **60**(25), 3102-3104 (1992).

[8] H. Yoshida, C. H. Lee, Y. Matsuhisa, A. Fujii, and M. Ozaki, “Bottom-up fabrication of photonic defect structures in cholesteric liquid crystals based on laser-assisted modification of the helix,” Adv. Mater. **19**, 1187-1190 (2007).

[9] H. Coles, and S. Morris, “Liquid-crystal lasers,” Nat. Photon. **4**, 676-685 (2010).

[10] Y. Inoue, H. Yoshida, K. Inoue, Y. Shiozaki, H. Kubo, A. Fujii, and M. Ozaki, “Tunable lasing from a cholesteric liquid crystal film embedded with a liquid crystal nanopore network,” Adv. Mater. **23**, 5498-5501 (2011).

[11] D. –K. Yang, J. W. Doane, Z. Yaniv, and J. Glasser, “Cholesteric reflective display: drive scheme and contrast,” Appl. Phys. Lett. **64**(15), 1905-1907 (1994).

[12] M. –H. Lu, “Bistable reflective cholesteric liquid crystal display,” J. Appl. Phys. **81**(3), 1063-1066 (1997).

[13] N. Y. Ha, Y. Ohtsuka, S. M. Jeong, S. Nishimura, G. Suzaki, Y. Takanishi, K. Ishikawa, and H. Takezoe, “Fabrication of a simultaneous red-green-blue reflector using single-pitched cholesteric liquid crystals,” Nat. Mater. **7**, 43-47 (2007).

[14] S. –Y. Lu and L. C. Chien, “A polymer-stabilized single-layer color cholesteric liquid crystal display with anisotropic reflection,” Appl. Phys. Lett. **91**(13), 131119 (2007).

[15] S. S. Choi, S. M. Morris, W. T. S. Huck, and H. J. Coles, "Electrically tuneable liquid crystal photonic bandgaps," Adv. Mater. **21**, 3915-3918 (2009).

[16] K. Funamoto, M. Ozaki, and K. Yoshino, "Discontinuous shift of lasing wavelength with temperature in cholesteric liquid crystal," Jpn. J. Appl. Phys. **42**(12B), L1523–L1525 (2003).

[17] P. Pollmann and H. Stegemeyer, "Pressure dependence of the helical structure of cholesteric mesophases," Chem. Phys. Lett. **20**(1), 87-89 (1973).

[18] T. J. White, S. A. Cazzell, A. S. Freer, D. -K. Yang, L. Sukhomlinova, L. Su, T. Kosa, B. Taheri, and T. J. Bunning, "Widely tunable, photoinvertible cholesteric liquid crystals," Adv. Mater. **23**, 1389-1392 (2011).

[19] B. Kang, H. Choi, M. Jeong, and J. W. Wu, "Effective medium analysis for optical control of laser tuning in a mixture of azo-nematics and cholesteric liquid crystal," J. Opt. Soc. Am. B **27**(2), 204–207 (2010).

[20] D. –K. Yang, J. L. West, L. C. Chien, and J. W. Doane, "Control of reflectivity and bistability in displays using cholesteric liquid crystals," J. Appl. Phys. **76**(2), 1331-1333 (1994).

[21] Y. C. Yang, R. S. Zola, Y. Cui, D. –K. Yang, H. Y. Chen, C. C. Hsu, C. J. Chen, and C. C. Liang, "Master parameter governing the response time of reflective cholesteric liquid crystal displays," SID Symp. Digest Technical Papers **42**(1), 400-403 (2011).

[22] F. Du, Y. Lu, H. Ren, S. Gauza, and S. –T. Wu, "Polymer-stabilized cholesteric liquid crystal for polarization independent variable optical attenuator," Jpn. J. Appl. Phys. **43**(10), 7083–7086 (2004).

[23] R. A. M. Hikmet and H. Kemperman, "Electrically switchable mirrors and optical components made from liquid-crystal gels," Nature **392**, 476-479 (1998).

[24] Y. Inoue, H. Yoshida, H. Kubo, and M. Ozaki, "Deformation-free, microsecond electro-optic tuning of liquid crystals," Adv. Opt. Mater. **1**, 256-263 (2013).

[25] H. Kim, J. Kobashi, Y. Maeda, H. Yoshida, and M. Ozaki, "Pitch-length independent threshold voltage of polymer/cholesteric liquid crystal nano-composite," Crystals **5**(3), 302-311 (2015).

[26] J. Kobashi, H. Kim, H. Yoshida, and M. Ozaki, "Polarization-independent submillisecond phase modulation utilizing polymer/short-pitch cholesteric liquid crystal composite," Opt. Lett. **40**(22), 5363-5366 (2015).

[27] H. Kim, Y. Inoue, J. Kobashi, Y. Maeda, H. Yoshida, and M. Ozaki, "Deformation-free switching of polymer-stabilized cholesteric liquid crystals by low-temperature polymerization," Opt. Mater. Express **6**(3), 705-710 (2016).

[28] H. Kim, J. Kobashi, Y. Maeda, H. Yoshida, and M. Ozaki, "Helical pitch dependence of the electro-optic characteristics in polymer/cholesteric liquid crystal nanocomposites," Opt. Mater. Express **6**(4), 1138-1145 (2016).

[29] P. G. de Gennes and J. Prost, *The Physics of Liquid Crystals* (Clarendon Press, 1993).

[30] P. Yeh and C. Gu, *Optics of Liquid Crystal Displays* (John Wiley & Sons, 2010).

[31] R. B. Meyer, "Effects of electric and magnetic fields on the structure of cholesteric liquid crystals," Appl. Phys. Lett. **12**(9), 281-282 (1968).

[32] D. –K. Yang and S. –T. Wu, *Fundamentals of Liquid Crystals Devices* (John Wiley & Sons, 2006).

[33] W. Helfrich, "Deformation of cholesteric liquid crystals with low threshold voltage," Appl. Phys. Lett. **17**(12), 531-532 (1970).

[34] T. Aoki, M. Kokai, K. Shinohara, and E. Oikawa, "Chiral helical conformation of the polyphenylacetylene having optically-active bulky substituent," Chem. Lett. **22**(12), 2009-2012 (1993).

[35] T. Aoki, T. Kaneko, N. Maruyama, A. Sumi, M. Takahashi, T. Sato, and M. Teraguchi, "Helix-sense-selective polymerization of phenylacetylene having two hydroxy groups using a chiral catalytic system," J. Am. Chem. Soc. **125**(21), 6346-6347 (2003).

[36] D. J. Broer, J. Lub, and G. N. Mol, "Wide-band reflective polarizers from cholesteric polymer networks with a pitch gradient," Nature **378**, 467-469 (1995).

[37] S. W. Kang, S. Sprunt, and L. C. Chien, "Structure and morphology of polymer-stabilized cholesteric diffraction gratings," Appl. Phys. Lett. **76**(24), 3516-3518 (2000).

[38] S. N. Lee, L. C. Chien, and S. Sprunt, "Polymer-stabilized diffraction gratings from cholesteric liquid crystals," Appl. Phys. Lett. **72**(8), 885-887 (1998).

[39] U. Theissen, S. J. Zilker, T. Pfeuffer, and P. Strohriegl, "Photopolymerizable cholesteric liquid crystals-new materials for holographic applications," Adv. Mater. **12**(22), 1698-1700 (2000).

[40] S. Relaix, C. Bourgerette, and M. Mitov, "Broadband reflective liquid crystalline gels due to the ultraviolet light screening made by the liquid crystal," Appl. Phys. Lett. **89**(25), 251907 (2006).

[41] B. Fan, S. Vartak, J. N. Eakin, and S. M. Faris, "Surface anchoring effects on spectral broadening of cholesteric liquid crystal films," J. Appl. Phys. **104**, 023108 (2008).

[42] M. E. McConney, T. J. White, V. P. Tondiglia, L. V. Natarajan, D. -K. Yang, and T. J. Bunning, "Dynamic high contrast reflective coloration from responsive polymer/cholesteric liquid crystal architectures," Soft Matter **8**, 318-323 (2012).

[43] F. Castles, F. V. Day, S. M. Morris, D. –H. Ko, D. J. Gardiner, M. M. Qasim, S. Nosheen, P. J. W. Hands, S. S. Choi, R. H. Friend, and H. J. Coles, "Blue-phase templated

fabrication of three-dimensional nanostructures for photonic applications," Nat. Mater. **11**, 599-603 (2012).

[44] M. Onoda, Y. Manda, and K. Yoshino, "Anisotropy of absorption and photoluminescence spectra of stretched poly(3-alkylthiophene)," Jpn. J. Appl. Phys. **29**(8), 1490-1494 (1990).

[45] S. Nagamatsu, W. Takashima, K. Kaneto, Y. Yoshida, N. Tanigaki, and K. Yase, "Polymer field-effect transistors by a drawing method," Appl. Phys. Lett. **84**(23), 4608-4610 (2004).

[46] T. Higashi, N. Yamasaki, H. Utsumi, H. Yoshida, A. Fujii, and M. Ozaki, "Anisotropic properties of aligned p-conjugated polymer films fabricated by capillary action and their post-annealing effects," Appl. Phys. Express **4**(9), 091602 (2011).

[47] T. Higashi, N. Yamasaki, H. Utsumi, H. Yoshida, A. Fujii, and M. Ozaki, "Thermal annealing effects on optical anisotropy of aligned thiophene-based p-conjugated polymer films fabricated by capillary action," Jpn. J. Appl. Phys. **51**, 02BK11 (2012).

[48] R. L. Sutherland, V. P. Tondiglia, L. V. Natarajan, T. J. Bunning, and W. W. Adams, "Electrically switchable volume gratings in polymer-dispersed liquid crystals," Appl. Phys. Lett. **64**(9), 1074-1076 (1994).

[49] D. Coates, "Polymer-dispersed liquid crystals," J. Mater. Chem. **5**(12), 2063-2072 (1995).

[50] X. Zhou and Y. Huang, "Temperature dependence of the phase separation in ethyl cyanoethyl cellulose/poly(acrylic acid)/4′-n-pentyl-4-cyano-biphenyl composite films," J. Polym. Sci. Part B: Polym. Phys. **40**(13), 1334-1341 (2002).

[51] S. Matsumoto, M. Houlbert, T. Hayashi, and K. Kubodera, "Fine droplets of liquid crystals in a transparent polymer and their response to an electric field," Appl. Phys. Lett. **69**(8), 1044-1046 (1996).

[52] J. A. Jung and B. K. Kim, "Controls of solubility parameter and crosslinking density in polyurethane acrylate based holographic polymer dispersed liquid crystal," Opt. Comm., **247**, 125-132 (2005).

[53] J. H. Wang and B. Y. Zhang, "The kinetics and morphology of polymer dispersed liquid crystals by doped crylic acid," Polym. Comp., **32**(10), pp. 1523-1531.

[54] S. V. Kostromin, S. V. Bronnikov, and V. V. Zuev, "Kinetics of formation of polymer dispersed liquid crystals in a liquid-crystalline polymer matrix," Polym. Sci. Ser. A **53**(4), 317-322 (2011).

[55] N. H. Nataj, A. Jannesari, E. Mohajerani, F. Najafi, and H. Jashnsaz, "Photopolymerization behavior and phase separation effects in novel polymer dispersed liquid crystal mixture based on urethane trimethacrylate monomer," J. Appl. Polym. Sci. **126**(55), 1676-1686 (2012).

[56] R. A. M. Hikmet, "Electrically induced light scattering from anisotropic gels," J. Appl. Phys. **68**(9), 4406-4412 (1990).

[57] C. V. Rajaram, S. D. Hudson, and L. C. Chien, “Morphology of polymer-stabilized liquid crystals,” Chem. Mater. **7**(12), 2300-2308 (1995).

[58] R. A. M. Hikmet, “Anisotropic gels in liquid crystal devices,” Adv. Mater. **4**(10), 679-683 (1992).

[59] I. Dierking, “Polymer network-stabilized liquid crystals,” Adv. Mater. **12**(3), 167-181 (2000).

[60] L. Komitov, G. Hegde, and D. Kolev, “Fast liquid crystal light shutter,” J. Phys. D: Appl. Phys. **44**, 442002 (2011).

[61] C. –Y. Huang, H. –C. Pan, and C. –T. Hsieh, “Electrooptical properties of carbon-nanotube-doped twisted nematic liquid crystal cell,” Jpn. J. Appl. Phys. **45**(8A), 6392-6394 (2006).

[62] H. –Y. Chen, W. Lee, and N. A. Clark, “Faster electro-optical response characteristics of a carbon-nanotube-nematic suspension,” Appl. Phys. Lett. **90**, 033510 (2007).

[63] Y. –J. Lee, Y. –K. Kim, S. I. Jo, K. –S. Bae, B. –D. Choi, J. –H. Kim, and C. –J. Yu, “Fast vertical alignment mode with continuous multi-domains for a liquid crystal display,” Opt. Express **17**(26), 23417-23422 (2009).

[64] Y. Inoue, H. Yoshida, and M. Ozaki, “Nematic liquid crystal nanocomposite with scattering-free, microsecond electro-optic response,” Opt. Mater. Express **4**(5), 916-923 (2014).

[65] S. Relaix, C. Bourgerette, and M. Mitov, “Broadband reflective cholesteric liquid crystalline gels: volume distribution of reflection properties and polymer network in relation with the geometry of the cell photopolymerization,” Liq. Cryst. **34**(9), 1009-1018 (2007).

[66] G. Agez, S. Relaix, and M. Mitov, “Cholesteric liquid crystal gels with a graded mechanical stress,” Phys. Rev. E Stat. Nonlin. Soft Matter Phys. **89**(2), 022513 (2014).

[67] Y. Inoue “架橋された液晶構造体を用いた光学素子に関する研究”, Ph.D Thesis, (Osaka Univ., 2013).

[68] H. Imura and K. Okano, “Temperature dependence of the viscosity coefficients of liquid crystals,” Jpn. J. Appl. Phys. **11**(10), 1440-1445 (1972).

[69] J. Sun, Y. Chen, and S. T. Wu, “Submillisecond-response and scattering-free infrared liquid crystal phase modulators,” Opt. Express **20**(18), 20124-20129 (2012).

[70] M. R. Wilson and D. J. Earl, “Calculating the helical twisting power of chiral dopants,” J. Mater. Chem. **11**, 2672-2677 (2001).

[71] R. Cano, “Interprétation des discontinuités de grandjean,” Bull. Soc. Fr. Mineral. Cristallogr. **91**, 20-27 (1968).

[72] H. Nemati, D. –K. Yang, K. –L. Cheng, C. –C. Liang, J. –W. Shiu, C. –C. Tsai, and R. S. Zola, “Effect of surface alignment layer and polymer network on the Helfrich deformation in cholesteric liquid crystals,” J. Appl. Phys. **112**(12), 124513 (2012).

[73] C. V. Rajaram, S. D. Hudson, and L. C. Chien, “Effect of polymerization temperature on the morphology and electrooptic properties of polymer-stabilized liquid crystals,” Chem. Mater. **8**(10), 2451-2460 (1996).

[74] R. A. M. Hikmet and R. Polesso, “Patterned multicolor switchable cholesteric liquid crystal gels,” Adv. Mater. **14**(7), 502-504 (2002).

Achievements

I. Publications

1. **Hoekyung Kim**, Junji Kobashi, Yasutaka Maeda, Hiroyuki Yoshida, and Masanori Ozaki, "Helical pitch dependence of the electro-optic characteristics in polymer/cholesteric liquid crystal nanocomposites" *Opt. Mater. Express*, **6**(4), pp.1138-1145 (2016).
2. **Hoekyung Kim**, Yo Inoue, Junji Kobashi, Yasutaka Maeda, Hiroyuki Yoshida, and Masanori Ozaki, "Deformation-free switching of polymer-stabilized cholesteric liquid crystals by low-temperature polymerization" *Opt. Mater. Express*, **6**(3), pp.705-710 (2016).
3. Junji Kobashi, **Hoekyung Kim**, Hiroyuki Yoshida, and Masanori Ozaki, "Polarization independent submillisecond phase modulation utilizing polymer/short-pitch cholesteric liquid crystal composite" *Opt. Lett.*, **40**(22), pp.5363-5366 (2015).
4. **Hoekyung Kim**, Junji Kobashi, Yasutaka Maeda, Hiroyuki Yoshida, and Masanori Ozaki, "Pitch-length independent threshold voltage of polymer/cholesteric liquid crystal nano-composites" *Crystals*, **5**, pp.302-311 (2015).

II. Proceedings

1. **Hoekyung Kim**, Junji Kobashi, Hiroyuki Yoshida, and Masanori Ozaki, "Electro-optic properties of nano-pore dispersed cholesteric liquid crystals with varying chiral concentrations" *IEICE Technical Report OME2014-45*, **114**(241), pp.45-49 (2014).

III. International Conferences

1. [**Poster**] **H. Kim**, Y. Inoue, J. Kobashi, H. Yoshida, and M. Ozaki, "Improvement of electro-optic characteristics in a polymer-cholesteric liquid crystal nano-composite by low temperature polymerization" 16th Topical Meeting on the Optics of Liquid Crystals (OLC2015), Grand Hotel Sopot, Sopot, Poland, September 13–18 (2015).
2. [**Oral**] J. Kobashi, H. Yoshida, **H. Kim**, and M. Ozaki, "Submillisecond, polarization independent phase modulation using a polymer-cholesteric liquid crystal nanocomposite" 16th Topical Meeting on the Optics of Liquid Crystals (OLC2015), Grand Hotel Sopot, Sopot, Poland, September 13–18 (2015).
3. [**Invited**] Hiroyuki Yoshida, Junji Kobashi, **Hoekyung Kim**, Yo Inoue, Yasutaka Maeda, and Masanori Ozaki, "Properties and applications of nano-pore dispersed liquid crystals" SPIE Photonics West, Emerging Liquid Crystal Technologies X, The Moscone Center, San Francisco, California, USA, February 7–15 (2015).
4. [**Poster**] **Hoekyung Kim**, Junji Kobashi, Hiroyuki Yoshida, and Masanori Ozaki, "Dependence of the electro-optic response on the helical pitch in nano-pore dispersed

cholesteric liquid crystals" The 2nd Asian Conference on Liquid Crystals (ACLC 2015), Haeundae Grand Hotel, Busan, Korea, January 19–21 (2015).

5. [**Invited**] Masanori Ozaki, Yo Inoue, Junji Kobashi, **Hoekyung Kim**, and Hiryouki Yoshida, "Scattering-Free, Microsecond Electro-Optic Response Based on Polymer/LC Nanocomposite" The 21st International Display Workshops (IDW '14), TOKI MESSE Niigata Convention Center, Niigata, Japan, December 3–5 (2014).
6. [**Keynote**] Masanori Ozaki, Yo Inoue, **Hoekyung Kim**, and Hiroyuki Yoshida, "Micro-second electro-optic modulation in polymer/liquid-crystal nanocomposite films" SPIE Optics and Photonics, Liquid Crystals XVIII, San Diego Convention Center, San Diego, California, United States, August 17–21 (2014).
7. [**Invited**] Hiroyuki Yoshida, Yo Inoue, **Hoekyung Kim**, and Masanori Ozaki, "Sub-millisecond Electro-optic switching in Nano-pore Dispersed Liquid Crystals" International Symposium on nanophotonics and Nanomaterials 2014 (ISONP 2014), Beijing, China, January 15–17 (2014).
8. [**Invited**] Masanori Ozaki, Yo Inoue, **Hoekyung Kim**, and Hiroyuki Yoshida "Micro-second Electro-optic Modulation in Photo-polymerized Liquid Crystal Films Containing Nano-size Liquid-crystal Droplets" 15th Topical Meeting on the Optics of Liquid Crystals (OLC2013), Ala Moana Hotel, Hawai'I, USA, September 29–October 4 (2013).
9. [**Invited**] Masanori Ozaki, Yo Inoue, **Hoekyung Kim**, and Hiroyuki Yoshida, "Micro-second electro-optic switching in liquid crystal film with nano-pore filled with liquid crystal" The 13th International Meeting on Information Display (IMID 2013), Daegu, Korea, August 26–29, 2013.

IV. Domestic Conferences

1. [口頭発表] **Hoekyung Kim**, Junji Kobashi, Hiroyuki Yoshida, and Masanori Ozaki 「Electro-optic properties of nano-pore dispersed cholesteric liquid crystals with varying chiral concentrations」 2014 年 電子情報通信学会 有機エレクトロニクス研究会 (OME)、大阪大学中之島センター, 2014 年 10 月 10 日.
2. [口頭発表] 小橋淳二, **金會慶**, 吉田浩之, 尾﨑雅則「高分子ーコレステリック液晶複合材料を用いた高速偏光回転素子」2014 年第 75 回応用物理学会秋季学術講演会、北海道大学、2014 年 9 月 17 日－20 日.
3. [口頭発表] 小橋淳二, **金會慶**, 吉田浩之, 尾﨑雅則「高分子ーコレステリック液晶複合材料を用いた偏光無依存な高速位相変調素子」2014 年日本液晶学会討論会、島根県松江市　くにびきメッセ、2014 年 9 月 8 日－10 日.
4. [ポスター発表] **金會慶**, 小橋淳二, 吉田浩之, 尾崎雅則「Dependence of the threshold voltage on the chiral dopant concentration in nano-pore dispersed cholesteric liquid crystals」

2014 年日本液晶学会討論会、島根県松江市 くにびきメッセ、2014 年 9 月 8 日－10 日.

5. [口頭発表] 小橋淳二，**金會慶**，吉田浩之，尾﨑雅則「高分子-液晶コンポジット材料を用いた高速応答光変調素子に関する研究」第 294 回電気材料技術懇談会 大阪大学中之島センター、大阪大学中之島センター、2014 年 7 月 23 日.
6. [ポスター発表] **金會慶**, 吉田浩之, 井上曜, 小橋淳二, 尾崎雅則「Characterization of the optical properties of nano-pore dispersed cholesteric liquid crystals」2013 年日本液晶学会討論会、大阪大学豊中キャンパス、2013 年 9 月 8 日－10 日.